Copyright Warning & Restrictions

The copyright law of the United States (Title 17, United States Code) governs the making of photocopies or other reproductions of copyrighted material.

Under certain conditions specified in the law, libraries and archives are authorized to furnish a photocopy or other reproduction. One of these specified conditions is that the photocopy or reproduction is not to be "used for any purpose other than private study, scholarship, or research." If a, user makes a request for, or later uses, a photocopy or reproduction for purposes in excess of "fair use" that user may be liable for copyright infringement,

This institution reserves the right to refuse to accept a copying order if, in its judgment, fulfillment of the order would involve violation of copyright law.

Please Note: The author retains the copyright while the New Jersey Institute of Technology reserves the right to distribute this thesis or dissertation

Printing note: If you do not wish to print this page, then select "Pages from: first page # to: last page #" on the print dialog screen

NJIT New Jersey's Science & Technology University

The Van Houten library has removed some of the personal information and all signatures from the approval page and biographical sketches of theses and dissertations in order to protect the identity of NJIT graduates and faculty.

ABSTRACT

NOVEL PHOTOBASE GENERATORS FOR PHOTOINDUCED POLYMERIZATION AND PH REGULATION

by

Shupei Yu

Photochemistry encompasses the investigation of chemical processes instigated by light absorption. As important branches of photochemistry, photosensitive and optical materials have attracted extensive research interests in both academia and industry. Photosensitive and optical materials are composed of polymers / small molecules with photo-responsive properties. These materials not only can absorb light in the desired energy spectrum, but also exhibit chemical / physical reactions, which can be applied to different fields such as photoredox, photo-heat, phototherapy, solar cells, diodes, etc. Among them, photobase generators (PBGs) are a series of photosensitive compounds, which absorb the incident light, then release the basic species that can trigger the consequent reactions such as thiol-Michael reaction and ring-opening polymerization reactions.

Boron-dipyrromethene (BODIPY)-based chromophores have emerged as highly intriguing moieties within the realm of chromophores. The prominence is attributed to its remarkable properties, including a high fluorescent quantum yield, pronounced chemical stability, and minimal Stokes shift. The core structures of BODIPY have been subject to thorough investigations and refinements, resulting in the development of a spectrum of BODIPY derivatives that find applications within the domain of chemical synthesis and biological science.

In this work, three projects about BODIPY-based photobase generators are included with demonstration and discussion of their bio-applications. Firstly, BODIPY based PBGs are synthesized and the photochemical/photophysical properties are characterized. Secondly, the applications of BODIPY based PBGs in photoinduced thiol Michael reaction and ring-opening reaction are explored. Thirdly, the feasibility of using PBGs in lysosome pH regulation light is demonstrated and the potential usage in cancer therapy is discussed.

NOVEL PHOTOBASE GENERATORS FOR PHOTOINDUCED POLYMERIZATION AND PH REGULATION

by
Shupei Yu

A Dissertation
Submitted to the Faculty of
New Jersey Institute of Technology
in Partial Fulfillment of the Requirements for the Degree of
Doctor of Philosophy in Chemistry

Department of Chemistry and Environmental Science

December 2023

Copyright © 2023 by Shupei Yu

ALL RIGHTS RESERVED

.

APPROVAL PAGE

NOVEL PHOTOBASE GENERATORS FOR PHOTOINDUCED POLYMERIZATION AND PH REGULATION

Shupei Yu

Dr. Yuanwei Zhang, Dissertation Advisor — Date
Assistant Professor of Chemistry and Environmental Science, NJIT

Dr. Kevin D Belfield, Committee Member — Date
Dean of College of Science and Liberal Arts
Professor of Chemistry and Environment Science, NJIT

Dr. Hao Chen, Committee Member — Date
Professor of Chemistry and Environmental Science, NJIT

Dr. Michael Eberhart, Committee Member — Date
Assistant Professor of Chemistry and Environmental Science, NJIT

Dr. Xiaoyang Xu, Committee Member — Date
Associate Professor of Chemical and Materials Engineering, NJIT

BIOGRAPHICAL SKETCH

Author: Shupei Yu

Degree: Doctor of Philosophy

Date: December 2023

Undergraduate and Graduate Education:

- Doctor of Philosophy in Chemistry,
  New Jersey Institute of Technology, Newark, NJ, 2023

- Bachelor of Material Science in Material Chemistry,
  Qingdao University of Science and Technology, Qingdao, P. R. China, 2017

Major: Chemistry

Presentations and Publications:

Yu, Shupei, Ojasvita Reddy, Alperen Abaci, Yongling Ai, Yanmei Li, Hao Chen, Murat Guvendiren, Kevin D. Belfield, and Yuanwei Zhang. "Novel BODIPY-Based Photobase Generators for Photoinduced Polymerization." ***ACS Applied Materials & Interfaces*** 15, no. 38 (2023): 45281-45289.

Wan, Zhaoxiong, Shupei Yu, Qi Wang, Karthik Sambath, Roshena Harty, Xiangshan Liu, Hao Chen, Chen Wang, Xuan Liu, and Yuanwei Zhang. "Far-red BODIPY-based Oxime Esters: Photo-uncaging and Drug Delivery." ***Journal of Materials Chemistry B*** (2023).

Grebel, Haim, Shupei Yu, and Yuanwei Zhang. "Supercapacitors with Gold Colloids That Are Placed at a Short Distance from Active-Carbon Electrodes; The Case for a Plasmonic Effect at the Electrolyte/Electrode Interface." ***In Electrochemical Society Meeting Abstracts 243***, no. 1, pp. 446-446. The Electrochemical Society, Inc., 2023.

Liu, Yuwei, Shupei Yu, Yuanwei Zhang, and Xuan Liu. "Label-free Full-field Doppler Phase Microscopy Based on Optical Computation." ***Biomedical Optics Express*** 14, no. 1 (2023): 441-452.

Dou, Jie, Shupei Yu, Ojasvita Reddy, and Yuanwei Zhang. "Novel ABA Block Copolymers: Preparation, Temperature Sensitivity, and Drug Release." ***RSC Advances*** 13, no. 1 (2023): 129-139.

Grebel, H., Shupei Yu, and Yuanwei Zhang. "Active Carbon Based Supercapacitors with Au Colloids: The Case of Placing The Colloids in Close Proximity to The Electrode Interface." ***Nanoscale Advances*** 5, no. 1 (2023): 179-190.

Wan, Zhaoxiong, Shupei Yu, Qi Wang, John Tobia, Hao Chen, Zhanjun Li, Xuan Liu, and Yuanwei Zhang. "A BODIPY-Based Far-Red-Absorbing Fluorescent Probe for Hypochlorous Acid Imaging." ***ChemPhotoChem*** 6, no. 4 (2022): e202100250.

Yeh, SC A., Jue Hou, J. W. Wu, S. Yu, Y. Zhang, K. D. Belfield, F. D. Camargo, and C. P. Lin. "Quantification of Bone Marrow Interstitial pH and Calcium Concentration by Intravital Ratiometric Imaging." ***Nature communications*** 13, no. 1 (2022): 393.

Yang, Hongyan, Yanmei Li, Yuling Zhao, Shupei Yu, Hailin Ma, Long Qian, Ruidong Wang, Tianzhi Yu, and Wenming Su. "Four New Bipolar Indolo [3, 2-b] Carbazole Derivatives for Blue OLEDs." ***Dyes and Pigments*** 187 (2021): 109096.

Zhao, Tinghan, Zhaoxiong Wan, Karthik Sambath, Shupei Yu, Mehrun Nahar Uddin, Yuanwei Zhang, and Kevin D. Belfield. "Regulating Mitochondrial pH with Light and Implications for Chemoresistance." ***Chemistry–A European Journal*** 27, no. 1 (2021): 247-251.

Yu, Tianzhi, Yuying Niu, Shupei Yu, Zixuan Xu, Yuling Zhao, and Hui Zhang. "Synthesis, Photo-and Electro-luminescence of Novel Red Phosphorescent Ir (III) Complexes with a Silsesquioxane Core." ***Journal of Organometallic Chemistry*** 830 (2017): 85-92.

Yu, Tianzhi, Lijing Ma, Shupei Yu, Zixuan Xu, Yuling Zhao, and Hui Zhang. "Synthesis, Characterization, and Photo-and Electro-luminescence of New Ir (III) Complexes with Carrier Transporting Group-functionalized Dibenzoylmethane Ligand for Green Phosphorescent OLEDs." ***Synthetic Metals*** 209 (2015): 319-328.

FOR MY FAMILY
希望我的家人身体健康

ACKNOWLEDGMENTS

I want to express my sincere gratitude to my dissertation advisor Dr. Yuanwei Zhang and co-advisor Dr. Kevin Belfield, who have not only served as my academic guides but also as continual sources of support, inspiration, and motivation. Throughout my Ph.D. studies, they provided invaluable assistance and guidance in my research endeavors. Additionally, they encouraged my participation in various collaborative programs and readily offered commendable references when needed. In essence, the exceptional enthusiasm and positive research-oriented approach of Dr. Yuanwei Zhang and Dr. Kevin Belfield have been the driving forces behind my successful graduate journey at the New Jersey Institute of Technology, and I am indebted to them for their unwavering support, without which I would not have completed my doctoral studies.

I want to express my gratitude to each member of my committee, Dr. Hao Chen, Dr. Michael Eberhart, and Dr. Xiaoyang Xu, for their unwavering patience, professional guidance, and valuable assistance. Special thanks are due to Dr. Carlos Pacheco for providing indispensable support in NMR spectroscopy. Additionally, I express my sincere appreciation for the research funding received from the National Institute of General Medical Sciences of the National Institutes of Health (award numbers 5R21AA028340-02 and 1R15GM148990-01) and the New Jersey Health Foundation (award numbers PC 57-20 and PC 25-22).

Also, I express my gratitude to Yuwei Liu and Dr. Xuan Liu for their assistance with phase images. Special appreciation is extended to Yongling Ai and Prof. Hao Chen

for their support in Mass spectroscopy. I’m grateful for the enduring companionship of my family members TianZhi Yu and Yuling Zhao, as well as my girlfriend Yanmei Li.

TABLE OF CONTENTS

TABLE OF CONTENTS
(Continued)

Chapter **Page**

TABLE OF CONTENTS
(Continued)

Chapter **Page**

LIST OF TABLES

LIST OF FIGURES

LIST OF FIGURES
(Continued)

Figure **Page**

LIST OF FIGURES
(Continued)

Figure **Page**

LIST OF SCHEMES

LIST OF SYMBOLS

©	Copyright
∫	Integration
≈	Approximately
ε	Extinction coefficient
Φ	quantum yield
τ	lifetime
λ	wavelength

LIST OF DEFINITIONS

PBG	Photobase generator. A category of compound that could release organic base once upon light irradiation
PAG	Photoacid generator. A category of compound that could release proton once upon light irradiation
BODIPY	Boron-dipyrrolemethene
DMSO	Dimethyl sulfoxide
DCM	Dichloromethane
μM	Micro mol per liter
IC50	a quantitative measure that indicates how much of a particular inhibitory substance (e.g. drug) is needed to inhibit, in vitro, a given biological process or biological component by 50%.
NMR	Nuclear magnetic resonance
HeLa cells	Henrietta Lacks's cancer cells
DDQ	2, 3-Dichloro-5, 6-dicyano-1, 4-benzoquinone
DIPEA	N,N-Diisopropylethylamine
MS	Mass spectroscopy
ROS	Reactive oxygen species
UV	Ultraviolet light
VIS	Visible light
PPG	Photoprotecting group
NIR	Near infrared
DMF	Dimethylformamide

CHAPTER 1

PHOTOBASE GENERATORS AND BODIPY

1.1 Photobase Generators

A photobase generator (PBG) is a type of photolatent compound that generates organic bases upon exposure to light. PBGs have been systematically developed to cater to diverse applications within the domain of polymer science and technology. These applications encompass a spectrum of processes, including photo-induced polymerization, depolymerization, crosslinking, de-crosslinking, and photo-imaging. The versatility of PBGs positions them as invaluable tools for manipulating and controlling polymerization reactions with precision and adaptability. PBGs are desirable because they can be used to generate organic bases under mild conditions, without the need for high temperatures.

1.1.1 Introduction

Similar to PBGs, photoacid generators (PAGs) are chemical compounds that have the ability to initiate polymerization reactions by liberating acid species upon exposure to light.[1] Within the realm of polymer science, PAGs find extensive applications in various domains, including coatings, adhesives, inks, and semiconductor materials.[2] Over the years, significant developments have taken place in the field of PAGs, particularly to facilitate photoinitiated cationic polymerization processes. This advancement has paved the way for the utilization of a myriad of monomeric materials, including vinyl ether, epoxy and oxetane. Each of these materials boasts distinct attributes, such as exceptional

adhesion, mechanical strength, and chemical resistance.[3] Ionic PAGs primarily encompass onium salt derivatives,[4] a class of compounds with a century-long history in applications such as deprotection methods in chemically-amplified photoresists. However their utilization in photopolymerization has only been recently developed. Onium salts comprise an onium functional group as the cationic component, exemplified by diarylhalonium and triarylsulfonium, paired with a counter anion. When exposed to light, onium salts undergo photolysis, a process leading to the concurrent generation of Brønsted acids and cations.[5] The rate at which these acids are liberated is influenced by both the cationic and anionic constituents. Indeed, the cation plays a direct role in photochemical reactions, the anion dictates the acid's strength resulting from the cation's photolysis and regulates the kinetics of polymerization.

Cationic photopolymerization offers distinct advantages, primarily due to the absence of termination reactions, ensuring high curing efficiency.[6] Additionally, it exhibits insensitivity to oxygen and affords a wide range of polymer backbones. Moreover, the reliance on high-energy UV light (wavelengths < 300 nm) introduces several drawbacks, including potential harm to cells and tissues, as well as limited penetration depth. Consequently, significant research efforts have been directed towards the development of compounds that are sensitive to visible light, addressing these concerns.[6]

In comparison to PAGs, PBGs have seen comparatively less development. The inception of organic photobase generators dates back to 1990, as initially introduced by Fréchet’s group.[7] They employed a photo-response carbamate group to yield basic species through photochemical activation. Subsequent to this seminal work, various other

classes of PBGs have been formulated, encompassing salts and O-acyloximes. These photolatent compounds have found utility in diverse applications, acting as crosslinking agents, and more recently, garnering acknowledgment for their role as initiator in base-catalyzed reactions.[8] Recent progress in PBGs has focused on the synthesis of ionic derivatives that exhibit easy tunability. Their ionic characteristics enable the adjustment of the photosensitive fragment, with the goal of enhancing quantum yield and absorption at extended wavelengths. Furthermore, these derivatives allow for the easy incorporation of diverse active protonated latent superbases through a straightforward acid-base reaction.

PBGs have many advantages. For example, they can be used to initiate polymerization reactions under mild conditions, such as at room temperature, and with low-energy visible light, which is less damaging to cells and tissues than high-energy UV light. PBGs can also be used to initiate anionic polymerization reactions in the presence of oxygen and water.[9]

PBGs have found applications in various domains, notably in the synthesis of polyurethanes and the ring-opening polymerization (ROP) of epoxides and lactones. (1) In the synthesis of polyurethanes, PBGs serve as initiators for the polymerization of isocyanates and polyols, leading to the formation of polyurethanes. This polymerization process boasts the advantage of being feasible under mild conditions, including room temperature, and with the utilization of low-energy visible light.[10] (2) PBGs play a crucial role in initiating the ROP of epoxides and lactones, offering a versatile approach for crafting polymers with diverse properties.[11] (3) Step-growth polymerization: PBGs have been used to initiate step-growth polymerization reactions, which can be used to

synthesize a variety of polymers, including polyesters and polyamides.[12] (4) Fabrication of micro- and nanostructures: PBGs have been used in the fabrication of micro- and nanostructures, such as photonic crystals and microfluidic devices. PBGs exhibit the capability to initiate polymerization reactions in designated regions of a substrate, thereby enabling meticulous control over the dimensions and configurations of the ensuing structures.[13] Overall, PBGs have shown great potential for use in a wide range of applications in the field of photopolymerization. Their ability to initiate polymerization reactions under mild conditions and with low-energy visible light makes them an attractive alternative to traditional thermal polymerization methods. However, due to the relatively high cost of PBGs and the fact that almost any base generated during use is easily oxidized into colored substances and difficult to remove from polymer products. This greatly limits the application of PBGs in photopolymerization. Therefore, it is necessary to develop a new generation of PBGs.

1.1.2 Recent Development of Photobase Generators

1.1.2.1 Salt

The utilization of salts as precursors for the generation of bases initially manifested in the form of quaternary ammonium salts (QAs), as documented in a foundational study conducted by Sarker et al. in the year 1998.[14, 15] The investigation conducted by Sarker and colleagues centered on the conversion of QAs to tertiary amines in the presence of borate anions, the chemical structures of which are delineated in Figure 1.1a.[16, 17] Notably, ammonium salts possess the capacity to liberate free amines upon exposure to irradiation. Consequently, irradiation of quaternary ammonium salts (QASs) results in the

production of tertiary amines. A distinctive characteristic of QAs lies in their structural configuration, defined by a direct linkage with a chromophore. Under the UV light irradiation, this chromophore undergoes homolytic cleavage of the C-N bond, thereby engendering the formation of the corresponding amine.[9]

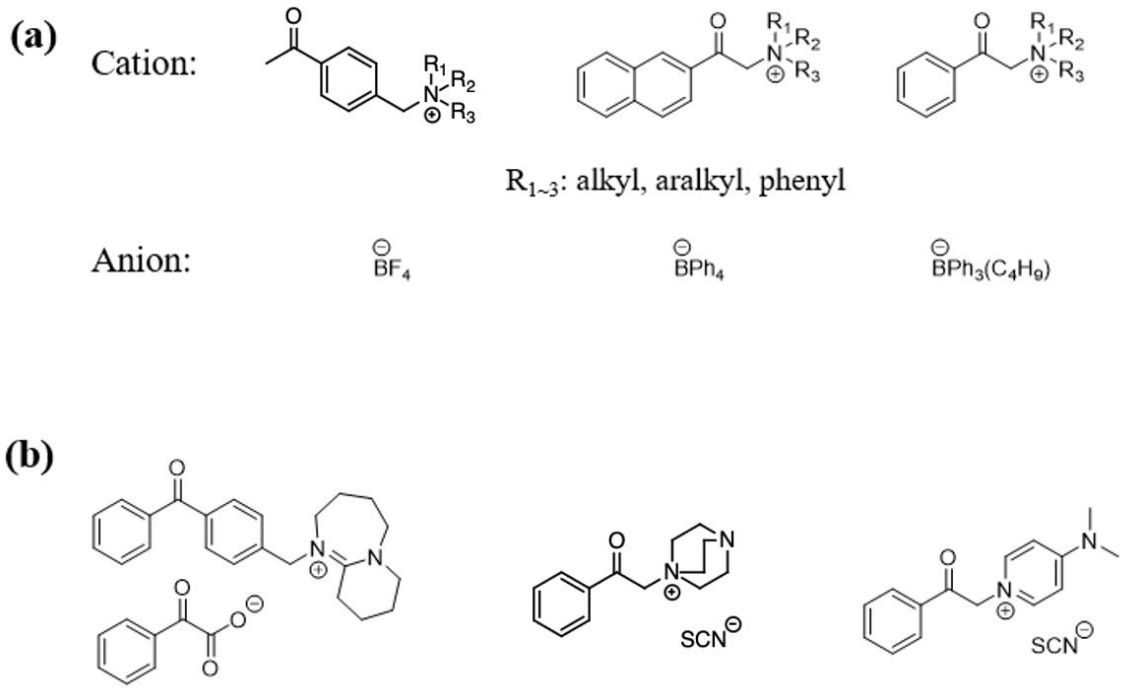

Figure 1.1 a) QAs with borate anions as PBGs. b) Examples of QAs.

Source: Zivic, Nicolas, et al. "Recent Advances and Challenges in the Design of Organic Photoacid and Photobase Generators for Polymerizations." *Angewandte Chemie International Edition* 58.31 (**2019**): 10410-10422.

These compounds, marking a significant breakthrough, ushered in the ability to liberate tertiary amines, thereby broadening the scope of utilization for photobase generators (PBGs) to encompass a wider array of bases (as shown in Fig 1.1b).[9] Figure 1.2 elucidates the proposed photochemical mechanism, wherein an initial single electron transfer (SET) transpires from the borate anion to the cation, yielding an intermediate species. Subsequently, homolytic cleavage of the C-N bond within the

cation takes place in the subsequent step, culminating in a secondary SET event from an unspecified species to the cation, ultimately leading to the formation of a radical and an amine.[18] Significantly, the experimental results highlight the absence of concurrent side reactions, and product analysis confirms the nearly quantitative efficiency in amine generation. The quantum yield of QAs photolysis is contingent upon the electron-donating propensity of the anions and the steric effects associated with the cations.

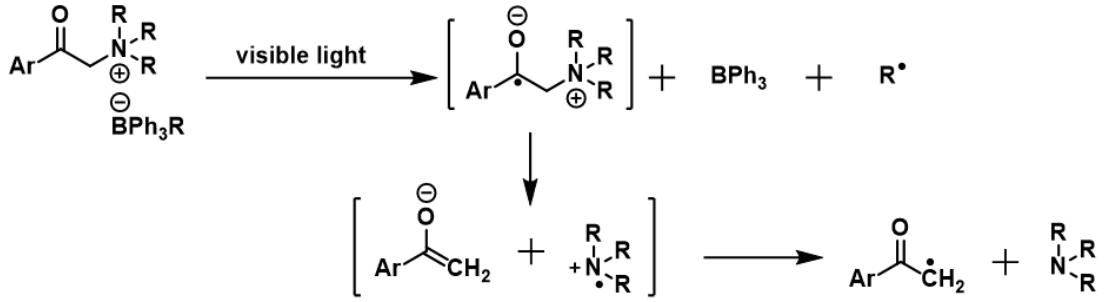

Figure 1.2 Photochemical reactions of QAs with borate anions.

Source: Suyama, Kanji, and Masamitsu Shirai. "Photobase Generators: Recent Progress and Application Trend in Polymer Systems." *Progress in Polymer Science* 34.2 (**2009**): 194-209.

Nevertheless, it is crucial to highlight that a significant fraction of these compounds exhibits restricted solubility and compromised stability when exposed to organic solvents, notably demonstrating diminished thermal endurance. Additionally, it is salient to acknowledge that the photolytic efficiency predominantly hinges upon the specific structural attributes of the amines, thereby rendering the endeavor to engender versatility in the incorporation of amines into QA compounds inherently impracticable.[9]

To address these constraints, Sun and colleagues developed a series of PBGs based on tetraphenylborate salts of 1,5,7-Triazabicyclo[4.4.0]dec-5-ene (TBD·$HBPh_4$). Upon short-wave UV light irradiation these PBGs exhibit the ability to effectuate the photo-induced liberation of the free base through a process in which the BPh_4^- anion undergoes a structural rearrangement and subsequently acquires a proton from $TBD{\cdot}H^+$

(Scheme 1.1).[19] It is noteworthy that the pKa value of TBD in acetonitrile is recorded at 26.03. This distinctive attribute plays a pivotal role in facilitating the process of photoinduced living ring-opening polymerization of cyclic esters and the photoinduced cross-linking of a diverse range of polymeric materials incorporating the hydroxyl ester functional group.[9] However, it is worth noting that the PBGs based on tetraphenylborate salts are limited to the absorption of high-energy UV light, thereby impacting their potential utility in biological applications. This limitation is primarily due to the fact that UV light can induce substantial photodamage in cells and tissues, in addition to its limited penetration depth compared to visible light. Furthermore, it is important to note that the quantum yields for base generation of these PBGs (Φ_{254}=0.18 for TBD salt) are typically low which can be unfavorable for photo-triggered polymerization reactions.

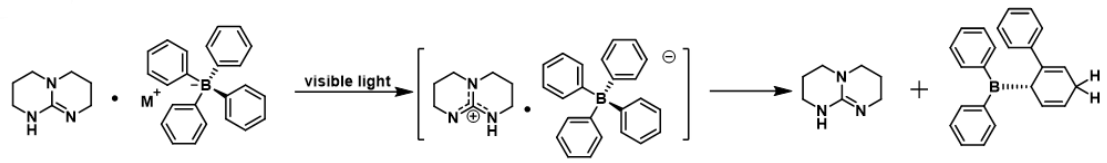

Scheme 1.1 Proposed mechanism for the photo-generation of TBD from TBD*$HBPh_4$.

Source: Sun, Xun, Jian Ping Gao, and Zhi Yuan Wang. "Bicyclic Guanidinium Tetraphenylborate: A Photobase Generator and A Photocatalyst for Living Anionic Ring-opening Polymerization and Cross-linking of Polymeric Materials Containing Ester and Hydroxy Groups." *Journal of the American Chemical Society* 130.26 (**2008**): 8130-8131.

1.1.2.2 Carbamates

The carbamate-based photobase generator involve employing a photolabile protecting group (PPG) attached to an amine through a carbamate linker. This configuration undergoes photodecarboxylation, resulting in the liberation of primary or secondary amines (as shown in Scheme 1.2).[9] Compared with the salt-based PBGs, the carbamate-

based PBGs provide higher base photo-releasing efficiencies, and better solubilities in organic solvents. Therefore, many of these PBGs are commonly used to date. However, these PBGs are only able to liberate relatively weak base that are generally inefficient in the activation of anionic polymerizations during their early applications. In addition, due to the weak bases released, the system needs a second thermal treatment to form the polymeric network, which may affect the final polymer structure.

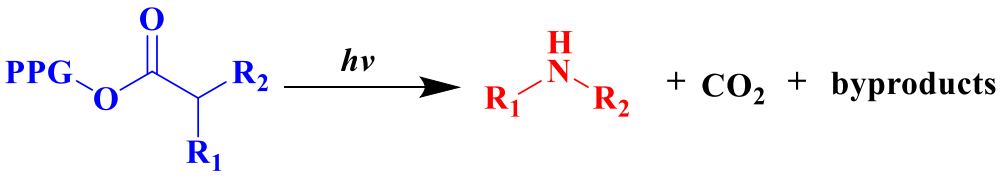

PPG: photoremovable protecting group
R_1,R_2: alkyl

Scheme 1.2 General photolysis of photolabile carbamates.

Source: Zivic, Nicolas, et al. "Recent Advances and Challenges in the Design of Organic Photoacid and Photobase Generators for Polymerizations." *Angewandte Chemie International Edition* 58.31 (**2019**): 10410-10422.

This situation was changed in 2014, Bowman and colleagues showcased the photo-uncaging of a robust base, specifically 1,1,3,3-tetramethylguanidine (TMG, pKa=23.4 in MeCN), through the use of carbamate bond photo-cleavage property. The researchers employed 2-(2-nitrophenyl)propoxycarbonyl (NPPOC) as the PPG, a compound previously recognized for its high quantum yields at 365 nm (Φ_{365}=0.15) (Scheme 1.3).[20] Subsequently, NPPOC-TMG was employed in the photoinduced thiol-Michael addition reaction involving a tetrathiol and a trimethacrylate, resulting in expeditious polymerization within a brief time frame.

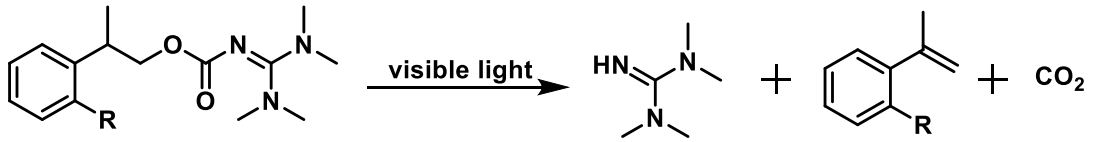

Scheme 1.3 Photolysis of NPPOC-TMG.

Source: Xi, Weixian, et al. "Spatial and Temporal Control of Thiol-Michael Addition via Photocaged Superbase in Photopatterning and Two-stage Polymer Networks Formation." *Macromolecules* 47.18 (**2014**): 6159-6165.

The expeditious kinetics observed in this process facilitated a further demonstration of precise spatial control via photopatterning. This control was instrumental, particularly in scenarios where rapid network formation is imperative to curtail catalyst diffusion and achieve high-resolution patterning. The attainment of spatial control in this context would have been rendered unfeasible in the presence of primary or secondary amines. This is substantiated by the observation that the thiol-Michael addition reaction exhibited considerable deceleration when conducted in the presence of compounds like hexylamine or diethylamine.[21]

In 2018, Bowman and his colleagues further optimized the structure of NPPOC-TMG.[22] They enhanced the performance by modifying the structure of the (3,4-methylenedioxy-6-nitrophenyl)-propyloxycarbonyl (MNPPOC) protected base. This modification facilitated photocleavage kinetics and led to a red-shifted absorption. This allows for low-energy, visible light irradiation to initiate thiol-Michael addition polymerizations with limited visible light exposure, reducing photochemical side reactions and avoiding damage to UV sensitive cells or tissues in biomedical applications. The investigation proposes that o-nitrobenzyl-based PBGs hold promise for applications in biocompatible and UV-sensitive materials. Additionally, they could find utility in the synthesis of gene assembly, nucleopeptide/peptide microarrays. The

researchers also discussed the importance of minimizing photo released radical side products or intermediates during the photolysis of PBGs to avoid radical-mediated homopolymerization and maintain the orthogonality of the thiol-Michael system.

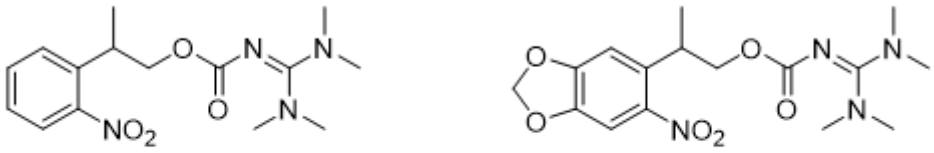

NPPOC-TMG MNPPOC-TMG

Figure 1.3 o-Nitrobenzyl-based photobase generators.

Source: Zhang, Xinpeng, et al. "o-Nitrobenzyl-based Photobase Generators: Efficient Photoinitiators for Visible-light Induced Thiol-michael Addition Photopolymerization." *ACS Macro Letters* 7.7 (**2018**): 852-857.

To enable PBGs to absorb within the visible-light range, Xinpeng Zhang et al. developed a new strategy for efficient network formation in thiol-Michael polymerizations using a coumarin-based photobase generator.[23] The photobase generator is devised to shield a potent base, TMG, utilizing a visible-light-responsive group, specifically a coumarin derivative. Under visible-light irradiation, the TMG coupled with the coumarin derivative demonstrates exceptional catalytic activity in initiating the thiol-Michael reaction, including thiol-Michael addition-based polymerization. This leads to a stoichiometric reaction involving both thiol and vinyl functional groups. This pioneering approach exhibits promise for its application in additional visible-light-induced, base-catalyzed thiol-click processes, such as reactions involving thiol-isocyanate and thiol-epoxy network formation. They also explain the advantages of using the thiol-Michael addition "click" reaction in materials science. This includes the easy creation of strong,

interconnected polymeric materials with high success rates. The reaction happens quickly, and it can be carried out under mild conditions.

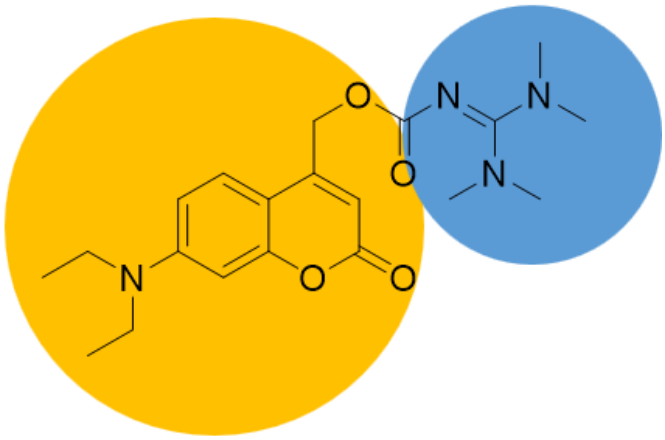

Figure 1.4 Coumarin-based photobase generators.

Source: Zhang, Xinpeng, et al. "Visible-light-initiated Thiol-Michael Addition Polymerizations with Coumarin-based Photobase Generators: Another Photoclick Reaction Strategy." *ACS macro letters* 5.2 (**2016**): 229-233.

1.1.2.3 *O*-Acyloximes

O-Acyloximes constitute a subset of PBGs designed to produce organic bases upon exposure to light. This class of PBGs stands out as a promising candidate, characterized by its notable photosensitivity, robust thermal stability, and low toxicity profile. *O*-Acyloximes have found utility across a diverse spectrum of applications within the realms of polymer science and technology, encompassing photo-crosslinking, photo-patterning, and photo-cleavage.

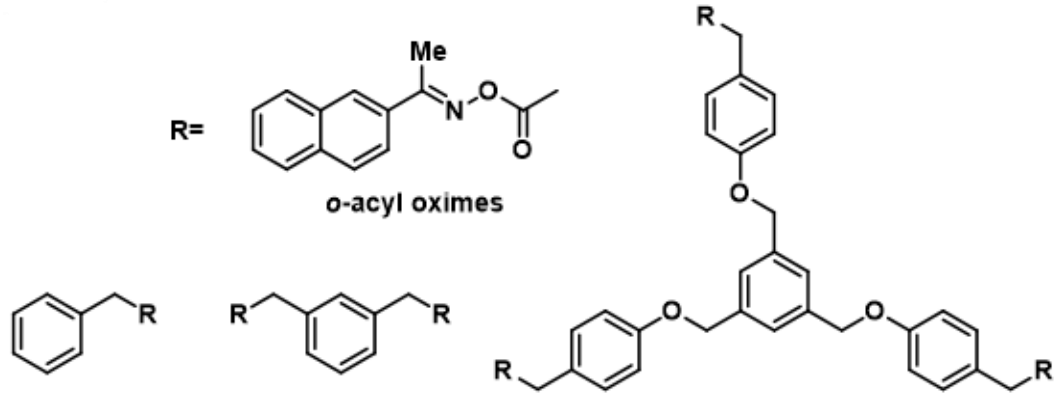

Figure 1.5 Multifunctional *O*-acyloximes.

Source: Suyama, Kanji, and Masamitsu Shirai. "Photobase Generators: Recent Progress and Application Trend in Polymer Systems." *Progress in Polymer Science* 34.2 (**2009**): 194-209.

A notable advantage inherent to *O*-acyloximes is their ability to effectuate the generation of organic bases under mild reaction conditions, obviating the necessity for elevated temperatures or strong acidic environments. Their relative ease of synthesis and potential for customization to suit specific applications through structural modifications of the acyloxime group further enhances their appeal.[24]

However, it is pertinent to acknowledge a few limitations associated with *O*-acyloximes. Their susceptibility to moisture-induced degradation, leading to premature decomposition, poses a notable challenge. Additionally, their lower quantum yields in comparison to alternative PBG varieties can curtail their overall efficiency in specific applications.[25]

The photolysis mechanism underlying *O*-acyloximes-based PBGs is predicated upon the absorption of incident light by the PBG molecule, thereby engendering the transient formation of an excited state. The ensuing fate of this excited state is contingent upon the specific structural attributes of the PBG molecule and the prevailing reaction conditions (Figure 1.6).[9] In the context of *O*-acyloximes, the excited state undergoes a

homolytic cleavage reaction, culminating in the generation of an acyloxime radical and a carbonyl compound. The acyloxime radical, in turn, engages in a subsequent reaction with a proton source, such as water or a protic solvent, ultimately yielding an organic base.[8]

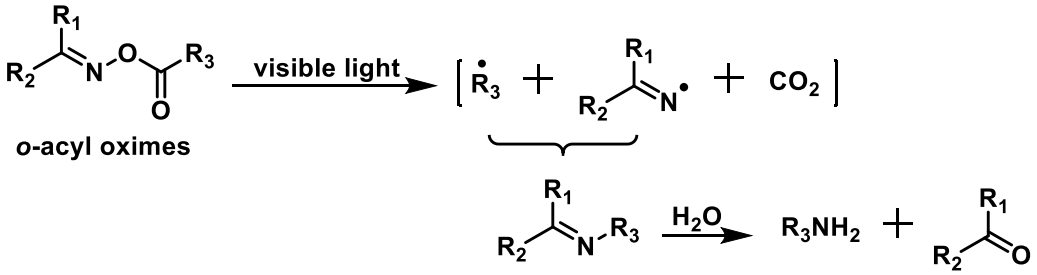

Figure 1.6 Photochemical reactions of *O*-acyloximes.

Source: Suyama, Kanji, and Masamitsu Shirai. "Photobase Generators: Recent Progress and Application Trend in Polymer Systems." *Progress in Polymer Science* 34.2 (**2009**): 194-209.

1.2 BODIPY

BODIPY is a fluorescent dye widely applied in science, medicine, and biotechnology due to its high fluorescence quantum yield and chemical stability, making it valuable for various applications, including molecular imaging and biosensing.[26] BODIPY dyes are characterized by their high molar extinction coefficients, high fluorescence quantum yields, and excellent photostability. They are also highly tunable, with a wide range of absorption and emission wavelengths, and can be easily functionalized with various reactive groups for further derivatization. BODIPY dyes play a multifaceted role in medical diagnostics, antimicrobial applications, biomolecule labeling, and the functionalization of drug micro- and nanocarriers. Additionally, they serve as valuable fluorescent probes for bioimaging, allowing for the precise targeting of various biomolecules both within and outside cellular environments. In the field of material chemistry, BODIPY dyes have been instrumental in crafting novel light-responsive

materials, ranging from energy cassettes and light-harvesting substances to laser dyes and polymers. Their versatile applications extend to areas like photovoltaics, artificial models of photosynthesis, BODIPY–porphyrin conjugates, and dye-sensitized solar cells.[27,28] Furthermore, BODIPY derivatives linked to metal centers serve as multifaceted tools in life sciences, demonstrating their efficacy in photodynamic therapy (PDT).[29]

1.2.1 Core Structure

The core structure of BODIPY (boron dipyrromethene) is a boron-dipyrrin complex, which consists of a central boron atom, two pyrrole rings, and two meso carbon atoms. The boron atom in BODIPY carries a formal negative charge, while the positive charge is distributed across the ring structure. The central 8-position is termed the meso-position, a concept derived from porphyrin chemistry. Importantly, the BODIPY core structure remains electrically neutral, emphasizing the molecule's relatively nonpolar nature.[26]

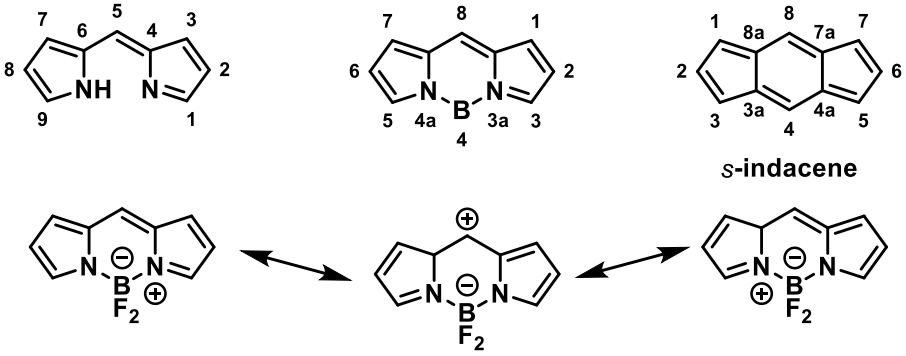

Scheme 1.4 Core structure of BODIPY.

Source: Boens, Noel, et al. "Synthesis of BODIPY Dyes Through Postfunctionalization of the Boron Dipyrromethene Core." *Coordination Chemistry Reviews* 399 (**2019**): 213024.

Additionally, one can alter the photophysical properties by attaching functional groups at appropriate positions in the BODIPY structure. For positions 2, 6, and 8, extending the π-conjugated system by connecting benzene rings did not result in a

significant increase in excitation/emission wavelengths. In contrast, for positions 3, 5, and 7, a direct attachment of benzene rings through a C=C bond led to a significant increase in excitation/emission wavelengths, resulting in a redshift. When designing novel BODIPY derivatives with good photostability, it is essential to study the correlation between photophysical properties and molecular structure. Therefore, this family of fluorescent dyes plays a crucial role in long-wavelength emission markers used in biological applications.

1.2.2 Modification of BODIPY Structure

BODIPY, a fluorescent dye molecule, has garnered widespread recognition owing to its commendable optical and structural stability.[27, 28] Nevertheless, the native form of BODIPY is associated with certain constraints that curtail its utility in specific domains.[29] For instance, the emission wavelength of BODIPY falls below the 600 nm threshold, limiting its suitability for imaging applications that necessitate longer wavelengths.[30-32] Moreover, BODIPY is intrinsically hydrophobic, rendering its utilization in aqueous environments challenging and imposing constraints on its biocompatibility.[33]

To ameliorate these inherent limitations, researchers have diligently devised diverse strategies for the structural modification of BODIPY. Such structural refinements can enhance various properties of BODIPY, encompassing its water solubility, emission wavelength, and biocompatibility, thus rendering it more adaptable across a spectrum of applications (Fig 1.7).[34] For example, introducing structural modifications at specific positions of the BODIPY molecule, such as aryl, ethynyl, and styryl substitutions, can lead to a significant redshift in both the UV absorption maximum and fluorescence

emission.[35] The introduction of charged or neutral groups can similarly enhance the water solubility of BODIPY, facilitating its deployment in aqueous environments.[36, 37]

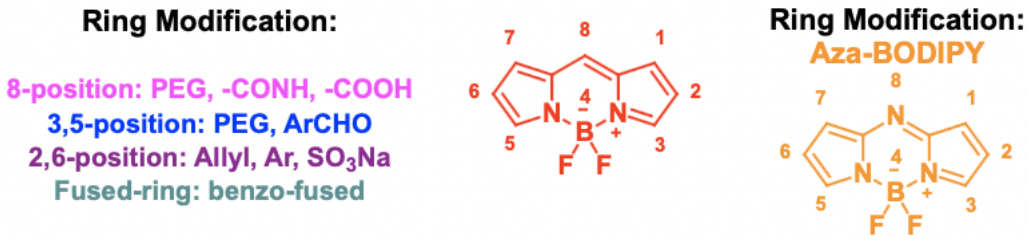

Figure 1.7 The modification of BODIPY.

Source: Lu, Hua, et al. "Structural Modification Strategies for the Rational Design of Red/NIR Region BODIPYs." *Chemical Society Reviews* 43.13 (**2014**): 4778-4823.

1.2.2.1 8/meso-Substituted BODIPY

8/meso-substituted BODIPY entails a structural modification of the BODIPY molecule, characterized by the introduction of a substituent at the 8/meso-position. This particular adaptation has minimal influence on the absorption and emission wavelengths of BODIPY. Consequently, researchers predominantly concentrate their efforts on enhancing the water solubility of the molecule by introducing neutral or charged groups.[38, 39]

Numerous strategies have been devised to enhance the water solubility of 8/meso-substituted BODIPY. One viable approach involves the incorporation of a water-soluble polymer chain, such as poly(ethylene glycol), at the 8/meso-position. Alternatively, the introduction of an acid-functional substituent, such as carboxylic acid, emerges as another strategy, known for its capacity to augment the fluorescence of BODIPY in aqueous environments.[40] This enhancement not only empowers effective labeling through

the plasma membrane but also bolsters the overall biocompatibility of 8/meso-substituted BODIPY.

In essence, the structural modification of 8/meso-substituted BODIPY represents an avenue conducive to heightening the water solubility of BODIPY through the introduction of neutral or charged groups.[39] This adaptation broadens the spectrum of applications by enhancing the versatility of BODIPY in aqueous environments, consequently augmenting its utility in diverse domains.[41]

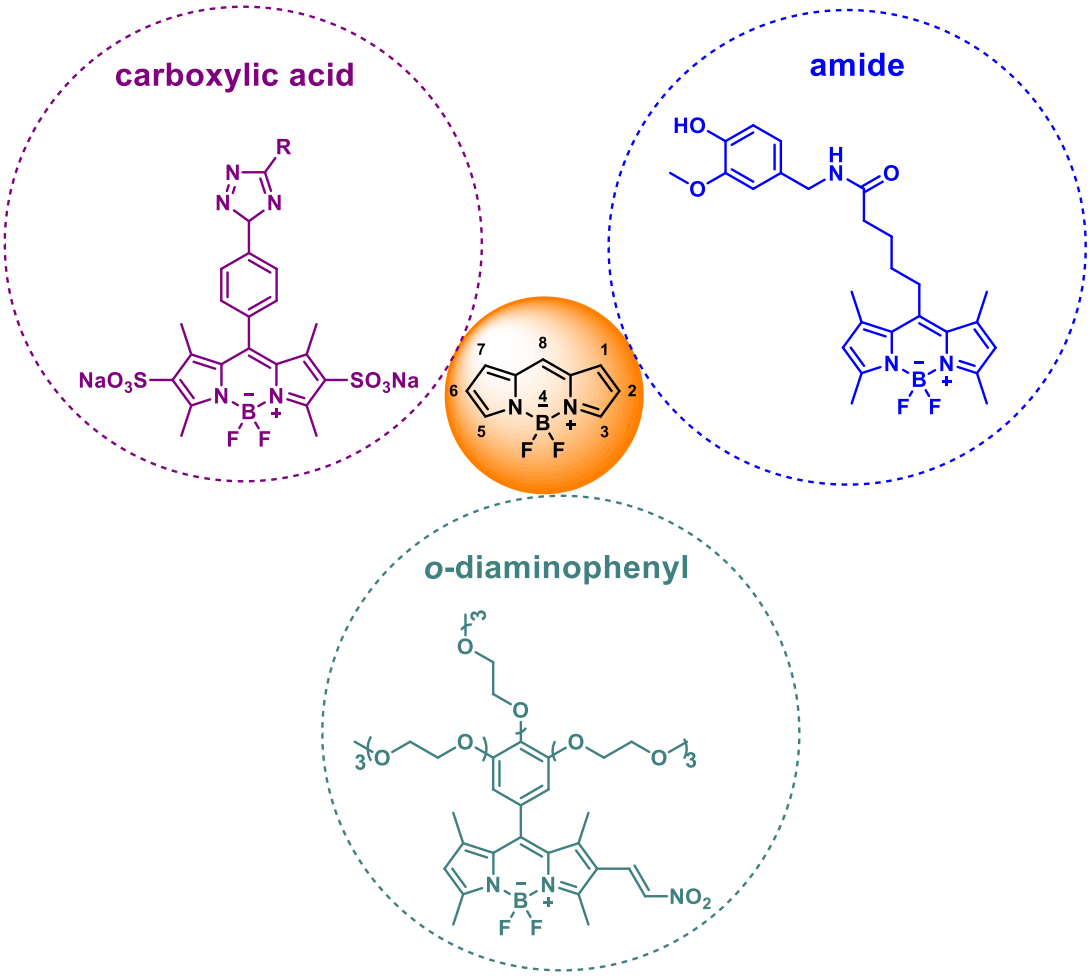

Figure 1.8 Selected structurally modified 8/meso-substituted BODIPY.

Source: Lu, Hua, et al. "Structural Modification Strategies for the Rational Design of Red/NIR Region BODIPYs." *Chemical Society Reviews* 43.13 (**2014**): 4778-4823.

1.2.2.2 2/6-Substituted BODIPY

2/6-Substituted BODIPY denotes a structural alteration of the BODIPY molecule, characterized by the introduction of a substituent at the 2/6-position. This specific adaptation serves to ameliorate the water solubility of BODIPY, thereby broadening its utility in aqueous environments and augmenting its versatility across a myriad of applications.[42]

One prevalent strategy for the modification of 2/6-substituted BODIPY entails the introduction of a hydrophilic group, exemplified by sulfonate or carboxylate functionalities, at the 2/6-position.[43] This approach effectively amplifies the water solubility of the molecule and elevates its fluorescence emission through the establishment of a p-p conjugated system.

Another modification avenue for 2/6-substituted BODIPY revolves around the incorporation of a near-infrared (NIR) fluorophore at the 2/6-position. This modification effectuates a shift in the emission wavelength of BODIPY into the NIR region, which holds considerable relevance for imaging applications reliant on longer wavelengths.[44]

In summation, the structural modification known as 2/6-substituted BODIPY stands as an instrumental means to enhance the water solubility and fluorescence properties of BODIPY. This adaptation, by enhancing the biocompatibility of BODIPY and enabling its efficacious deployment in aqueous environments, engenders a heightened degree of versatility across diverse applications.

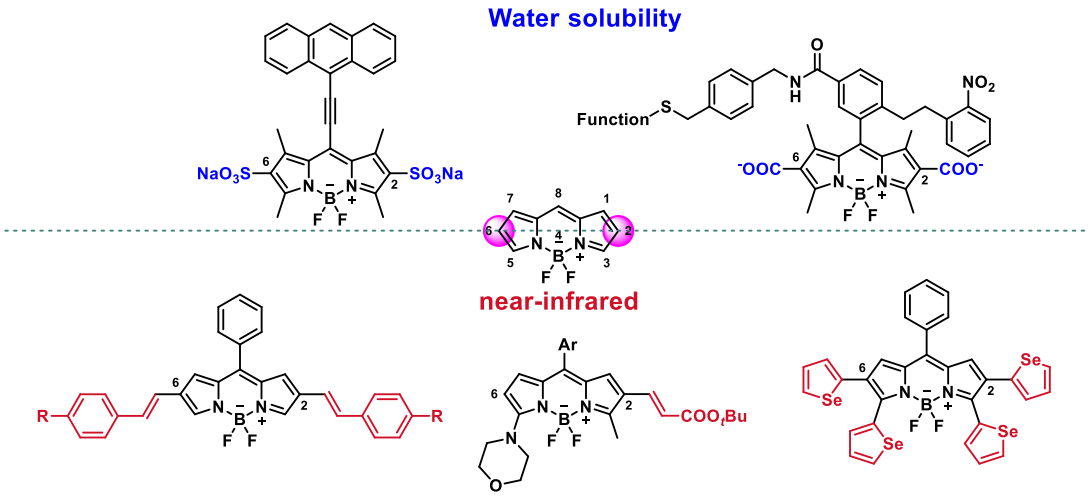

Figure 1.9 Selected structurally modified 2/6-substituted BODIPY.

Source: Lu, Hua, et al. "Structural Modification Strategies for the Rational Design of Red/NIR Region BODIPYs." *Chemical Society Reviews* 43.13 (**2014**): 4778-4823.

1.2.2.3 3/5-Substituted BODIPY

Concerning 3/5-Substituted BODIPY, this pertains to a structural alteration of the BODIPY molecule, entailing the introduction of a substituent at the 3/5-position. This specific modification finds its primary utility in effecting a wavelength shift in the emission spectrum of fluorescent dyes, facilitating emission in the NIR region.[45]

Through the strategic introduction of a substituent at the 3/5-position, it becomes feasible to shift the emission wavelength of BODIPY into the near-infrared range. This adjustment holds particular significance in imaging applications that necessitate longer wavelengths. Moreover, this structural adaptation concurrently contributes to the enhancement of water solubility and augments the biocompatibility of BODIPY, thereby rendering it a more versatile entity for a diverse array of applications. 3/5-substituted BODIPY stands as a pivotal structural modification capable of enhancing the emission

wavelength and water solubility of BODIPY.[46] This adaptation not only elevates the biocompatibility of BODIPY but also renders it amenable to utilization within aqueous environments, thus endowing it with greater versatility across an array of applications.

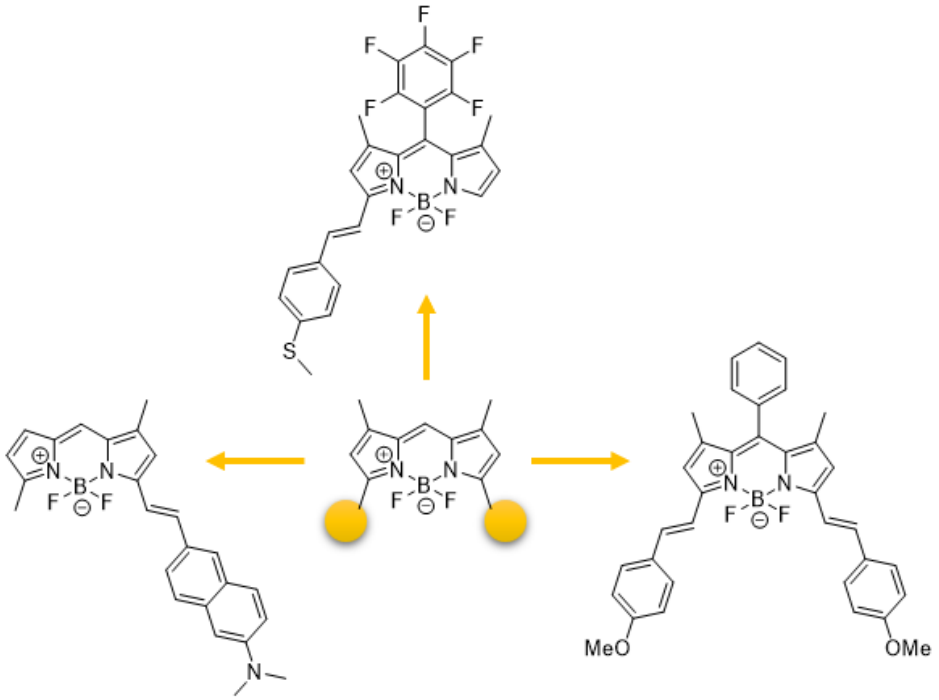

Figure 1.10 Selected structurally modified 3/5-substituted BODIPY.

Source: Lu, Hua, et al. "Structural Modification Strategies for the Rational Design of Red/NIR Region BODIPYs." *Chemical Society Reviews* 43.13 (**2014**): 4778-4823.

1.2.3 BODIPY based photoremovable protecting groups (PPGs)

Photoremovable protecting groups (PPGs) are temporary functional group protections that can be removed by light irradiation. PPGs play a crucial role in shielding specific functional groups from undesired chemical alterations, offering a high level of precision in their removal with spatial and temporal control. In the realm of biological research, PPGs are particularly valuable, allowing for the targeted release of biologically active compounds with exceptional precision. Because of BODIPY dyes offer several notable advantages. For examples, firstly, they exhibit high absorption coefficients, enabling

efficient light absorption. Furthermore, BODIPY dyes possess high quantum yields of fluorescence, facilitating the straightforward detection and monitoring of the photocage. In addition, they are known for their stability and can be readily synthesized with a variety of functional groups, rendering them versatile for a wide range of applications. Therefore, BODIPY is highly suitable for use as a photoprotective group. In 2017, Winter and colleagues utilized BODIPY photocages to explore the mechanism of photorelease of a leaving group (LG) and to determine the ideal structural features for achieving high quantum yields of photorelease.[47]

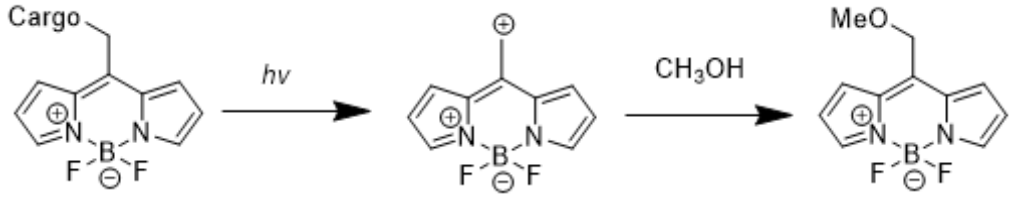

Scheme 1.5 Photorelease of a leaving group (LG) from the BODIPY cage.

Source: Slanina, Tomas, et al. "In Search of The Perfect Photocage: Structure–reactivity Relationships in Meso-methyl BODIPY Photoremovable Protecting Groups." *Journal of the American Chemical Society* 139.42 (**2017**): 15168-15175.

The process of photoreleasing a LG from a BODIPY photocage involves the absorption of light by the photocage, which promotes the molecule to an excited state. In the realm of BODIPY photocages, the excited state can take the form of either a singlet or a triplet state. Subsequently, intersystem crossing (ISC) transpires, giving rise to the triplet state. This triplet state plays a crucial role in liberating the LG and engendering the carbocation. The efficiency of photorelease is notably influenced by substituent effects, with superior LGs being released much more efficiently than less favorable ones. Derivatives with higher intersystem crossing quantum yields show improved quantum

yields of photorelease, and the presence of core heavy atoms can facilitate this enhancement. The optimal structural feature for achieving high quantum yields of photorelease with BODIPY photocages include the use of better LGs and core heavy atoms (Scheme 1.5).

Moreover, Winter and his team undertook modifications to the BODIPY core structure, leading to the development of a family of BODIPY-derived photocages.[48] These photocages are distinguished by their ability to be cleaved by individual photons of visible/near-infrared light. Notably, they exhibit tunable absorption profiles across the visible/near-infrared spectrum and have the capacity to release chemical cargo upon irradiation. The discussion in the study centers on the advantages inherent to the utilization of these photocages in comparison to other commonly employed photocages, along with an examination of the influence of appended styryl groups on their absorption properties.

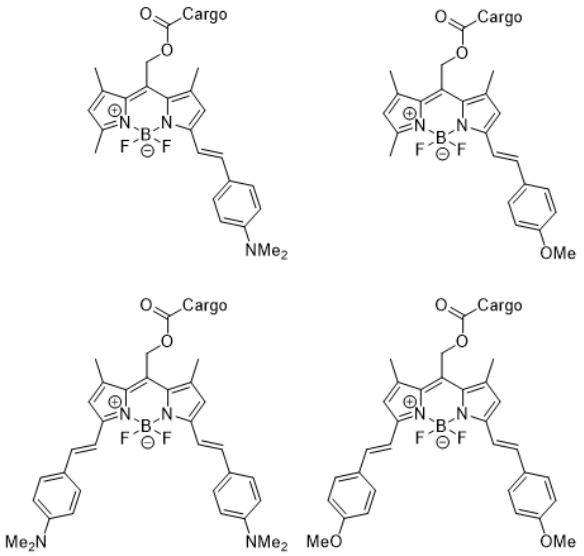

Figure 1.11 BODIPY based photocages.

Source: Peterson, Julie A., et al. "Family of BODIPY Photocages Cleaved by Single Photons of Visible/near-infrared Light." *Journal of the American Chemical Society* 140.23 (**2018**): 7343-7346.

1.2.4 BODIPY Based PAGs

PAGs represent a class of compounds designed to induce the generation of acid upon exposure to light, thereby serving as initiators for polymerization reactions.[1] The development of PAGs has been driven by the desire to facilitate polymerization reactions under mild conditions, including ambient temperature, and with the utilization of low-energy visible light, which minimizes potential damage to cells and tissues compared to high-energy UV light.[49]

PAGs offer several advantages over traditional thermal polymerization methodologies. Notably, they enable polymerization reactions to proceed in the presence of oxygen, a feat unattainable with thermal polymerization. Additionally, PAGs afford precise spatial control, empowering the meticulous regulation of resulting structure dimensions and configurations.[2]

Nonetheless, PAGs are not without their limitations. Their sensitivity to water presence can potentially disrupt polymerization reactions, presenting a challenge. Furthermore, the synthesis of PAGs can be intricate, and their quantum yields may be modest, thereby impacting their efficiency in initiating polymerization reactions.

Our research group has introduced an innovative strategy aimed at mitigating chemoresistance in cancer treatment.[50] This strategy leverages a triarylsulfonium photoacid generator (BD-PAG) featuring a BODIPY chromophore, with the primary objective of modulating mitochondrial pH and inducing mitochondrial membrane depolarization. To substantiate the efficacy of this approach, we conducted comprehensive cell viability assays and live cell imaging studies. The results of our

research hold promise for the advancement of more efficacious cancer treatment modalities in the future.

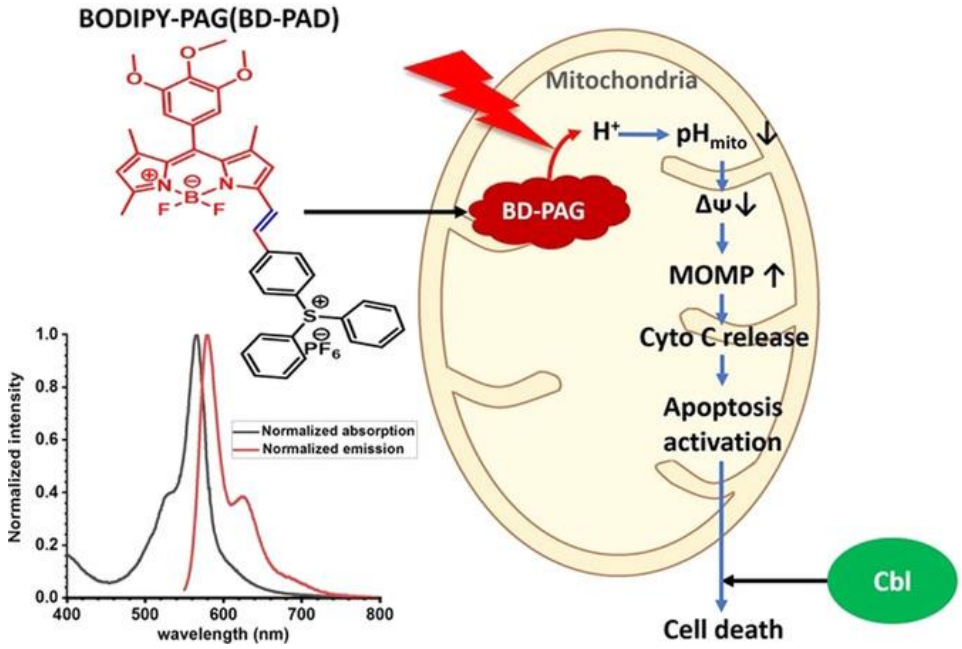

Figure 1.12 Molecular structure of BD-PAG and photophysical properties (left). Illustration of photo-induced pH drop in mitochondria and potential pathway leading to cell death (right).

Source: Zhao, Tinghan, et al. "Regulating Mitochondrial pH with Light and Implications for Chemoresistance." *Chemistry–A European Journal* 27.1 (**2021**): 247-251.

CHAPTER 2

DESIGN, SYNTHESIS, PHOTOCHEMICAL AND PHPTPPHYSICAL PROPERTIES OF NOVEL BODIPY-BASED PHOTOBASE GENERATOR

2.1 Introduction

PBGs are a series of photosensitive compounds, which absorb the incident light, then release the basic species that can deprotonate a thiol and trigger the consequent reactions. The ideal characteristics of PBGs include: (1) strong absorption in the visible region; (2) high quantum yield to generate a base; and (3) chemical stability in the dark before photolysis.[51] Compared with PAGs, PBGs are much less developed and the common structures are based on quaternary ammonium salts (QAs),[16, 52, 53] tetraphenylborate salts (TBD),[54] and carbamates.[12, 20, 22] Most of these common PBGs are only able to liberate relatively weak primary and secondary amines that are generally inefficient in the activation of anionic polymerizations.[9] For example, Sarker's group utilized QAs to generate tertiary amines upon UV light irradion.[16, 55] In addition, due to the weak bases released, the system still needs a second thermal treatment to form the polymeric network, which may affect the final polymer structure.

Another challenge that remains in the field is the design and synthesis of visible light-sensitive PBGs.[9] Most typical PBGs absorb strongly only under high-energy UV and/or blue light, which presents a series of fatal disadvantages including: (1) causing irreversible damage to cells and tissues limiting their applications in biological environments, and (2) shallow light penetration depth.[56] Recently, there has been increasing interest in the development of photoinitiators that work under visible light

excitation and the popularity of energy efficient LED light paved the way for low energy consumption and low heat generation. For example, Hillet et al. reported a photopolymerziation approach for facial soft tissue restoration in small animals,[57] and Pioletti et al. studied the photopolymerization process of a hydrogel behind a soft tissue.[58] For these reasons, new classes of photobase systems were reported by Bowman et al., who utilized 2-(2-nitrophenyl)-propyloxycarbonyl (NPPOC), (3,4-methylenedioxy-6-nitrophenyl)-propyloxycarbonyl (MNPPOC), and coumarin as PPGs to photocage the strong base 1,1,3,3-tetramethylguanidine (TMG, pKa =13.6).[22, 23] In another work, Truong et al. reported a thioxanthone based structure for 1,8-diazabicyclo[5.4.0]undec-7-ene (DBU) release under blue light and used this for polymer crosslinking.[59]

Although, these reports extended the excitation wavelengths, the compounds that based on coumarin and thioxanthone are still absorbed primarily in the blue region - around 400 nm. Therefore, there is an urgent need for novel PBGs that can generate strong bases with absorption at wavelengths further in the visible range for deep tissue regeneration and engineering.

2.2 Design of Photobase Generators

Compared with chromophores used in the reported PBGs (such as nitrobenzene or coumarin), BODIPY derivatives have several advantageous properties, such as stability in various media, sharp absorbance spectra, high molar absorptivity, low toxicity, high quantum yields, and color shifts by simple structure modification.[60] For these reasons, BODIPY derivatives have experienced wide use as fluorescent probes,[61-65] photocatalysts,[66, 67] photosensitizers in photodynamic therapy,[68, 69] and cell visualization agents[30, 70] in biolabeling,[71, 72] and bioimaging.[73, 74] Recently, Winter and co-workers

reported a family of BODIPY-derived photocages that can release carboxylic acid under targeted light irradiation. The BODIPY core in 3, 5 meso-position was modified with different substituents to adjust conjugation and hydrophilic properties, which greatly changed the λmax and deprotection efficiency of the target molecule.[48, 75] Moreover, Sitkowska and co-workers reported a series of BODIPY-based photo-protecting groups for primary and secondary amines.[60] Inspired by these promising findings, we designed novel BODIPY-based PBGs that utilized BODIPY core as the photocage and TMG as the leaving group, while retaining the excellent photophysical properties of BODIPYs. The strong basicity of TMG is used to efficiently trigger the thiol-ene Michael addition reactions in a light guided manner. Moreover, to improve the photo-uncaging efficiency, heavy atom iodine was introduced to the BODIPY structure (BD-I-TMG).[76] Compared with the derivative without iodine (BD-TMG), BD-I-TMG exhibit increased intersystem crossing (ISC) and, consequently, improved the release of TMG from the long-lived triplet excited state.[77]

To investigate the photoactivating ability of BD-TMG and BD-I-TMG, we employed various thiols and vinyl-containing compounds as model reactions. The reaction kinetics and yields were monitored by ^{1}H NMR. Furthermore, butyl 3-mercaptopropionate and ethyl acrylate were implemented to investigate the photoactivator's efficiency by monitoring the conversion of thiol function groups through FT-IR spectral analyses. The synthetic route for the BD-TMG and BD-I-TMG is presented in Scheme 1. The BD-OH and BD-I-OH were synthesized through a modified version of the reported methods.[60, 77] All reactions were conducted under mild conditions.

2.3 Experimental Section

2.3.1 Materials and Instruments

2,4-Dimethylpyrrole, N,N-diisopropylethylamine, pentaerythritol tetrakis(mercaptoacetate) were purchased from TCI America. Acetoxyacetyl chloride, and boron trifluoride diethyl etherate were purchased from Thermo Scientific. Triphosgene, N-iodosuccinimide, 1,1,3,3-tetramethylguanidine, butyl thioglycolate, divinyl sulfone, ethyl acrylate, butyl 3-mercaptopropionate and trimethylolpropane trimethacrylate were purchased from Sigma-Aldrich. All chemicals were used as received and without further purification. ^{1}H NMR (500 MHz) and ^{13}C NMR (126 MHz) spectra were recorded on a 500 MHz Bruker ultrashield spectrometer. Mass spectra were recorded on a high-resolution Orbitrap Q Exactive mass spectrometer (Thermo Scientific, San Jose, CA). UV-vis absorption spectra were obtained on a Tecan Infinite M200 PRO plate reader spectrometer in 1 cm path length quartz cuvettes. Fluorescence spectra were recorded on an Edinburgh FLS980 fluorescence spectrometer. FT-IR spectra were recorded using a SHIMADZU IRAffinity-1 instrument. The letter mold used for photopolymerization is made of silicone and the size of each letter is about 0.6 × 0.3 × 0.3 inches.

2.3.2 Synthesis Route

The synthesis began with the preparation of the BODIPY core with an ester at the meso-position (BODIPY-OAc) by reacting 2,4-dimethyl pyrrole with acetoxyacetyl chloride. Then the ester was hydrolyzed to liberate the hydroxyl group for postmodification in the

following steps. The hydrolysis procedure was modified based on a reported protocol.[60] To introduce a heavy atom to the BODIPY core, NIS was used in THF under the dark as the iodination agent to add an iodine atom to the BODIPY core at 2-positon (Scheme 2.1). When compared to other heavy atoms, such as bromine and chlorine, iodine can greatly enhance the spin-orbit coupling that results in an efficient intersystem crossing rate.[78, 79] At this stage, we obtained two photocages BD-OH and BD-I-OH that we will further conjugate with TMG to realize photolysis and photobase release.

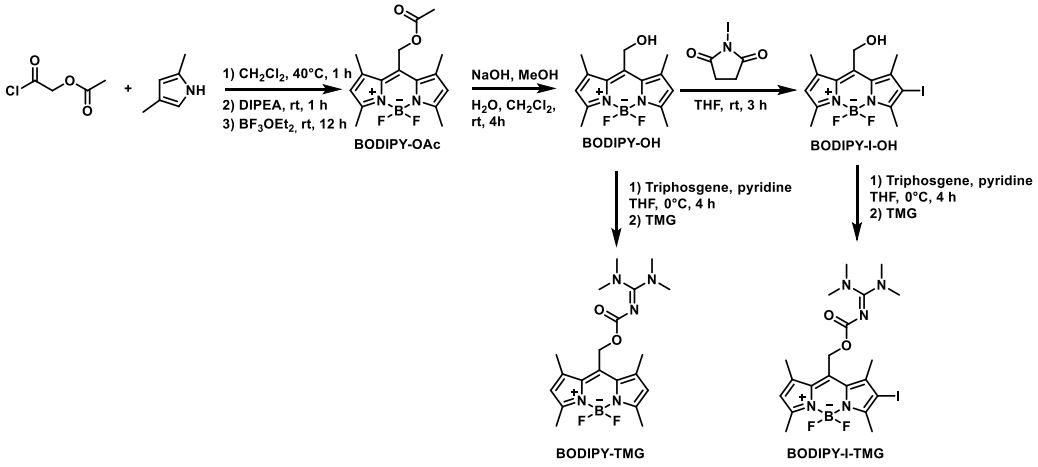

Scheme 2.1 Synthesis of BODIPY-TMG and BODIPY-I-TMG

In the last step, we attempted to use the transesterification mechanism to convert the alcohol of BD-OH and BD-I-OH into ester through carbonyldiimidazole (CDI) under the catalysis of the DMAP.[30] However, we rarely obtained the final product via this synthetic route. We then tried to convert the alcohol of BD-OH and BD-I-OH into chloroformate with triphosgene, and then used it to react with the amino group of TMG to give the final products. Here, we first reported the method to conjugate TMG with BODIPY esters by amidation. This approach provides a high yield and high reaction rate, such that BD-OH and BD-I-OH were obtained separately as dark red and dark purple

solids with reasonable yields of 28% and 31%, respectively. It is worth noting that the preparation of the derivative with di-iodine failed using a similar synthesis approach.

Synthesis and characterization of BODIPY-OAc: 2,4-dimethyl pyrrole (3.00 g, 31.53 mmol) was dissolved in dry CH2Cl2 (40 mL) under nitrogen. Acetoxyacetyl chloride (2.58 g, 18.92 mmol) was added into the solution dropwise, and the mixture was stirred at room temperature for 30 min. The solution was then refluxed at 40 ˚C for 2 h. The solution was cooled to room temperature and then N,N-diisopropylethylamine (DIPEA, 8.15 g, 63.06 mmol) was added dropwise. After stirring for 1 h, BF_3•OEt_2 (8.95 g, 63.06 mmol) was added dropwise, and the mixture was stirred for another 1 h. After this time, the solvents were partially evaporated and the residue was extracted with CH_2Cl_2 (3 × 20 mL), then the mixture was washed with brine (2 × 20 mL) and dried over anhydrous Na_2SO4. The mixture was then evaporated to remove the solvent, and the residue was purified on a silica column using CH2Cl2 and hexanes (1:2, v/v), affording BODIPY-OAc as a dark red solid, as reported in literature80 (3.120g, 51.5% yield). 1H NMR (500 MHz, CDCl3) δ (ppm): 6.08 (s, 2H), 5.30 (s, 2H), 2.53 (s, 6H), 2.36 (s, 6H), 2.13 (s, 3H).

Synthesis and characterization of BODIPY-OH: The synthesis was slightly modified based on a reported method.[81] A mixture of NaOH water solution (13 mL, 0.10 M) and methanol (40 mL) was stirred for 10 min and then added to a solution BODIPY-OAc (1.00 g, 3.12 mmol) in CH_2Cl_2 (20 mL). The reaction mixture was then stirred overnight in the dark at room temperature. Next, the solvents were partially evaporated, and the residue was extracted with CH_2Cl_2 (3 × 20 mL). The combined organic layers were then washed with 1 M HCl (2 × 20 mL) and brine (1 × 20 mL), and dried over

anhydrous Na_2SO_4. BODIPY-OH was purified on a silica column using ethyl acetate, CH_2Cl_2, and hexanes (1:18:2, v/v/v), yielding red precipitate (0.55 g, 63.1% yield). ^1H NMR (500 MHz, CDCl3) δ (ppm): 6.24 (s, 2H), 5.54 (s, 1H), 4.73 (s, 2H), 2.51 (s, 6H), 2.42 (s, 6H).

Synthesis and characterization of BODIPY-I-OH: similar to a reported method,82 BODIPY-OH (60 mg, 0.22 mmol) was dissolved in dry tetrahydrofuran (2.5 mL) in dark conditions under nitrogen. A solution of N-iodosuccinimide (106 mg, 0.475 mmol) in dry THF (3 mL) was added dropwise into the preceding solution. The mixture was stirred at room temperature for 4 h and evaporated to remove the solvent. The residue was extracted with CH_2Cl_2 (3 × 20 mL), and then the organic layer was washed with brine (2 × 10 mL) and dried over anhydrous Na_2SO_4. BODIPY-I-OH was purified on a silica column using ethyl acetate and CH_2Cl_2 (1:20, v/v), providing a purple solid (53.6 mg, 60% yield). ^1H NMR (500 MHz, $CDCl_3$) δ (ppm): 6.17 (s, 1H), 5.33 (s, 1H), 4.95 (s, 2H), 2.64 (s, 3H), 2.57 (s, 3H), 2.55 (d, 6H).

Synthesis and characterization of BD-TMG: BODIPY-OH (50 mg, 0.18 mmol) and triphosgene (37.3 mg, 0.13 mmol) were added to a cold anhydrous CH_2Cl_2 solution (40 mL, 0 ˚C). A solution of pyridine (35.6 mg, 0.45 mmol) and anhydrous CH_2Cl_2 (2 mL) was stirred for 2 min and then added into the above solution dropwise. The mixture was stirred for 30 min at 0 ˚C. Next, the solution of TMG (49.7 mg, 0.43 mmol) and anhydrous CH_2Cl_2 was stirred for 2 min and then added to the above mixture. The reaction mixture was stirred overnight at room temperature. After this, the solvent was carefully evaporated, and the residue was washed with brine (3 × 30 mL). The organic layer was dried over anhydrous Na_2SO_4 and purified by silica gel chromatography with

CH_3OH and CH_2Cl_2 (1:20, v/v), affording BODIPY-TMG as a dark purple solid. (21 mg, 28% yield). ^1H NMR (500 MHz, $CDCl_3$) δ (ppm): 6.05 (s, 2H), 5.25 (s, 2H), 2.88 (s, 12 H), 2.52 (s, 6H), 2.44 (s. 6H). ^{13}C NMR (126 MHz, $CDCl_3$) δ (ppm): 166.65, 159.75, 155.74, 155.59, 141.75, 135.46, 121.84, 121.77, 58.13, 39.89, 15.62, 14.64. HRMS (ESI+) calculated for $[M+H]^+$ ($C_{20}H_{29}BF_2N_5O_2$) 420.23769; Found 420.23828.

Synthesis and characterization of BD-I-TMG: BODIPY-I-OH (50 mg, 0.12 mmol) and triphosgene (36.7 mg, 0.12 mmol) were added to a cold anhydrous DCM solution (40 mL, 0 ˚C). The solution of pyridine (29.4 mg, 0.37 mmol) and anhydrous DCM (2 mL) was stirred for 2 min and then added into the above solution dropwise. The mixture was stirred for 30 min at 0 ˚C. Next, the solution of TMG (42.8 mg, 0.37 mmol) and anhydrous DCM was stirred for 2 min and then added to the above mixture. The reaction mixture was stirred overnight at room temperature. After this, the solvent was carefully evaporated, and the residue was washed with brine (3 × 30 mL). The organic layer was dried over anhydrous Na_2SO_4 and purified by silica gel chromatography with CH_3OH and CH_2Cl_2 (1:20, v/v). BODIPY-I-TMG as the final product (21 mg, 31% yield). ^1H NMR (500 MHz, $CDCl_3$) δ (ppm): 6.10 (s, 1H), 5.24 (s, 2H), 2.88 (s, 12H), 2.58 (s, 3H), 2.52 (s, 3H), 2.45 (d, 6H). ^{13}C NMR (126 MHz, $CDCl_3$) δ (ppm): 166.74, 159.62, 158.37, 154.64, 143.88, 141.56, 135.30, 133.62, 132.20, 123.08, 58.28, 39.94, 29.72, 17.71, 15.98. HRMS (ESI+) calculated for $[M+H]^+$ ($C_{20}H_{28}BF_2IN_5O_2$) 546.13433; Found 546.13460.

2.4 Photophysical and Photochemical Properties

The photophysical properties of BD-TMG and BD-I-TMG were then investigated by UV-vis absorption and steady-state fluorescence emission spectroscopy (as shown in Figure 2.1). The absorption spectra of BD-TMG and BD-I-TMG showed an intense peak centered at 520 nm and 535 nm, respectively, and the emission was located at 531 nm and 551 nm, respectively. Furthermore, the molar absorptivity values (ε) of BD-TMG and BD-I-TMG were 5.69×10^4 M^{-1} cm^{-1} and 3.13×10^4 M^{-1} cm^{-1}. Compared with BD-TMG, BD-I-TMG exhibited a red-shifted absorbance, emission, and molar absorptivity, which is similar to literature reports.[60, 77] The fluorescence quantum yields (Φ_f) were measured in dichloromethane, and calculated using Rhodamine 6G as the standard. The fluorescence quantum yield, Φ_f, values for BD-TMG and BD-I-TMG in CH_2Cl_2 were 0.84 and 0.09, respectively (Table 2.1). Moreover, the fluorescence lifetime (τ) of BD-I-TMG exhibited an obvious decrease compared with BD-TMG, consistent with a heavy atom effect from the iodination of the BODIPY core causing quenching of fluorescence by increasing the intersystem crossing (ISC) from the first excited singlet to the triplet state.

Table 2.1 Photophysical Properties of BD-TMG and BD-I-TMG

	λ_{max}^{abs} (nm)[a]	λ_{max}^{em} (nm)[b]	ε (10^4 M^{-1} cm^{-1})[c]	Φ_f[d]	τ (ns)[e]	Φ_{TMG}[f]	$\varepsilon\Phi_{TMG}$ (M^{-1} cm^{-1})
BD-TMG	520	531	5.69 ± 0.173	0.84	4.37	0.009	512.1
BD-I-TMG	535	551	3.13 ± 0.12	0.09	0.66	0.029	907.7

[a]Wavelength of maximum absorption. [b]Wavelength of maximum emission. [c]Extinction coefficient. [d]Fluorescence quantum yield (Error in measurement±1.2%). [e]Fluorescence lifetimes (Error in measurement ≤ 10 ps). [f]Photobase generation quantum yield (Error in measurement ±2.9%).

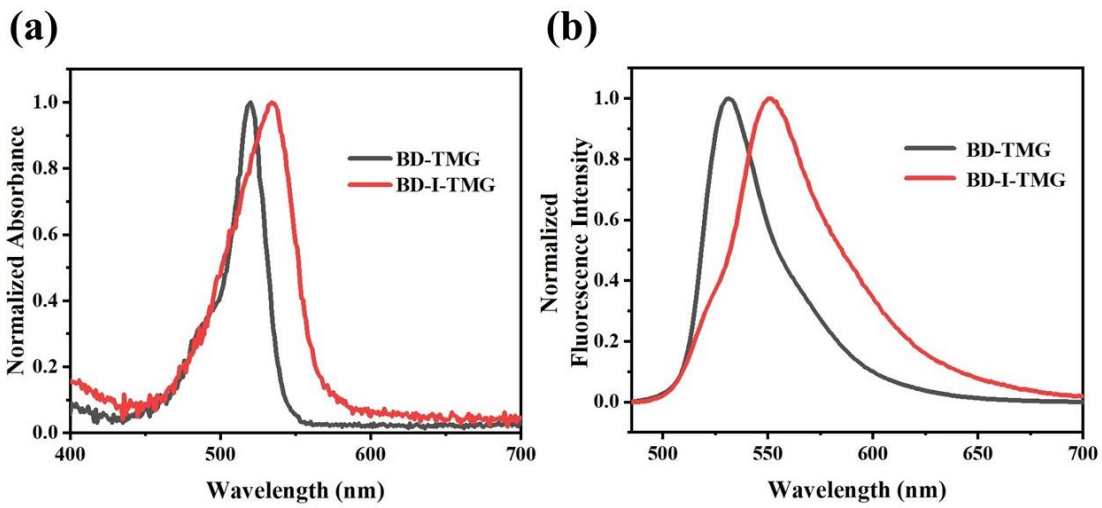

Figure 2.1 Normalized UV-vis absorption (a) and emission spectra (b, λ_{ex} = 480 nm for BD-TMG and 485 nm for BD-I-TMG) of BD-TMG and BD-I-TMG in CH_2Cl_2.

Before studying the release of TMG under light irradiation, we first explored the stability of our PBGs under dark conditions. The results showed that after 24 h in the dark, both BD-TMG and BD-I-TMG have a negligible change in their UV-vis spectra, indicating high dark stability (as shown in Figure 2.2). In addition, we also verified the stability with increased temperature and found the compounds were stable even at 60℃ (as shown in Figure 2.3).

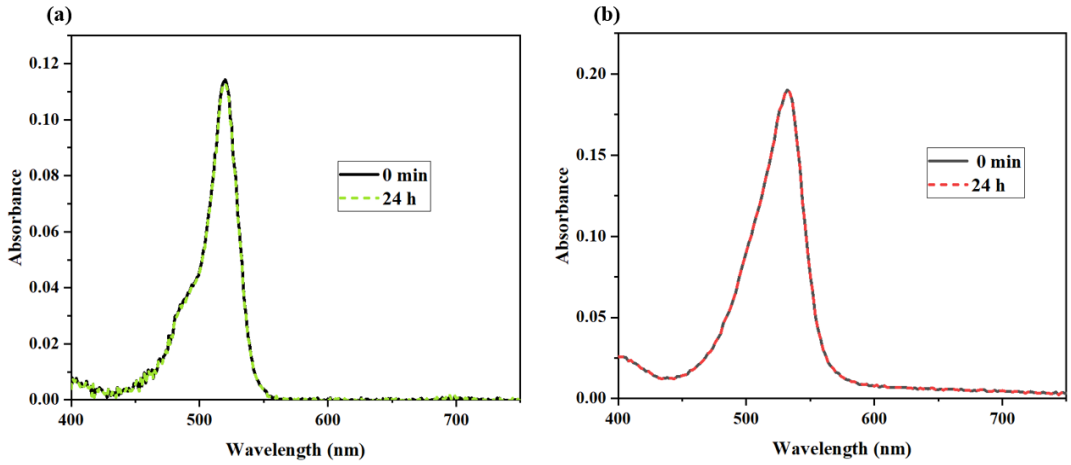

Figure 2.2 UV-vis absorption spectra of BD-TMG (a) and BD-I-TMG (b) at 0 min and 24 h in methanol in the dark condition (all measurements were conducted at room temperature).

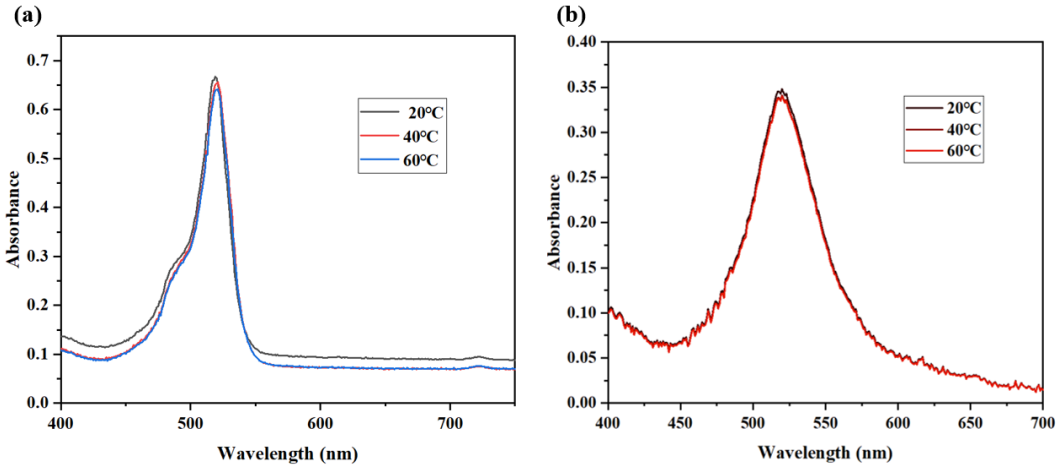

Figure 2.3 UV-vis absorption spectrums of BD-TMG (a) and BD-I-TMG (b) after kept at 20, 40, 60 °C for 30 min. Spectra were recorded after slowly cool down the solution to room temperature

Absorption, Emission spectra and fluorescent quantum yield of compound BD-TMG and BD-I-TMG: All steady-state absorption, fluorescence emission, of compound BD-TMG and BD-I-TMG were investigated in 10 mm path length quartz cuvettes at room temperature. The absorption spectra were measured with a Tecan Infinite M200 PRO plate reader spectrometer in 1 cm path length quartz cuvettes. Fluorescence emission and excitation spectra were obtained using an Edinburgh Photonics FLS980 spectrometer equipped with a thermoelectric cooled photo multiplier detector (Hamamatsu). All measurements were carried out with the optical density below 0.12 at the excitation wavelength to avoid reabsorption. The excitation and fluorescence emission spectra were corrected for the spectral sensitivity of Edinburgh Photonics excitation and detection sys using factory-measured correction files.

Fluorescence quantum yields were determined by a reference point method. Rhodamine 6G (Φ_f = 0.95) / exe at 490 nm in DCM (0.1 μM) was used as a standard

sample to calculate the fluorescence quantum yield of BD-TMG and BD-I-TMG. The equation is as follows.

$$\frac{\phi_s}{\phi_R} = \frac{A_s}{A_R}\,\frac{(Abs)_R}{(Abs)_s}\,\frac{\eta_s^2}{\eta_R^2} \tag{1.1}$$

Where Φ represents quantum yield, Abs represents absorbance, A represents area under the fluorescence curve, and η is refractive index of the medium. The subscripts S and R denote the corresponding parameters for the sample and reference, respectively.

LED light emission profile. In the photo-releasing and photopolymerization experiments, we select the green LED light (Thorlabs M505L3, nominal wavelength 505 nm with adjustable power control via voltage control). The emission profile of the LED light showed significant overlap with the absorption spectra of BD-TMG and BD-I-TMG, as shown below (Figure 2.4).

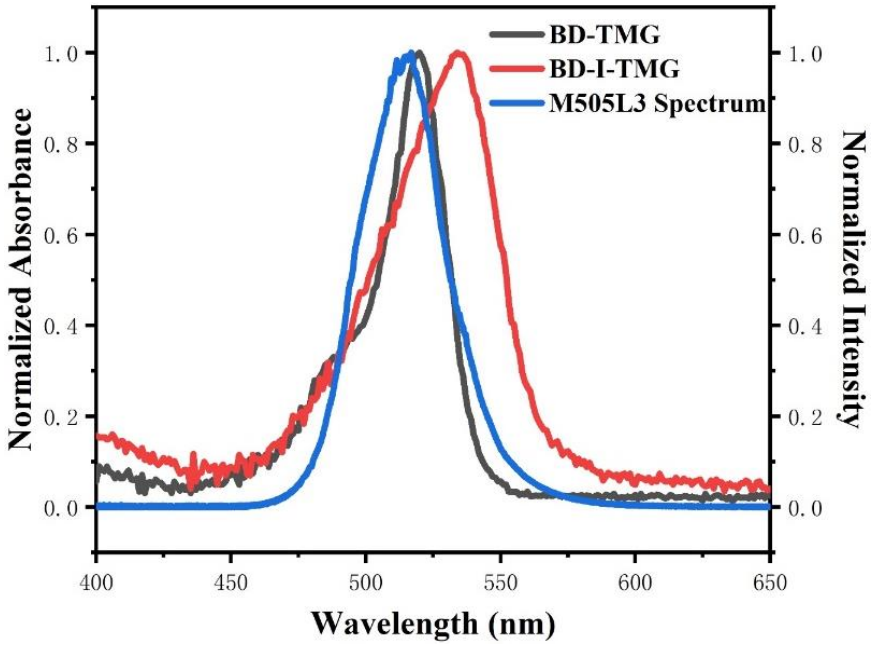

Figure 2.4 Normalized UV-vis absorption for BD-TMG and BD-I-TMG and the emission spectra of Thorlabs M505L3 LED light.

Quantum yield of base generation (Φ_b): we used UV-vis measurement of photolysis of BD-TMG and BD-I-TMG to monitored changes in the 450 to 500 nm region that correspond to base generation. BD-TMG and BD-I-TMG were dissolved in CD_3OD (~1×10^{-4} M) and then irradiated by 505 nm LED light in a 1 cm length path cuvette. The light source is Thorlabs M505L3 which has the nominal wavelength is 505 nm and the irradiance is 11 mW/cm^2. The distance between the LED light and the sample is 1 cm. After irradiation, the BD-TMG and BD-I-TMG samples were transferred and concentrated to NMR tube for NMR measurement. Because before and after photolysis the peaks of TMG only shifted from 2.85 ppm to 3.01 ppm, and the total integration is consistent, we used the ratio of TMG to calculate the rate of base production. The amount of photobase generators consumed was obtained by calculating the integral rate of the peak area of BD-TMG and BD-I-TMG in the target area of ^{1}H NMR. The power density of the LED light was determined using PM100D-Compact Power and Energy Meter Console manufactured by Thorlabs, and confirmed the value by using photometer IL1400A (International Light Inc.). The photon numbers were calculated by integrating the spectrum plot using power density times the percentage to the power of this wavelength region. All areas and accumulated number of photons was used for the calculation of rate of photon absorption.[83, 84] The quantum yield measurements were repeated three times with independently prepared samples. The equation is as follows.

$$\Phi_b = \frac{rate\ of\ photobase\ generator\ consumed}{rate\ of\ photon\ absorption} = \frac{rate\ of\ base\ production}{rate\ of\ photon\ absorption} \quad (1.2)$$

Where rate of photon absorption is expressed as moles of photons absorbed per unit volume per unit time.

Fluorescence lifetimes (τ_F) were determined with the single photon counting technique (TCSPC) and the same fluorescence spectrometer using a pulsed picosecond diode laser (EPL-505) as the excitation source. Molar absorption coefficient (ε) and maximum absorbance wavelengths (λ_{max}) were determined by Beer's law, from plots of absorbance vs. concentration (Figure 2.5). Recordings were performed in 10 mm path length quartz cuvettes at room temperature.

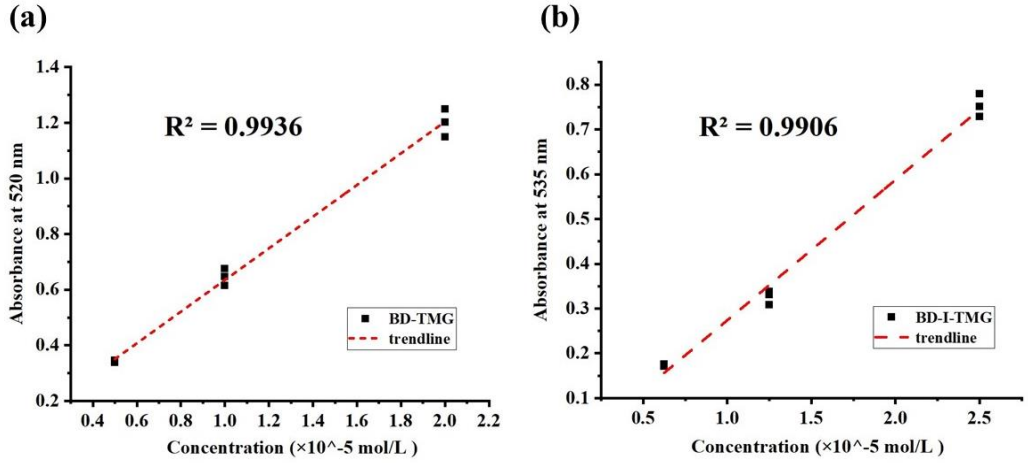

Figure 2.5 Extinction coefficient calculation fit lines of BD-TMG (a) and BD-I-TMG (b) measured in dichloromethane.

Photolysis of BD-TMG and BD-I-TMG: PBGs (2 ml of 0.6×10^{-3} M in methanol) were placed in quartz cuvette (10 mm path). The cuvettes were placed in front of a light source (Thorlabs M505L3) mounted LED that has a nominal wavelength 505 nm with a power density of 11 mW/cm^2, 1 cm distance and was irradiated for the indicated times. The photo-behaviors were monitored by UV-vis spectra.

To confirm the value of molar absorption coefficients for both compounds BD-TMG and BD-I-TMG, we measured the molar extinction coefficients in triplicate and

started from milligrams. We respectively weighed 5 mg, 10 mg, 20 mg of BD-TMG and BD-I-TMG to prepare the stock solutions. The detection concentrations of BD-TMG are 5 μM, 10 μM, and 20 μM, and the detection concentration of BD-I-TMG are 6.25 μM, 12.5 μM, and 25 μM. To ensure the accuracy of the measurements, each concentration was measured in triplicate. BD-TMG has a molar extinction coefficient of 5.69×10^4, and the value for BD-I-TMG is 3.13×10^4. Regarding the decrease in the molar extinction coefficient after iodination of BODIPY, and the half of typical value of molar extinction coefficient of BD-I-TMG, we looked at the reported values in literature and found out that this drop in molar extinction coefficient is common after modification with heavy atoms (such as Br and I).[60, 77, 85] For example, in 2018, Szymanski reported[60] the molar extinction coefficient for BODIPY core of 4.2×10^4 $M^{-1}cm^{-1}$ and after modified with one iodine atom the molar extinction coefficient dropped to 1.4×10^4 $M^{-1}cm^{-1}$. In another example, Ortiz reported[85] the molar extinction coefficient for the BODIPY core of 6.9×10^4 $M^{-1}cm^{-1}$ and after modified with one iodine atom the molar extinction coefficient dropped to 2.2×10^4 $M^{-1}cm^{-1}$.

Thermal stability: BD-TMG and BD-I-TMG (2 ml of 0.6×10^{-3} M in DCM) in a cuvette was merged in a water bath with controlled temperatures (20, 40, and 60 °C), separately. After 30 minutes, the cuvette was slowly cool down to room temperature for the UV-vis measurement. The absorbance showed ignorable changes in varied temperatures.

Dark stability: BD-TMG and BD-I-TMG (dissolved in methanol) was placed in quartz cuvette (10 mm path). The cuvettes were placed in the dark condition at room

temperature. After 24 hours the cuvette was analyzed by UV-vis absorbance spectra. There were no changes in the absorbance spectra.

2.5 BD-TMG and BD-I-TMG Photo Degradation and Photolysis Path

Furthermore, to show these structures can release TMG under green light irradiation, we investigated the photolysis process of BD-TMG and BD-I-TMG by monitoring the reaction with ^{1}H NMR. The PBGs were dissolved in CD_3OD. A 400 mW, 505 nm LED lamp was used to irradiate the sample (irradiance: 80 mW/cm^2) and the irradiation-time dependent ^{1}H NMR spectrums were recorded (Figure 2.6). With increasing irradiation time, the peak around 2.9 ppm decreased which corresponds to the methyl groups of TMG of BD-TMG and BD-I-TMG. This decreasing peak results from the photolysis process of the carbamate group on BD-TMG and BD-I-TMG. At the same time, the peak from free TMG at 3.01 ppm increases gradually. More importantly, the TMG releasing speed of BD-I-TMG is much faster than BD-TMG, with more TMG released within the first 2 min, and fully released TMG in the period of 60 min light irradiation. This also supports the heavy atom effect, in which the iodine in BD-I-TMG can enhance ISC and facilitate conversion from the singlet state to the triplet state. Furthermore, as reported in the literature,[77] BODIPY-based PBGs' carbamate cleavage relaxation mainly occurred from the T1 state, implying that iodination can improve the deprotection efficiency of TMG. The photolytic efficiency tests substantiated this.

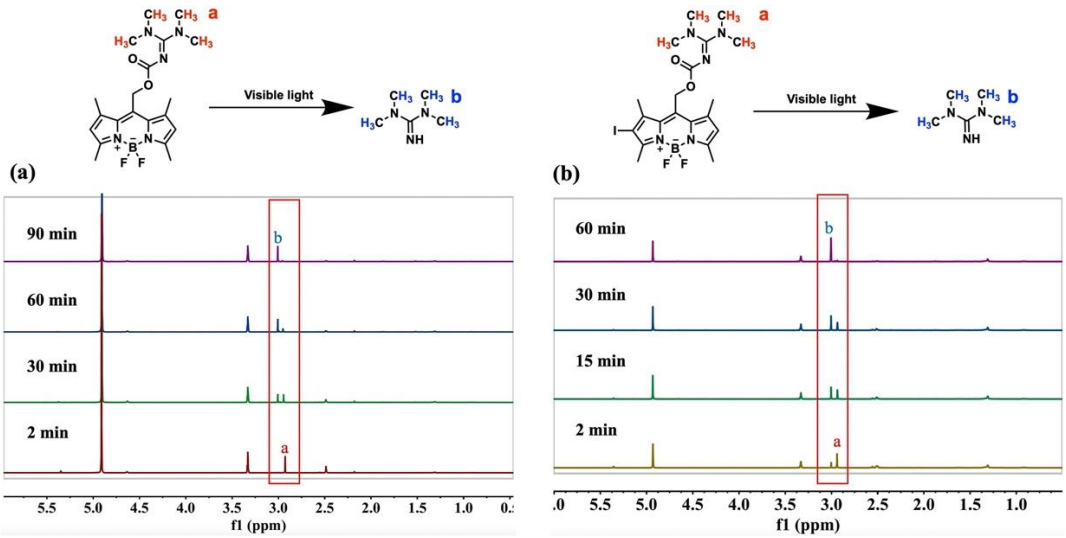

Figure 2.6 BD-I-TMG (a) and BD-TMG (b) photo degradation in CD_3OD. The samples were irradiated by Thorlabs M505L3 LED light source (nominal wavelength 505 nm, power density is 80 mW/cm^2, samples were concentrated for ^{1}H NMR measurements).

To further investigate the role of triplet states on the photo-releasing process, the Stern-Volmer quenching experiment was utilized. Photolysis of 1×10^{-5} M BD-I-TMG in dichloromethane was irradiated with or without the addition of 5 mM triplet quencher potassium sorbate (PS).[86] A significantly slower photolysis rate was observed using UV-vis when PS was introduced, confirming the improved TMG releasing efficiency is facilitated by the heavy atom effect (Figure 2.7). Moreover, we also studied the effect of oxygen in the solvent on the photolysis rate of BD-I-TMG. 1×10^{-5} M BD-I-TMG in degassed dichloromethane was prepared for the photolysis analysis. The irradiation time-dependent photolysis was monitored by UV-vis (Figure 2.8). The result showed that the rate of photolysis of BD-I-TMG in the degassed solvent is slightly higher than in the non-degassed solvent, indicating the energy transfer from triplet states to oxygen. However, the difference is minor and non-degassed conditions are used in the experiments below.

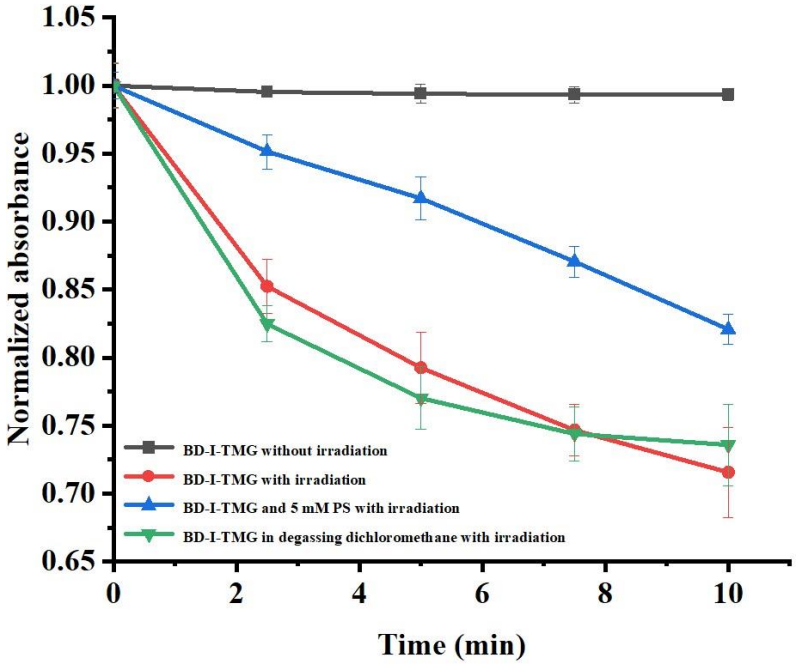

Figure 2.7 Time course of photolysis for the BD-I-TMG with different conditions (black curve: dark condition, blue curve: in presence of 5 mM of triplet quencher potassium sorbate (PS), red curve: with irradiation, green curve: BD-I-TMG in degassed dichloromethane). Concentration of BD-I-TMG is 1×10^{-5} M. BD-I-TMG was irradiated by 505 nm LED lamp (Thorlab's M505L3, power density: 80 mW/cm^2, 1 cm irradiated distance).

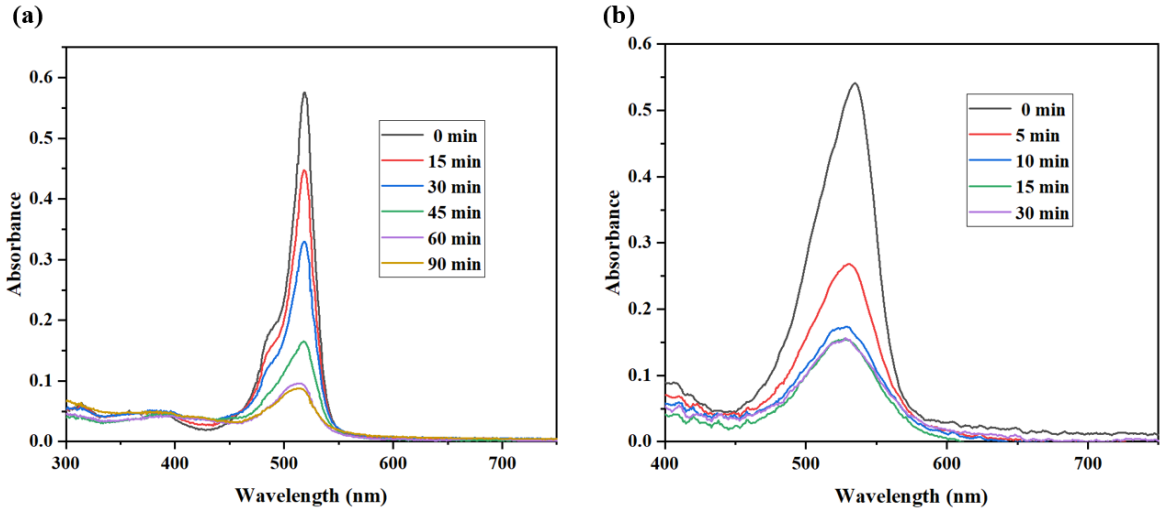

Figure 2.8 UV-vis absorption changes of BD-TMG (a) and BD-I-TMG (b) during photolysis in Methanol. BD-TMG and BD-I-TMG were irradiated by 505 nm LED lamp, separately.

The photobase generation quantum yield of BD-I-TMG (Φ_{TMG} = 0.029) and photolytic efficiency ($\varepsilon\Phi_{TMG}$ = 907.7) were superior to the BD-TMG (Φ_{TMG} = 0.009, $\varepsilon\Phi_{TMG}$ = 512.1) system. Moreover, the photolytic efficiency of BD-I-TMG is much greater than traditional o-nitrobenzyl-based PBGs,[22] and the quantum yield is close to the coumarin-based PBGs.[30] In addition, we observed a significant decrease in photolysis rate when aprotic $CDCl_3$ was used (as shown in Figure 2.9) as the solvent. This result indicates that the nucleophilic solvent (e.g., CH_3OH) facilitates the photodecomposition rate. Additionally, to confirm this photolysis process, time-dependent UV-vis measurements were used. As expected, under 505 nm light irradiation, a decrease in the peaks at 520 and 535 nm of BD-TMG and BD-I-TMG were observed, respectively.

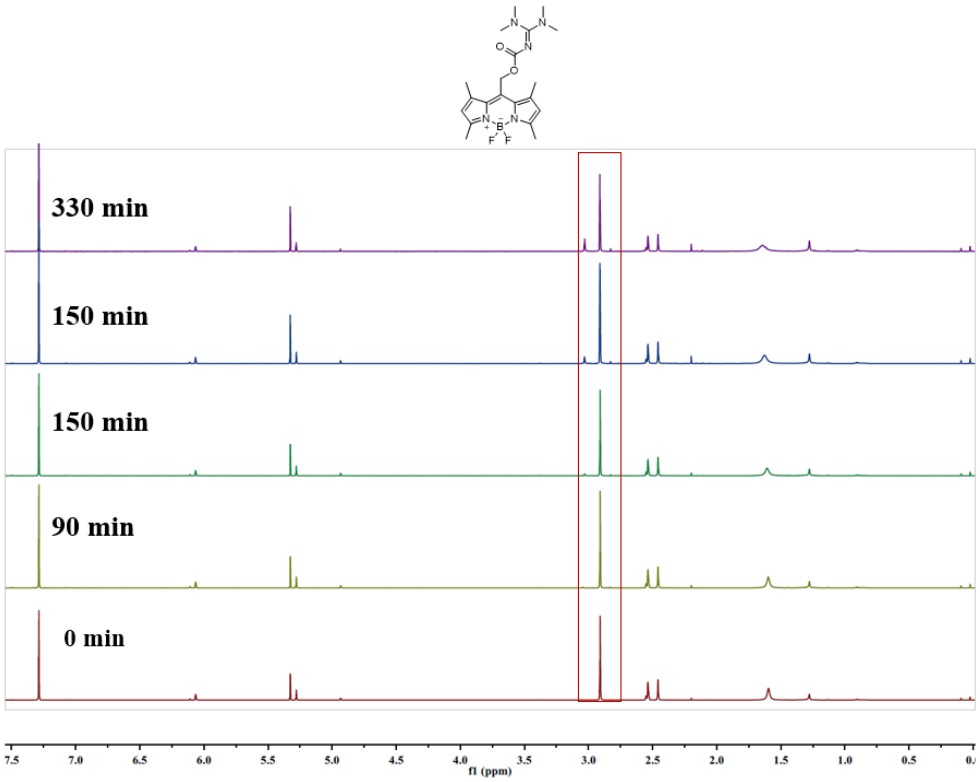

Figure 2.9 ^{1}H NMR of BD-TMG photo degradation test in $CDCl_3$.

We postulate that the photolysis mechanism of BD-TMG and BD-I-TMG proceeds as described in Scheme 2.2. A similar photo-heterolysis mechanism was reported by Winter et al. with similar BODIPY cage structures.[87] Under visible light irradiation, the BODIPY-based photocages were excited to the excited singlet and triplet states. A photocleavage process ensued, where the C-O bond broke and then produced the BODIPY methyl cation and the corresponding anion leaving group. Among them, the BODIPY methyl cation group was restabilized by nucleophiles such as MeOH while the carbamate anion underwent the decarboxylation process to produce TMG and CO_2.

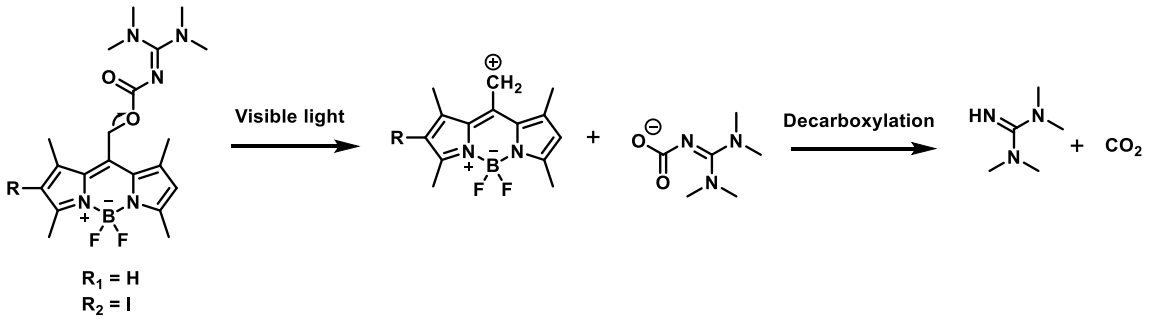

Scheme 2.2 Possible pathway for the photolysis of photocaged TMG.

To further study the photodegradation process and photolysis products of BD-TMG, we used ^{1}H NMR to monitor the mixture after green light irradiation (80 mW/cm^2, 505 nm LED light for 2 and 60 min, Figure 2.10). The ^{1}H NMR showed a peak at 5.53 ppm increases with irradiation time, which is corresponding to the OH after the carbocation intermedia reacts with H_2O in the solvent. Moreover, the CH_2 peak shifted from 5.32 ppm to 4.72 ppm, indicating the environment changes from an ester and an alcohol after TMG release. It is worth mentioning that the basicity of protected TMG and free TMG is significantly different[57] to allow the regulation of thiol-ene Michael addition reactions. BD-TMG and BD-I-TMG (dissolved in $CDCl_3$ or CH_3OD) was placed in

cuvette, and were subject for light irradiation (green LED light, irradiation distance: 1 cm, 80 mW/cm^2). After 30 minutes under light, the samples were concentrated to 0.5 mL for ^{1}H NMR measurements.

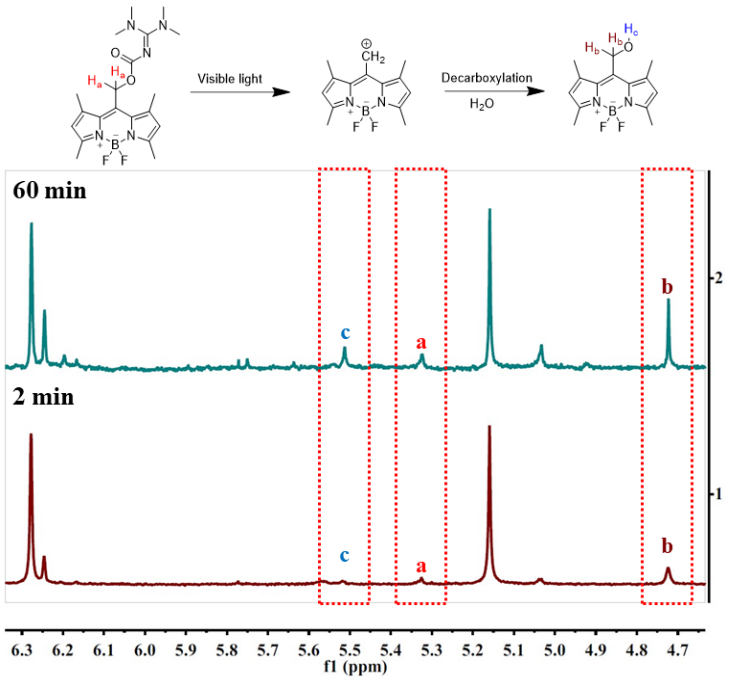

Figure 2.10 ^{1}H-NMR monitors photo-degradation process of BD-TMG in DMSO-d_6. The sample was irradiated by the Thorlab's M505L3 LED light source (nominal wavelength 505 nm, power density is 80 mW/cm^2, irradiated distance: 1 cm) for 2 min and 60 min respectively.

2.6 Conclusion

In summary, two novel BODIPY-based TMG-protected photobase generators, BD-TMG and BD-I-TMG, have been successfully synthesized for green light-initiated thiol-ene Michael addition photopolymerization. Both the PBGs' photophysical properties and photolysis efficiencies were studied. These two PBGs exhibited long wavelength absorption ability in the visible wavelength window above 500 nm. Compared with BD-TMG, the heavy atom (iodine) labeled BODIPY derivative, BD-I-TMG, had much greater photo-releasing efficiency resulting from the heavy atom effect.

CHAPTER 3

VISIBLE-LIGHT-INITIATED THIOL-MICHAEL ADDITION POLYMERIZATION AND RING-OPEN POLYMERIZATION ENABLED BY BODIPY-BASED PHOTOBASE GENERATOR

3.1 Introduction

Since the definition of a "click reaction" by Sharpless and co-workers in 2001,[88] this concept has been employed to great effect in bioconjugation, drug synthesis, materials science, and radiochemistry.[89] Among "click" reactions, the base-catalyzed thiol-ene Michael addition reaction is considered a prized tool in materials synthesis, which provides high functional group conversion, high reaction rate, and mild reaction conditions.[90] The thiol-ene Michael reaction proceeds via an anion-mediated pathway, in which a base deprotonates a thiol, forming a thiolate anion that reacts with electron-deficient alkenes to generate a thioether bond.[91] The versatility of the thiol-ene Michael reaction has been implemented in polymer science, including polymer-based gene delivery systems,[92] dendrimer synthesis,[93, 94] polymer surface modification,[95, 96] 3D printing,[97-99] hyperbranched polymers,[100, 101] and other polymer syntheses.[102] However, it is still challenging to provide the spatial and temporal control for the thiol-ene Michael reaction, because the polymerization reaction is initiated immediately after the introduction of the base.[103] To address this issue, PBGs have been utilized, which provide photoinduced control and are capable of releasing base species under irradiation of light at a specific wavelength (as shown in Figure 3.1).

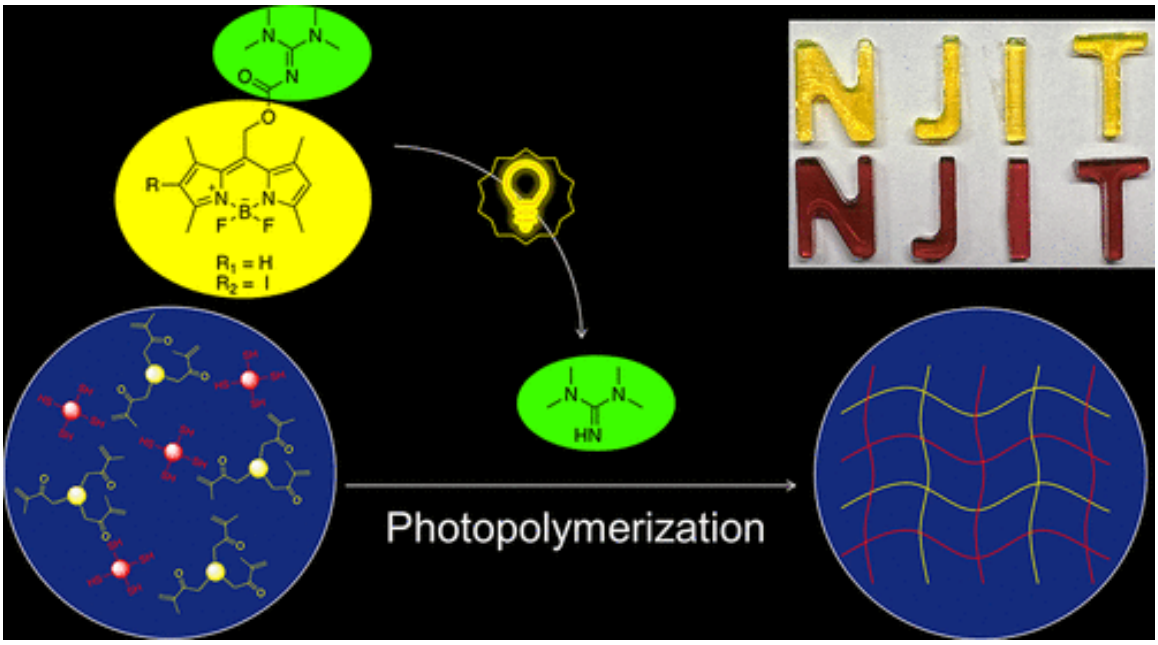

Figure 3.1 BODIPY based PBGs for photo-induced polymerization.

Moreover, Photobase generator also can induced ring-open polymerization. Photobase generator-induced ring-opening polymerization (photoinduced ROP) is a polymerization methodology predicated on light-induced initiation of the ring-opening of cyclic monomers, exemplified by lactones and lactides, for the synthesis of linear polymers.[104] In this modality, a photobase generator serves as the pivotal component, harnessing light exposure to engender a potent base that, in turn, catalyzes the commencement of the polymerization process. The distinctive merits of this approach encompass precise control over polymerization rates and the facilitation of milder reaction conditions when compared to conventional polymerization techniques. Furthermore, photoinduced ROP enables the tailored production of polymers possessing specific attributes, such as biodegradability and biocompatibility, rendering it a highly promising technique within the realm of biomedical applications.

3.2 Thiol-Michael Reaction Photo-induced by BODIPY Based PBGs

3.2.1 The applications of BD-TMG and BD-I-TMG in Thiol-Michael Reaction

To further explore the activation activity of BD-TMG and BD-I-TMG toward the thiol-ene Michael reaction, different monothiols were evaluated with ethyl acrylate and divinyl sulfone separately as model substrates. The light source used was Thorlabs M505L3 (nominal wavelength is 505 nm with an irradiance of 80 mW/cm^2, irradiated distance: 1 cm). The reaction yields were determined by ^{1}H NMR. 2.5 mol% of photobase generators was found to be efficient for the reaction Table 3.1 and Figure 3.2 includes the results, which indicate that using a 2.5 mol% catalyst loading of BD-TMG or BD-I-TMG showed high catalyst efficiency, and all the entries reaction conversions were completed in 30 min. The result shows that the activation of the thiol-ene additions with BD-I-TMG has a higher yield than the BD-TMG. This result can be attributed to the BD-I-TMG having much higher photolysis efficiency than BD-TMG. In addition, by comparing the reaction yield after 30 min of irradiation, both BD-TMG entries and BD-I-TMG were close to 100%, which indicated that 2.5 mol % of catalyst loading is in excess for the 1 mmol of thiol and ene.

Table 3.1 Scope of Photo Thiol-ene Michael Addition Catalyzed by BD-TMG and BD-I-TMG.

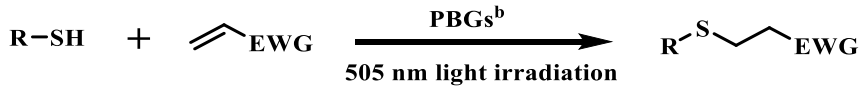

Entry	Thiol	Vinyl	Catalyst	Yield[a](%)
1	butyl thioglycolate	ethyl acrylate	BD-TMG	63
2	butyl 3-mercaptopropionate	divinyl sulfone	BD-TMG	94
3	butyl thioglycolate	divinyl sulfone	BD-TMG	68
4	butyl 3-mercaptopropionate	ethyl acrylate	BD-TMG	98
5	butyl thioglycolate	ethyl acrylate	BD-I-TMG	98
6	butyl 3-mercaptopropionate	divinyl sulfone	BD-I-TMG	95
7	butyl thioglycolate	divinyl sulfone	BD-I-TMG	76
8	butyl 3-mercaptopropionate	ethyl acrylate	BD-I-TMG	96

(a) Reaction yields are determined by ^{1}H NMR. (b) Reaction conditions: thiol (1 mmol), vinyl (1 mmol) and PBGs (2.5 mol%) irradiated using a 505 nm LED light source (power density is 80 mW/cm^2, irradiated distance: 1 cm) for 30 min

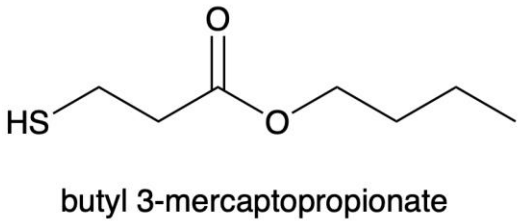

butyl 3-mercaptopropionate

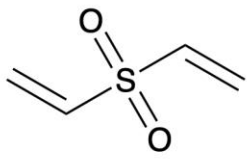

divinyl sulfone

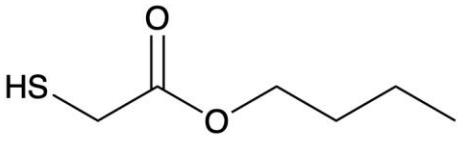

butyl thioglycolate

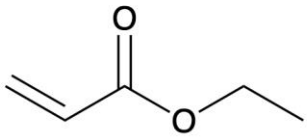

ethyl acrylate

Figure 3.2 The thiol and vinyl small molecules used in photo thiol-ene Michael addition model reaction.

To examine the kinetics of the photoactivation of the thiol-ene Michael reaction, BD-TMG and BD-I-TMG were implemented as photoactivators in the butyl thioglycolate and ethyl acrylate reaction under continuous visible light irradiation (505 nm, 80 mW/cm^2). The thiol conversion was monitored by FT-IR spectroscopy (Figure 3.3), monitoring the reduction of peak intensity around 2650 cm^{-1}, which corresponds to the thiol group of butyl thioglycolate. The final thiol conversion yield was confirmed by ^1H NMR.

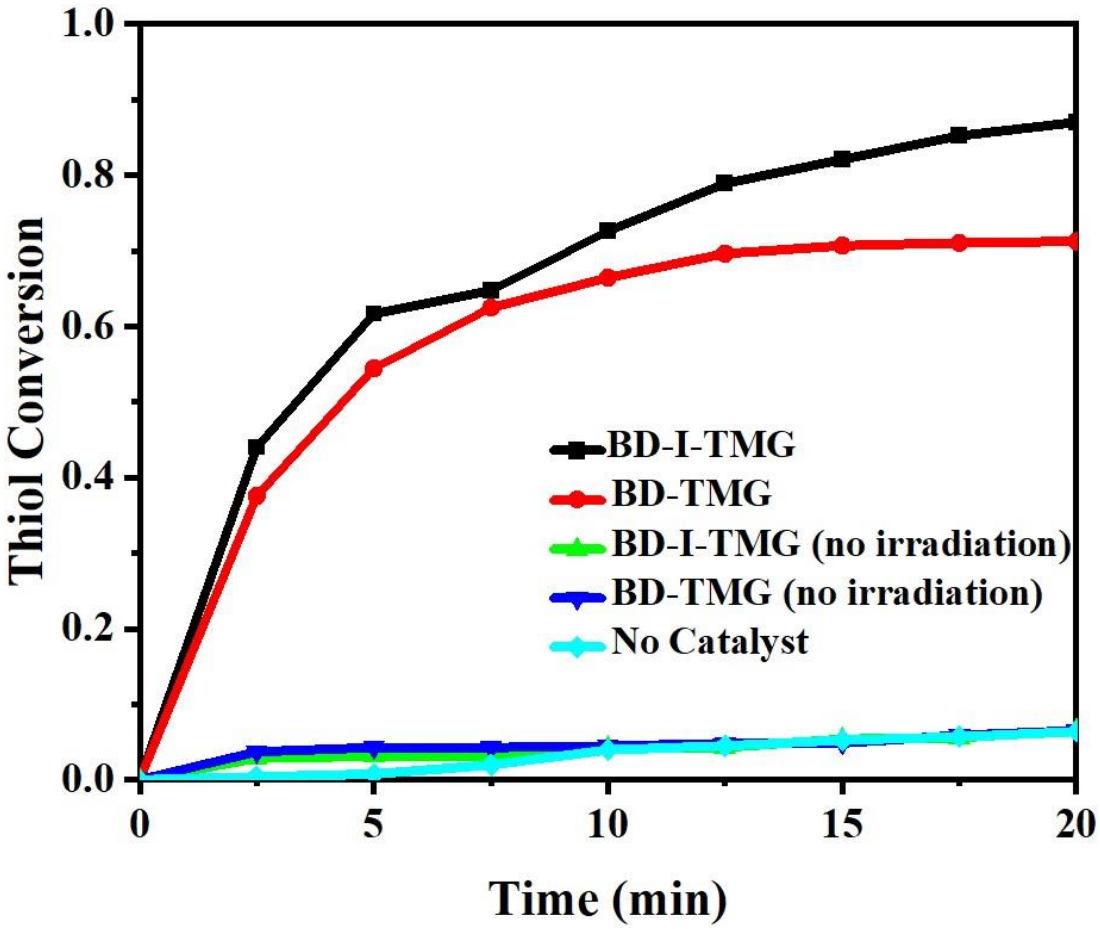

Figure 3.3 Thiol conversion versus time monitored by FT-IR for the model reaction between butyl thioglycolate and ethyl acrylate with 2.5 mol % photoinitiator loading. Light source: Thorlab's M505L3 LED light (nominal wavelength 505 nm, power density is 80 mW/cm^2, irradiated distance: 1 cm).

In Figure 3.3, the results indicate that both BD-TMG and BD-I-TMG exhibited fast reaction kinetics; however, the reaction rate of BD-I-TMG was higher than BD-TMG during the first 2.5 min of irradiation. In addition, the final thiol conversion of BD-I-TMG (ca. 85%) was also higher than BD-TMG (65%) under 20 min of continuous irradiation. Furthermore, it is shown that the PBGs and visible-light irradiation are both necessary to initiate the thiol-ene Michael reaction. In the absence of either PBGs or green light, no apparent reaction was observed. In addition, we also conducted the dark cure test for the BD-TMG and BD-I-TMG. The model reaction mixture was irradiated with LED light for 2.5 min and the thiol conversion was monitored in the dark using FT-IR (as shown in Figure 3.4). The result showed that BD-TMG and BD-I-TMG have the ability for dark cure, but the reaction rate after 2.5 min irradiation was slower than in continuous irradiation trials.

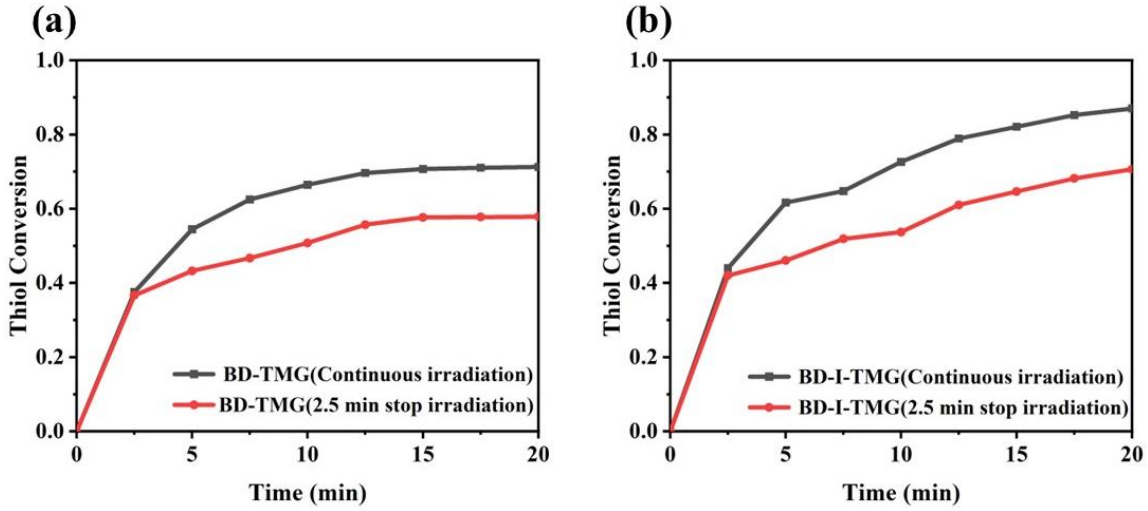

Figure 3.4 Thiol conversion versus time monitored by FT-IR: butyl thioglycolate and ethyl acrylate with 2.5 mol% BD-TMG (a) and BD-I-TMG (b) respectively, The mixture was initiated with the Thorlabs M505L3 LED light source (nominal wavelength 505 nm, power density is 80 mW/cm^2, irradiated distance: 1 cm). The controlled experiment was conducted under continuous irradiation (black curve), and the dark cure experiment was only irradiated for 2.5 min (red curve).

To demonstrate the utility of the BODIPY PBGs, a photopolymerization study was conducted. To form a polymer network, we implemented BD-I-TMG as the photoactivator. A mixture of pentaerythritol tetrakis(mercaptoacetate) (PETMA 1 mmol), trimethylolpropane trimethacrylate (TMPTMA 1 mmol), and 2.5 mol% of BD-I-TMG were well mixed and placed in a rubber mold. After 1 h of 505 nm LED light (80 mW/cm^2) irradiation, a soft rubbery polymer was obtained (Figure. 3.5), which indicated BD-I-TMG successfully initiated the polymerization reaction and formed cross-linked polymer during the photopolymerization process. Finally, to assess the mechanical properties of the polymer, the 0.5 mm thick film made of a stoichiometric mixture of PETMP and TMPTMA (molar ratio = 1:1) was cured in the presence of 2.5 mol% BD-I-TMG and tested via dynamic mechanical analysis (DMA) experiments (as shown in Figure. 3.5). Both the glass transition temperature (T_g = 17.36 ℃) and narrow tan δ indicated the formation of a homogeneous polymer network under the activation of BD-I-TMG and green LED light. In addition, we also evaluated rheological and mechanical properties of the BD-I-TMG-catalyzed crosslinked sample (Figure 3.6). The compressive modulus values obtained from compression tests were 11.9 ± 2.8 MPa (Figure 3.6a). The frequency sweep results confirm that the polymer is crosslinked and well structured, as the storage modulus (G') values were higher than the loss modulus (G") values over a wide range of frequencies (Figure 3.6b).

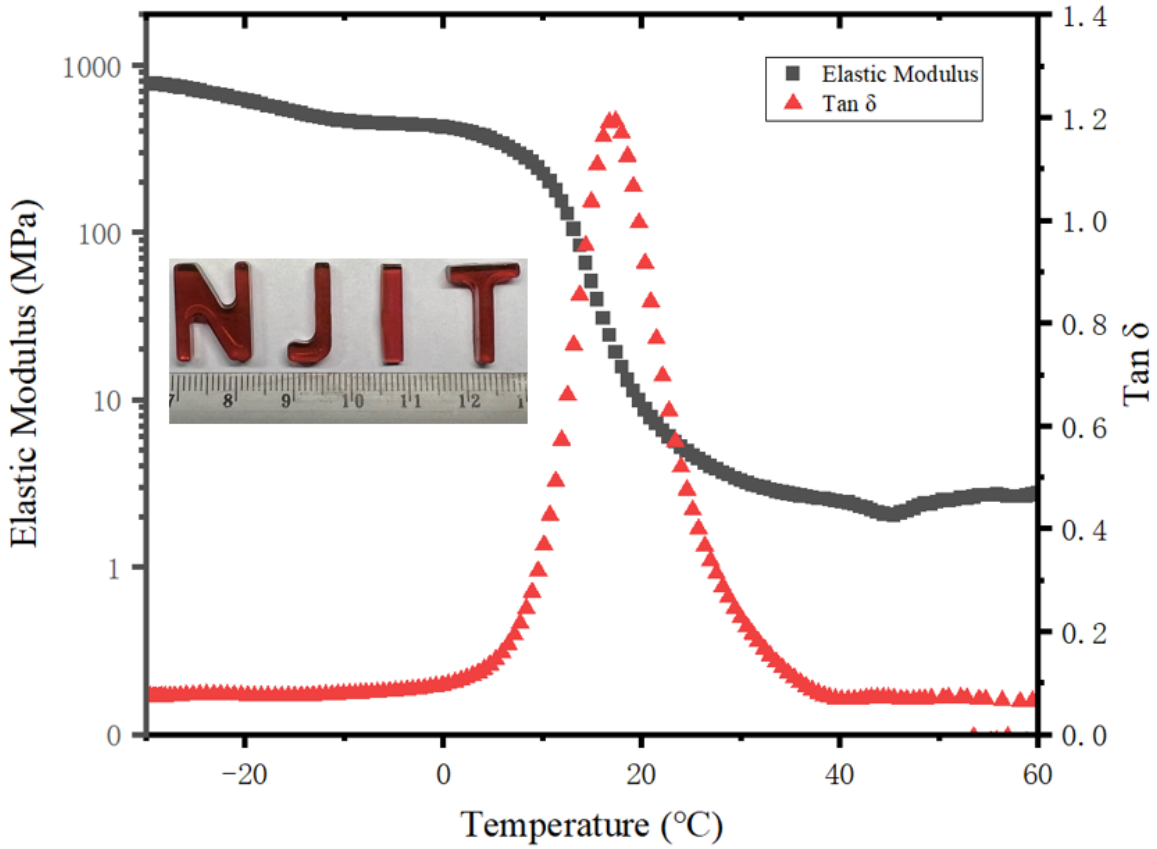

Figure 3.5 Plots of tan δ and elastic modulus vs temperature for polymer networks formed through the monomer cross-linking PETMP/ TMPTMA (molar ratio = 1:1) and 2.5 mol % BD-I-TMG catalyst loading. The sample was irradiated with 80 mW/cm^2, 505 nm LED light for 1 h. The irradiated distance is 1 cm.

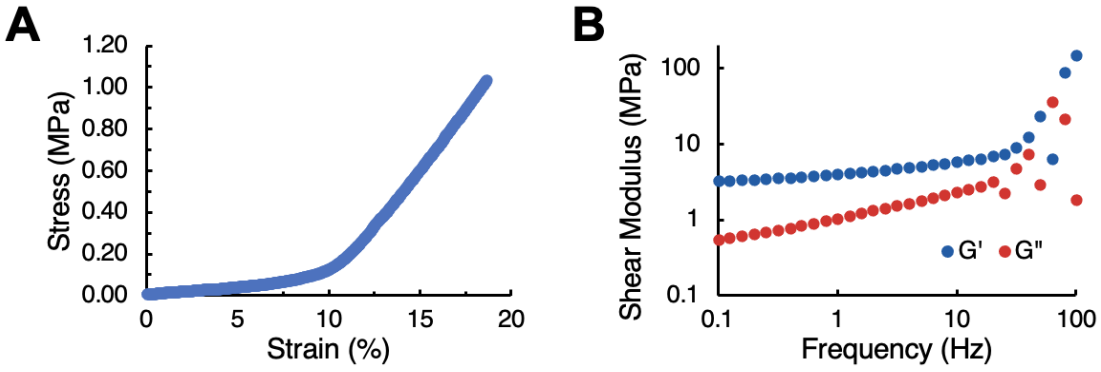

Figure 3.6 a) Representative stress-strain curve of a crosslinked sample under compressive force. b) Representative frequency sweep test of a crosslinked sample under 0.5% constant strain.

IR analyses were performed on FT-IR, SHIMADZU IRAffinity-1 instrument. Samples were injected into the space between two NaCl slides (the thickness of the NaCl plate is 5 mm). The LED lamp (nominal wavelength 505 nm, power density is 80 mW/cm^2, irradiated distance: 1 cm) was placed in the FTIR instrument to irradiate the sample vertically. The LED light was turned off when the sample is measured with FTIR. IR data was recorded every 2.5 minutes after LED light irradiation. By measuring IR peak area decreasing around 3150 cm^{-1}, and 2650 cm^{-1}, functional group conversion of vinyl and thiol can be calculated by the ratio of peak area to the peak area prior to the reaction.

To study the yield of thiol-ene Michael addition reaction with different PBGs catalyst loading, 1 mmol butyl 3-mercaptopropionate and 1 mmol ethyl acrylate with different BD-I-TMG loading (0.5 mol%, 1.5 mol%, 2.5 mol%, 3.5 mol%) were utilized. The mixture was placed 1 cm in front of the 505 nm LED light source (power density is 80 mW/cm^2), and irradiated for 30 min. The reaction yield monitored by ^1H NMR (as shown in Figure 3.7). The results shows that the yield reach to 85% even at 0.5% BD-I-TMG loading. Moreover, the yield reached a plateau at 2.5% BD-I-TMG loading. Therefore, we selected 2.5% catalyst loading for subsequent experiments.

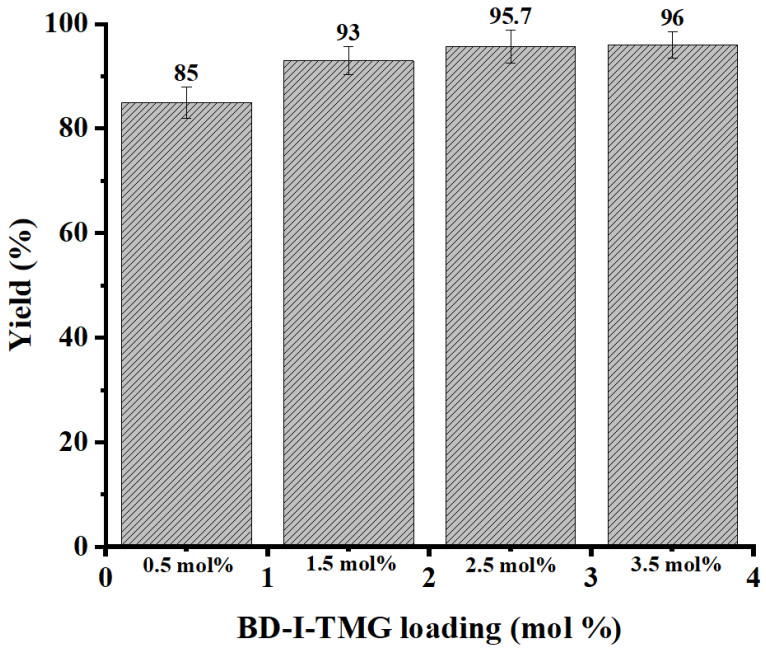

Figure 3.7 Photo thiol-ene Michael addition reaction yield versus different BD-I-TMG loading (0.5 mol%, 1.5 mol%, 2.5 mol%, 3.5 mol%) monitored by ^{1}H NMR for the model reaction between 1 mmol butyl 3-mercaptopropionate and 1 mmol ethyl acrylate. Light source: Thorlab's M505L3 LED light (nominal wavelength 505 nm, power density is 80 mW/cm^2, irradiated distance: 1 cm) for 30 min.

The polymerization conversion yield was determined by a gravimetric method. The yield was the weight ratio of the dried polymer product after soaking in DMSO for 3 days to the initial weight of starting materials including the photobase generator. Polymer was prepared using 1:1 ratio of PETMP and TMPTMA loaded with 2.5 mol% of BD-I-TMG under 30 min of green LED light irradiation at the power density of 80 mW/cm^2. The conversion yield was calculated to be 92.5%.

To monitor the BD-I-TMG induced photopolymerization reaction, FT-IR spectrum was utilized. 2.5 mol% BD-I-TMG was mixed with 1 mmol PETMA and 1 mmol TMPTMA. After measured the FT-IR spectrum of the mixture before LED light irradiation, the mixture was irradiated by Thorlabs M505L3 LED light (nominal wavelength 505 nm, power density is 80 mW/cm^2, irradiated distance: 1 cm) for 30 min

then measured the FT-IR spectrum again. The photopolymerization product was then soaked in DMSO overnight then dried by oven (120 °C, 6 h), then measured by FT-IR (as shown in Figure 3.8). The result shows that the S-H peak (around 2600 cm^{-1}) and the sp^2 C-H peak (around 3100 cm^{-1}) obviously decreased after photopolymerization, which proved that BD-I-TMG effectively initiated the thiol-Michael additional reaction.

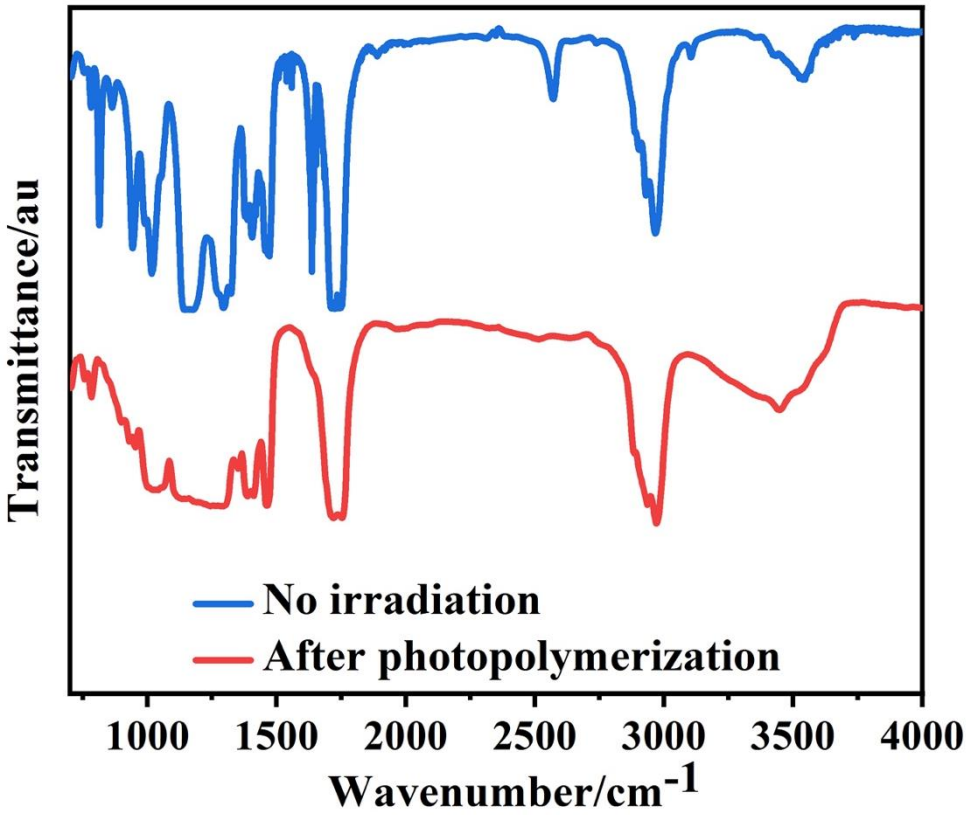

Figure 3.8 FTIR spectrum of the mixture of BD-I-TMG (2.5 mol%) with PETMA (1 mmol) and TMPTMA (1 mmol) in dark condition (blue line) and after 30min irradiation, the polymer was washed with DMSO 3 days (red line). Light source: Thorlab's M505L3 LED light (nominal wavelength 505 nm, power density is 80 mW/cm^2, irradiated distance: 1 cm, irradiation time: 30 min).

Mechanical property analysis of network photoinitiated polymer was utilized by DMA 850 dynamic mechanical analyzer. The standard film (0.5 mm thickness) made of a stoichiometric mixture of PETMP and TMPTMA (molar ratio = 1:1) and 2.5 mol % BD-I-TMG was prepared by injecting between two glass slides with 0.5 mm thickness spacer

and then the sample irradiated with 505 nm LED light (11 mW/cm^2) for 1 h. Then the film was demolded carefully and trimmed into disk shape with 20 mm diameter for the DMA test. The temperature was ramped at 3 °C / min with the frequency of 1 Hz.

Prior to rheological and mechanical characterization, BD-I-TMG catalysted crosslinked samples were immersed in DI water for one week to ensure equilibrium swelling. To analyze the rheological and mechanical properties of the samples, Mavern Ultra+ Rheometer (flat plate geometry, 4 mm) was used. All the tests were performed at room temperature. For the rheological characterization, storage (G') and loss (G") moduli values were recorded at 0.5% oscillatory strain from 0.1 to 100 Hz frequency. For the mechanical characterization, a compressive normal force was applied to 2.5 mm thick samples while recording the change in gap distance to calculate strain. 0.05 N initial force was applied to ensure contact between the upper plate and the sample. The compressive force was continuously increased (0.1 mm/s) up to 15 N. The compressive modulus (Young's modulus, E) was calculated from the slope of stress-strain curves obtained (using the linear range within 10 to 20% strain).

To find out if the BODIPY photoproduct can be removed from the polymer matrix or not, we formed a cross-linked polymer film (PETMP and TMPTMA) use BD-I-TMG under LED light. After solidifying, the as-prepared polymer was placed into DMSO and soaked for 7 days. After the polymer film was fully soaked in DMSO for 7 days, while the color of the polymer film faded a bit, we did not observe complete removal of the photoproduct (as shown in Figure 3.9). The color of film after soaking in DMSO still showed red, pink color evenly. Moreover, under UV lamp fluorescence was still observed. The high degree of polymer crosslinking may have impeded the extraction

of colored photoproducts (Figure 3.10). On the other hand, these properties will be helpful to apply BODIPY-based PBGs to biological and medical field with low leakage and potentially low toxicity.

Figure 3.9 Films preparation steps include mixing the PETMP, TMPTMA and BD-I-TMG (ratio: 1 mmol : 1 mmol : 0.05 mmol) in a glass vial, loading the mixtures in the mold, then the mixture was irradiated by the Thorlab's M505L3 LED light source (nominal wavelength 505 nm, power density is 80 mW/cm^2, irradiated distance: 1 cm) for 30 min. After solidifying, the film was soaked in DMSO for 7 days.

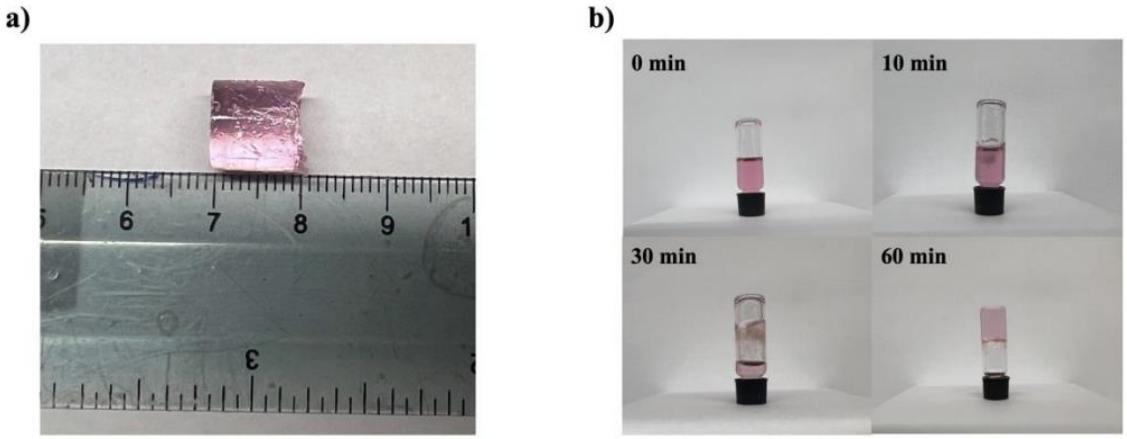

Figure 3.10 a) Green light-initiated polymer at the thickness of 10 mm. b) Photos of experiments demonstrating the photocuring conditions over different light irradiation time. The polymer networks formed through the monomer cross-linking PETMP/ TMPTMA (molar ratio = 1:1) and 2.5 mol % BD-I-TMG loading. The sample was irradiated with 80 mW/cm^2, 505 nm LED light for up to 60 min without dark cure. The irradiated distance is 1 cm.

3.3 The applications of BD-TMG in Ring-opening (ROP) Reaction

3.3.1 Background

Synthetic polypeptides, characterized by structural similarities to natural proteins, have garnered significant attention owing to their considerable potential for application in diverse domains, encompassing but not limited to tissue engineering, drug delivery, antimicrobial agents, and battery technologies.[105-107] The ring-opening polymerization (ROP) of α-amino acid N-carboxyanhydrides (NCAs) stands as a prominent approach for the large-scale synthesis of polypeptides.[108] Central to this process is the cleavage of the cyclic anhydride ring within NCA monomers, culminating in the establishment of peptide bonds among the monomeric units.[109] The ROP of NCAs may be activated by diverse catalysts and initiators, yielding polypeptides characterized by controlled molecular weights and dispersities. This method has been the subject of extensive investigation, leading to the development of diverse initiator-catalyst systems and polymerization conditions aimed at achieving both controlled and expeditious NCA polymerization.[110]

However, several limitations are associated with the ROP method. Firstly, the sensitivity of NCA ROP to reaction conditions, encompassing factors like temperature, pressure, and the presence of impurities, can impede the precise control of the polymerization process and influence the characteristics of the resultant polypeptides.[111] Secondly, the availability of appropriate initiators and catalysts can constrain the ROP of NCA. While an array of initiator/catalyst systems exists, certain systems may prove unsuitable for specific applications or exhibit limitations concerning their efficiency and selectivity.[112] Lastly, the accessibility of NCA monomers may present a limitation. While a diverse range of NCAs exists, some may be challenging to synthesize or have limited

availability, potentially impacting the scalability of the process. Therefore, it is urgent need for a new strategy to induced ring-opening polymerization.[113]

Photocaged superbase photoinduced ROP is a methodology wherein a photocaged superbase serves as the initiator for ROP upon exposure to UV irradiation.[114, 115] The photocaged superbase is characterized by its inactivity until subjected to UV light, at which point it liberates the superbase, instigating the polymerization process.[116] This approach offers several advantages over conventional ROP techniques, foremost among them the capacity to regulate the polymerization process via light exposure, affording meticulous control over both the molecular weight and dispersity of the resulting polymers.[117, 118] The origins of photocaged superbase photoinduced ROP date back to the early 2000s, when researchers embarked on explorations into light as a stimulus for external control over polymerization initiation.[119] Subsequently, the technique has undergone extensive examination in the realm of crafting non-biodegradable polymers through controlled radical polymerizations (CRP).[120-122] This avenue has facilitated precise surface modifications and the construction of intricate structures, catering to diverse applications. Photocaged superbase photoinduced ROP offers a series of notable advantages.[123] Foremost among them is the capacity to govern the polymerization process with light, affording meticulous control over both the molecular weight and dispersity of the resulting polymers.[108] Furthermore, this technique enables the initiation and termination of the polymerization process at will, achieved by the simple act of activating and deactivating the light source.[124] Additionally, the resultant polymers exhibit a high degree of molecular weight control, characterized by narrow dispersities, thereby yielding well-defined polymers. The applications of photocaged superbase photoinduced ROP

include the preparation of sophisticated materials where the precise control of space is essential, such as microelectronic devices and DNA microarrays.[125, 126] This technique can also be used in the preparation of biodegradable polymers such as aliphatic polyesters and polycarbonates, which has been hardly explored. The resulting polymers can be used in a wide range of biomedical applications, including medical implants and drug delivery.[109, 123]

3.3.2 Experimental Section

3.3.2.1 Preparation of γ-benzyl-L-glutamate N-carboxyanhydride NCA (BLG-NCA)

To a Mixture of γ-benzyl-L-glutamate acid (5 g, 0.021 mol) and triphosgene (4.5 g, 0,015 mol) under nitrogen was added anhydrous THF (200 ml). The solution was then heated to 50 °C for 4h, after which the solvent was removed under vacuum. A clear and colorless solution was obtained. The solvent was removed under vacuum. The residue (crude NCA) was transferred to a glovebox, dissolved in ca. 25 mL dry THF and recrystallized by layering 3 volumes of dry hexanes, and allowing to stand for 48 h. This procedure was repeated three times to yield a white crystalline.

3.3.2.2 General Polymerization Procedure using BD-TMG and Green LED Light

BLG-NCA (1 g, 3.80 mmol) was dissolved in DMF (1 mL) and H_2O (0.5 mL), followed by BD-TMG (80 mg, 0.19 mmol). The reaction solution was then subjected to green LED light for 3 h and purified by precipitation in hexane (3 ×) and ethyl ether (1 ×) to yield final product.

3.3.3 Results and Discussions

BLG-NCA was deliberately selected as the model monomer for this study, owing to its ready synthesis in high purity and favorable yield. The ring-opening polymerization of NCA was executed in the presence of BD-TMG (1 equivalent) and NCA (20 equivalent) within a dry DMF solvent under a nitrogen atmosphere at room temperature. As illustrated in Scheme 3.1, green light irradiation prompts the photo-uncaging of "superbase" TMG from BD-TMG, concurrently stabilizing the BODIPY cation to BD-OH. Subsequently, the alcohol group in BD-OH initiates the ring-opening of NCA, thus initiating the polymerization process. Simultaneously, the photo uncaged TMG serves to catalyze the polymerization reaction further. This reaction may persist until all NCA monomers have been consumed or until it is terminated via the introduction of a terminating agent, such as an acid. The resultant polypeptides, in turn, exhibit controlled molecular weights contingent on the ratio of BD-TMG to BLG-NCA. In contrast to traditional ROP of NCA, BD-TMG photoinduced ROP obviates the need for additional initiators and catalysts. Furthermore, it affords both temporary and spatial control over ROP polymerization.

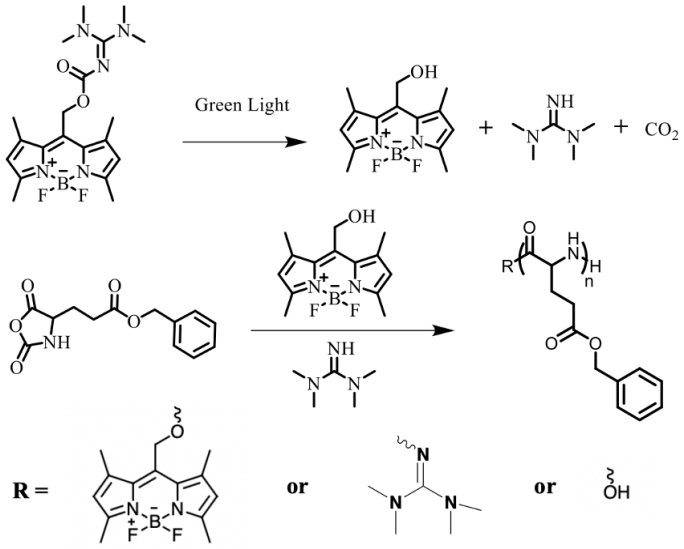

Scheme 3.1 Photo-triggered ROP of BLG-NCA using BD-TMG under green light irradiation.

Subsequently, the end groups of polypeptides prepared by the BD-TMG photoinduced ROP polymerization were investigated by mass spectroscopy (Fig. 3.11). As the Figure 3.11 shown, the end groups of the polypeptides can be either BODIPY, TMG or hydroxyl end group. This demonstrates that in the NCA ring-opening polymerization reaction, not only BD-OH but also TMG and water in the solvent can act as initiators. According to this reference,[108] the reactivity of the alcohol in ring-opening polymerization is significantly higher than that of TMG and water.

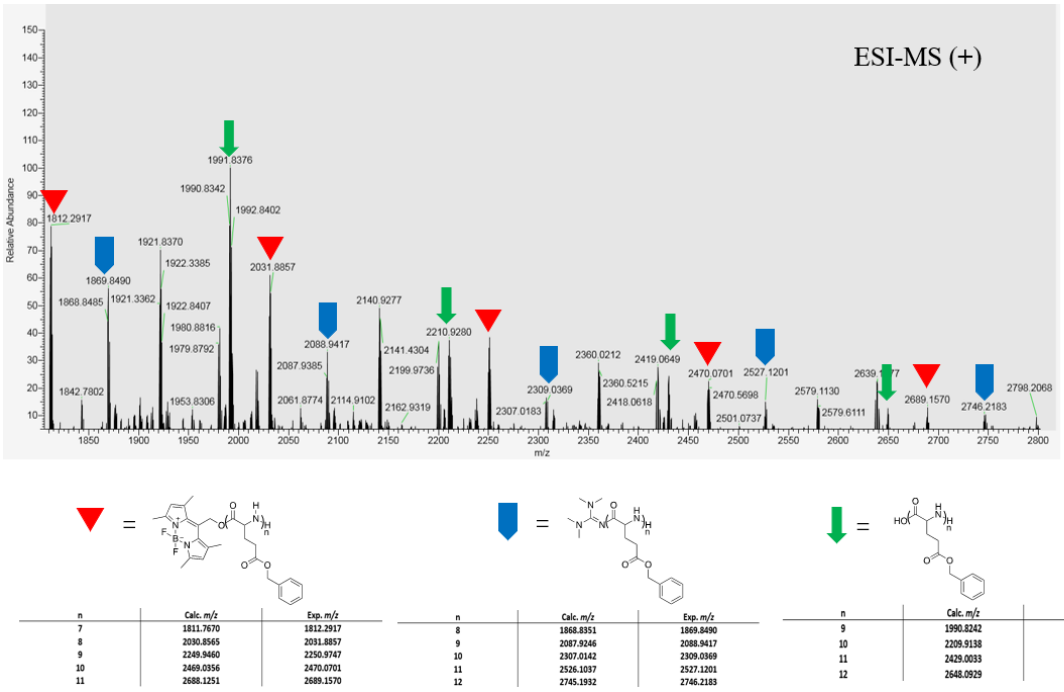

n	Calc. m/z	Exp. m/z
7	1811.7670	1812.2917
8	2030.8565	2031.8857
9	2249.9460	2250.9747
10	2469.0356	2470.0701
11	2688.1251	2689.1570

n	Calc. m/z	Exp. m/z
8	1868.8351	1869.8490
9	2087.9246	2088.9417
10	2307.0142	2309.0369
11	2526.1037	2527.1201
12	2745.1932	2746.2183

n	Calc. m/z	Exp. m/z
9	1990.8242	1991.8376
10	2209.9138	2210.9280
11	2429.0033	2419.0649
12	2648.0929	2649.0981

Fig 3.11 MS spectra of PBLG obtained via the initiation by BD-TMG.

3.3.4 Conclusion

In conclusion, we successfully employed BD-TMG as a photo-initiator and catalyst for the ring-opening polymerization of BLG-NCA. The inclusion of additional alcohol as an initiator for the ring-opening reaction is unnecessary in this process, as the photolysis product BD-OH from BD-TMG serves as an effective initiator for ring-opening polymerization. Moreover, the strong base TMG acts as a catalyst, further enhancing the polymerization reaction. High-resolution mass spectrometry was utilized to monitor the products of ring-opening polymerization, leading to the identification of three PBLG products with distinct end groups: polymers terminated with BODIPY, TMG, and OH. Our subsequent efforts involve controlling the photocatalytic ring-opening polymerization product by adjusting the initiator-to-monomer ratio. The purified polymer with BODIPY as the terminal group was subjected to cell imaging and toxicity testing.

CHAPTER 4

REGULATE LYSOSOMAL PH WITH LIGHT AND PHOTOBASE GENERATOR

4.1 Introduction

Lysosomes are membrane-bound, highly acidic intracellular organelles, that play important roles in numerous cellular processes including breakdown of macromolecules, worn-out organelles, endocytosis, autophagy, phagocytosis etc.[127] The pH value of the lysosomal is maintained at a range of 4.5 to 5.5, which provides an optimal catalytic environment for various acid hydrolysis enzymes that degrade engulfed biomolecules such as proteins, lipids, and nucleic acids.[128, 129] However, series of recent studies identified that impairment of lysosomal acidification affects the structural integrity and functional balance of lysosome.[127, 130, 131] In fact, dysregulation of lysosomal pH value disrupts cellular phagocytosis and autophagy, which leads to lysosomal membrane permeabilization (LMP) and causes the leakage of multiple contents, cascade hydrolysis of cytoplasmic contents, and extensive cytoplasmic acidification, thus result in irreversible cell damage and even cell death.[131] Moreover, impaired structure and function of lysosomes may directly or indirectly lead to various diseases, such as cancer, neurodegenerative diseases, metabolic disorders, and cardiovascular diseases.[132-135] Therefore, lysosomal pH has gained increasing attention as a therapeutic target as well as in disease prevention in recent years.

Most cancer cells are starved of oxygen (hypoxia), which significantly hinders the reactive oxygen sensitized photodynamic therapy (PDT) for cancer treatment.[136, 137] In contrast, an oxygen-independent approach that directly disrupts lysosomal pH balance may circumvent this limitation. Currently, there are limited methods that can specifically target lysosomes and precisely regulate lysosomal pH.[138-140] The reported reagents for lysosomal pH modulation can be divided into two categories: 1) decreasing the lysosomal pH, and 2) increasing the lysosomal pH. Materials that lower the lysosomal pH include polyester, poly (lactic-co-glycolic acid) (PLGA), and photo-activated nanoparticles (paNP).[141] For example, Grinstaff and teammates utilized PLGA nanoparticles (with diameters of $\approx$ 100 nm) to target lysosomes and released lactic (pKa is 3.86) and glycolic acid (pKa is 3.83) upon polymer degradation.[142] In general, drugs for lysosomal pH elevation are mostly hydrophobic and the pKa of the basic components are higher than the basal lysosomal pH. Such properties facilitate the travel of the substances across lipid membranes and accumulate in lysosomes thanks to the pH gradient between lysosomes and cytosol.[127, 141] For example, hydroxychloroquine (HCQ) and chloroquine (CQ) are weak bases that have been proved to be efficient in many anticancer treatment due to their ability to inhibit lysosomal acidification.[143-148] Furthermore, Obatoclax can also target lysosomes and induce lysosomal pH elevation, lysosomal dysfunction, subsequent lysosomal permeabilization, and cell apoptosis.[149, 150] In addition, Vegi's group discovered s-triazine analogs for the usage as a lysosomal autophagy inhibitor. These s-triazine derivatives are basic compounds that can deacidify lysosomes inhibit the maturation of lysosomal enzymes and cause lysosomal dysfunction.[151] In summary, regulating the lysosomal pH to induce cell apoptosis is an intriguing anticancer strategy

with great potential. However, current drugs used in regulating lysosomal pH still have limitations, such as 1) off-target effects due to the lack of spatial and temporal control; 2) the effective components are weak acids or bases; 3) the requirement of additional fluorescent probes for tracking.

The strategy of using PAGs and PBGs to induce lysosomal pH change may overcome the above-mentioned limitations. PAGs and PBGs are a series of photosensitive compounds, which absorb the incident light and then release the acidic or basic species. They have found many applications in click reaction, photopolymerization, and photodynamic therapy.[152] However, there have been few reports of regulating the lysosomal pH through PAGs or PBGs. We first reported a series of sulfonium-based PAGs and used one-photon and two-photon techniques to selectively induce cell death upon photo-released acid in lysosomes.[136] This work inspired us to attempt to modulate lysosomal pH by PBGs. Recently, we developed one novel BODIPY based green-light-sensitive PBGs (BD-TMG) that can release a strong base (tetramethyl guanidine, TMG, conjugate acid pKa = 13.6) for photoinduced polymerization..[153] Furthermore, we confirmed that BD-TMG has a great ability to target lysosomes in cells. BD-TMG also exhibited no acute toxic effects, over a range of concentrations, in dark conditions. In contrast, after green LED light irradiation, BD-TMG showed significant cytotoxicity in HeLa cells. More importantly, using a confocal microscope, we successfully monitored the process of lysosomal pH elevation under green light irradiation, followed by lysosome rupture, and cell apoptosis. In summary, herein, we provide the first report of using PBGs to regulate lysosomal pH to induce cancer cell apoptosis.

4.2 Experimental Section

4.2.1 Materials and General Equipment

BD-TMG was synthesized according to our previous reported procedures. (1) All other reagents and solvent were purchased from commercial suppliers and used without further purification. UV-vis absorption spectra were recorded on a Tecan Infinite M200 PRO plate reader spectrometer. Cell images were recorded by a Zeiss LSM 780 confocal microscope. All the cell images were processed by ImageJ.

4.2.2 Cell Culture

Human cervical cancer cells HeLa were cultured in Dulbecco's Modified Eagle Medium (DMEM) supplemented with 10% fetal bovine serum, 1% penicillin/streptomycin at 37 °C in a humidified 5% CO_2 incubator.

4.2.3 Dark Cell Viability

To assess the cytotoxicity of BD-TMG, HeLa cells were cultured in the Dulbecco's Modified Eagle Medium (DMEM) supplemented with 10% fetal bovine serum, 1% penicillin/streptomycin at 37 °C in a humidified 5% CO_2. Cells were placed in 96 well plates and incubated until there are no fewer than 5×10^3 cells per well for the experiments. Next, cells were incubated with different concentrations of BD-TMG (1, 2.5, 5, 10, 20, 40, and 80 μM). After 22 h incubation, replace fresh cell culture medium into each well and then 20 μL of the Cell Titer 96 Aqueous One solution reagent (for MTS assay) was added into each well, followed by further incubation for 2 h at 37 °C.

The respective absorbance values were read on a Tecan Infinite M200 PRO plate reader spectrometer at 490 nm. Cell viabilities were calculated based on the following equation:

$$Cell\ viability\ (\%) = \frac{Abs^{s}_{490nm} - Abs^{D}_{490nm}}{Abs^{c}_{490nm} - Abs^{D2}_{490nm}} \times 100\% \quad (4.1)$$

Where Abs^{s}_{490}nm is the absorbance of the cells incubated with different concentrations of experimental probe solutions, Abs^{D}_{490}nm is the absorbance of cell-free well containing only BD-TMG at the concentration that was studied, Abs^{c}_{490}nm is the absorbance of cells alone incubated in the medium, and Abs^{D2}_{490}nm is the absorbance of the cell-free well.

4.2.4 BD-TMG Dark Stability Test

BD-TMG dark stability in cell culture medium. 1×10^{-5} M BD-TMG were dissolved in cell culture medium (DMEM with 10% FBS and 1% PS) for 1h, 2h, 3h, and 4h in dark condition separately. UV-vis absorption was recorded by a Tecan Infinite M200 PRO plate reader spectrometer (Figure 4.1). There are no significant changes of BD-TMG absorbance in different time with cell culture medium which demonstrate BD-TMG is stable in cell culture medium in the dark condition.

BD-TMG dark stability in different pH solution. 1×10^{-5} M BD-TMG were dissolved in pH=4, pH=7, and pH=10 solutions in the dark condition separately. UV-vis absorption was recorded by a Tecan Infinite M200 PRO plate reader spectrometer (Figure 4.2). There are no significant changes of BD-TMG absorbance in different pH solutions which demonstrate BD-TMG is stable in cell culture medium in the dark condition.

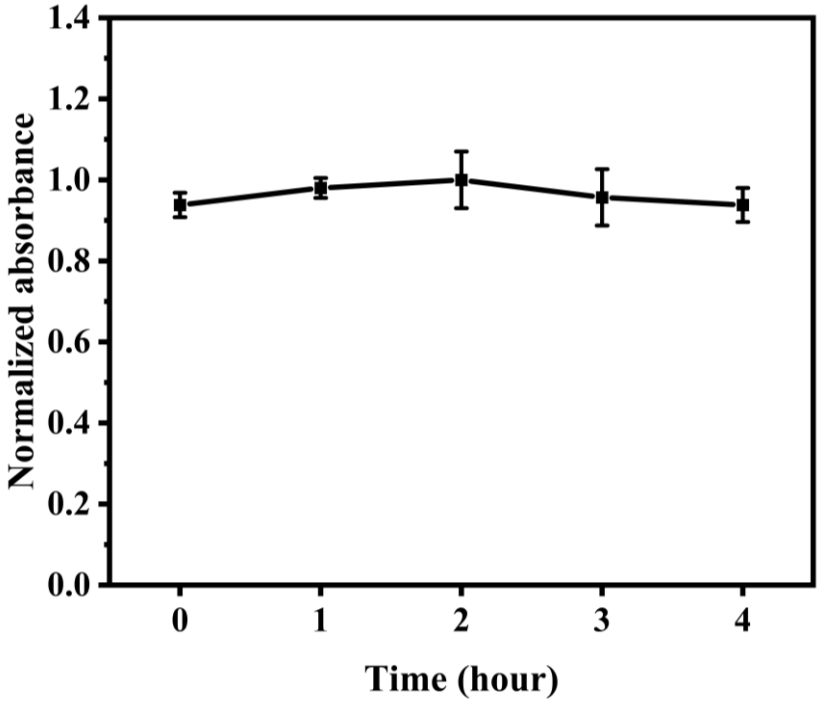

Fig 4.1 BD-TMG dark stability test in cell culture medium.

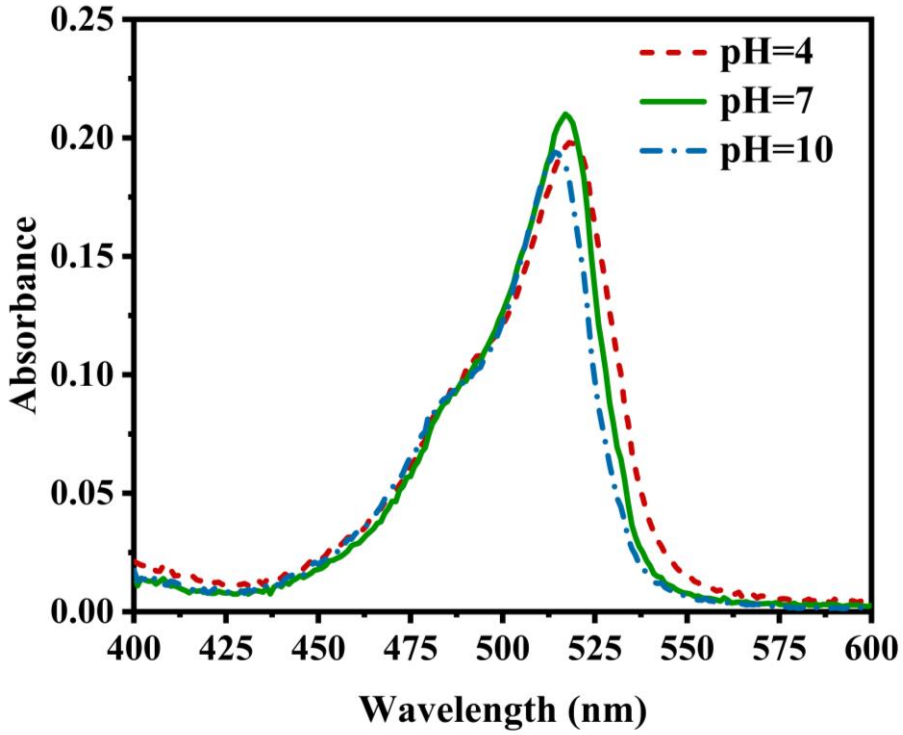

Fig 4.2 BD-TMG stability test in different pH environments.

4.2.5 Cellular Uptake and Colocalization

To investigate the efficiency and specificity of BD-TMG, HeLa cells were employed. All cells were seeded on confocal dish (MatTek) at the density of 4×10^4 cells per dish and incubated for 24 h at 37°C. Stock solution of BD-TMG dissolved in DMSO were prepared at a nominal concentration of 2 mM. The stock solution was diluted to 20 μM with DMEM cell medium and freshly placed over cells for a 30 min incubation period. Cells were washed three times with PBS and further incubated with LysoTracker™ Red DND-99 (working concentration: 75 nM) before cell imaging. Cells were then washed with PBS three times, and then the live cell imaging solution (Molecular Probes) was added to confocal dishes. Fluorescence images were obtained using a Zeiss LSM 780 confocal microscope (BD-TMG Ex: 514 nm, Em: 530~550 nm. LysoTracker™ Red DND-99 Ex: 561 nm; Em: 580 ~ 620 nm). Pearson's correlation coefficients were determined using ImageJ.

In addition, cell images for different concentrations of BD-TMG treated HeLa cell also collected. HeLa cells were treated with 5 μM, 10 μM, and 20 μM BD-TMG for 30 min separately. After washed with PBS three times, the live cell imaging solution was added. Fluorescence images were obtained using a Zeiss LSM 780 confocal microscope (BD-TMG Ex: 514 nm, Em: 530~550 nm). As Figure 4.3 shown.

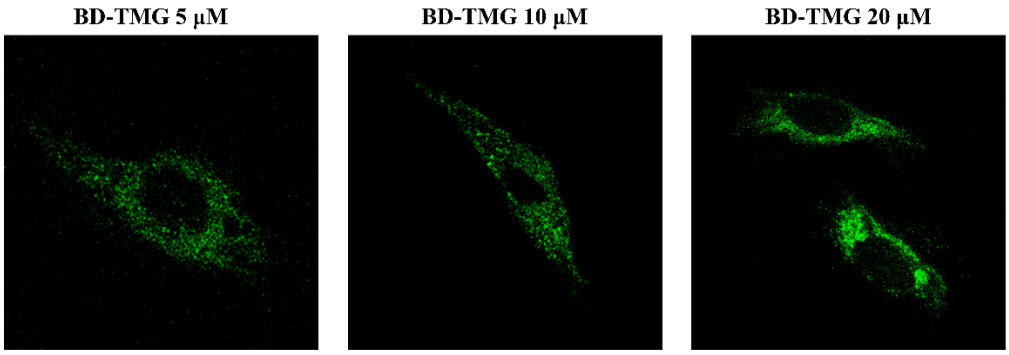

Figure 4.3 Cellular uptake image. HeLa cells were incubated with 5 μM, 10 μM, 20 μM of BD-TMG at 37 °C for 30 min separately, cell imaging was performed by confocal microscope after washing with PBS. (Ex: 514 nm, Em: 530~550 nm)

4.2.6 Lysosomal pH Measurement

For measuring the lysosomal pH changes in BD-TMG treated HeLa cells, HeLa cells were seeded on confocal dish at the density of 4×10^4 cells per dish and incubated for 24 h at 37°C. Then HeLa cells were incubated with 20 μM BD-TMG for 30 min. Cells were washed three times then 1000-fold dilution of pHLys Red (Lysosomal pH detection reagent. Order from Thermo Fisher Scientific) was added and incubated for another 30 min. In addition, for the control group, HeLa cells were only stained with 1000-fold dilution of pHLys Red for 30 min. The treated HeLa cells were used in photobleaching experiments by Zeiss LSM 780 confocal microscope.

Photobleaching experiments set up: photobleaching experiments performed on a Zeiss LSM780 scanning confocal microscope with 40× objective. The microscope was set to a pixel size of 0.19 μm and a pixel dwell time of 0.79 μsec. The pinhole was set to the maximum value. A 100 × 100 μm area was monitored by a 415 nm 100 mM diode laser at 100% maximum power for 80 scan cycles.

4.2.7 Time -lapse Cell Imaging

To observe lysosomal morphological changes during the BD-TMG photolysis. HeLa cells were employed. All cells were seeded on confocal dish (MatTek) at a density of 4 × 10^4 cells per dish and incubated for 24 h at 37 °C. HeLa cells were incubated with 20 μM of BD-TMG for 30 min. Cells were washed three times with PBS and the live cell imaging solution (Molecular Probes) was added to confocal dishes. BD-TMG was irradiated directly by the laser source of Zeiss LSM780 scanning confocal microscope a 415 nm 100 mM diode laser at 100% maximum power for 30 min.

4.3 Results and Discussion

BD-TMG is a BOIDPY-based PBG we developed recently that can absorb green light and then release a "super base" TMG (Figure 1a).[153] In addition, BD-TMG has a maximum absorbance of 520 nm and an emission maximum of 531 nm (Figure 4.4b). Compared with traditional PBGs that absorb high-energy UV and/or blue light, the advantages of visible light absorbance include less irradiation damage to cells and deeper light penetration depth.[56] Moreover, BD-TMG exhibits weak basicity before photolysis in the dark. The basicity of BD-TMG photo-released substance is much stronger than common lysosomal pH-elevating drugs, which helps alkalize the environment more efficiently. The mechanism of photolysis and release of TMG involves photo-cleavage and decarboxylation which is based on our previous report (Figure 4.4a).[153] It is worth noting that after releasing TMG, the main photolysis product is BD-OH in an aqueous solvent, which is a non-basic species. Moreover, the high fluorescence quantum yield of BD-TMG (Φ_f = 84%) permits easy tracking using a fluorescence confocal microscope.

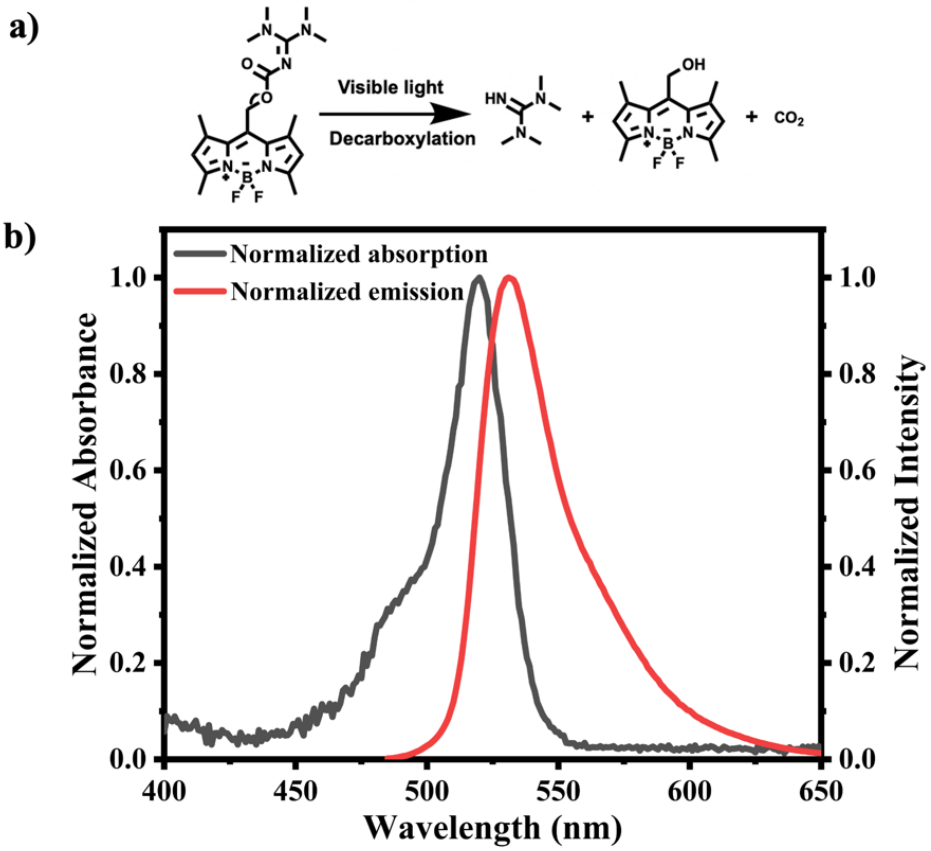

Figure 4.4 a) PBG BD-TMG releases strong base TMG under visible light. b) Normalized UV-vis absorption and emission of BD-TMG.

First, the dark stability of BD-TMG in a cell culture medium was performed by dissolving 1×10^{-5} M BD-TMG in a cell culture medium and UV-vis absorption was recorded to check the stability (Figure 4.1). During the measurement, there was no apparent change in BD-TMG absorption that indicated BD-TMG was stable in the cell culture medium in the absence of light. Moreover, we also dissolved 1×10^{-5} M BD-TMG in different pH solutions to analyze the pH stability. As Figure 4.2 showed, BD-TMG remains stable in different pH environments ranging from pH 4 to pH 10. After confirming the stability of BD-TMG in varied dark conditions, cellular uptake of BD-TMG was performed in HeLa cells after incubating with 5 μM, 10 μM, and 20 μM of BD-TMG at 37 °C for 30 min separately, After washing with PBS and replacing with

fresh cell culture medium, the treated cells showed clear fluorescence and the fluorescence intensity was increased with the increasing incubation concentration of BD-TMG, indicating higher cellular uptake (as shown in Figure 4.5).

In general, organic compounds that are hydrophobic and basic are easy to cross membranes and accumulate in lysosomes. For examples, daunorubicin (DNR), doxorubicin (DOX), mitoxantrone (MTX), chloroquine (CHQ), clomipramine (CLO).[154] Because BD-TMG is a weak base and hydrophobic, it should accumulate in lysosomes via the cation trapping mechanism due to the pH gradient between the cytoplasm and lysosomes.[155] Based on the reported lysosomal targeted hydrophobic weak base drug,[155] we presume that BD-TMG can diffuse across membranes because of its hydrophobicity and BD-TMG will be sequestered in lysosomal acid lumen caused by the protonation. To confirm the lysosomal targeting capability of BD-TMG, the colocalization study of BD-TMG in HeLa cells was monitored using a ZEISS confocal fluorescence microscopy and compared with commercial lysosomal targeting dye Lysotracker Red (as Figure 4.5 shown). HeLa cells were treated with 20 μM of BD-TMG for 30 min, after washing the cells were stained with LysoTracker Red (Ex: 561 nm; Em: 580 ~ 620 nm). Fluorescence images were recorded and the distribution of BD-TMG showed good colocalization with LysoTracker Red with Pearson's correlation coefficient value of 0.83. The degree of colocalization Pearson value indicates that BD-TMG was mainly localized in the lysosomes after 30 min of coincubation.

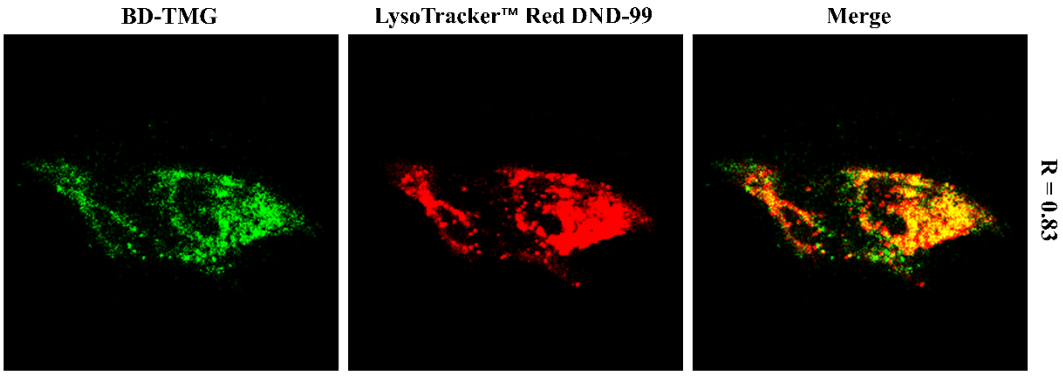

Figure 4.5 HeLa cell incubated with 20 μM of BD-TMG (green channel, Ex: 514 nm, Em: 530~550 nm) at 37 °C for 30 min. After washed by PBS 3 times, commercial dye (LysoTracker™ Red DND-99, 75 nM) was added in treated HeLa cell for another 30 min. Pearson's colocalization values is shown as R.

To further demonstrate the ability of BD-TMG in the regulation of lysosomal pH, we conducted co-staining experiments of HeLa cells with BD-TMG and pHLys Red. pHLys Red is a commercial lysosomal pH fluorescence indicator, which accumulates in the intact lysosome, and its fluorescence intensity decreases as the basicity increases. HeLa cells were incubated with 20 μM BD-TMG for 30 min, after washed with PBS, 1000-fold diluted pHLys Red was added and incubated for another 30 min. The treated HeLa cells were used in cell imaging (pHLys channel: Ex: 561nm, Em: 560 ~ 650 nm). As shown in Fig. 4.6a), the same group has HeLa cells treated with both BD-TMG and pHLys Red, and the pHLys channel exhibited a clear basicity increase when BD-TMG was activated under a 514 nm laser in a time-dependent manner. This result indicates that BD-TMG can increase lysosomal pH under green light. Moreover, to count the effects of pHLys Red photobleaching due to prolonged exposure to light, we also ran a control group that stained with pHlys Red only and conducted the laser irradiation experiments at the same condition. The results showed a slight fluorescence decrease in the control group due to photobleaching of pHLys, but not as significant as the sample when BD-

TMG was introduced. This further suggests that the elevation of lysosomal pH was caused by basic species release from BD-TMG. To quantitatively assess the fluorescence intensity changes from the light activation of BD-TMG, we carried out real-time intensity monitoring experiments (Figure 4.6). A confocal microscope was utilized to record the fluorescence intensity of the pHLys channel of the experimental group and control group. The results showed that the normalized fluorescence intensity of the control group only decreased by about 25%, however, there was an almost 60% fluorescence intensity decrease in the experimental group, which strongly indicates that BD-TMG is effective in elevating lysosomal pH.

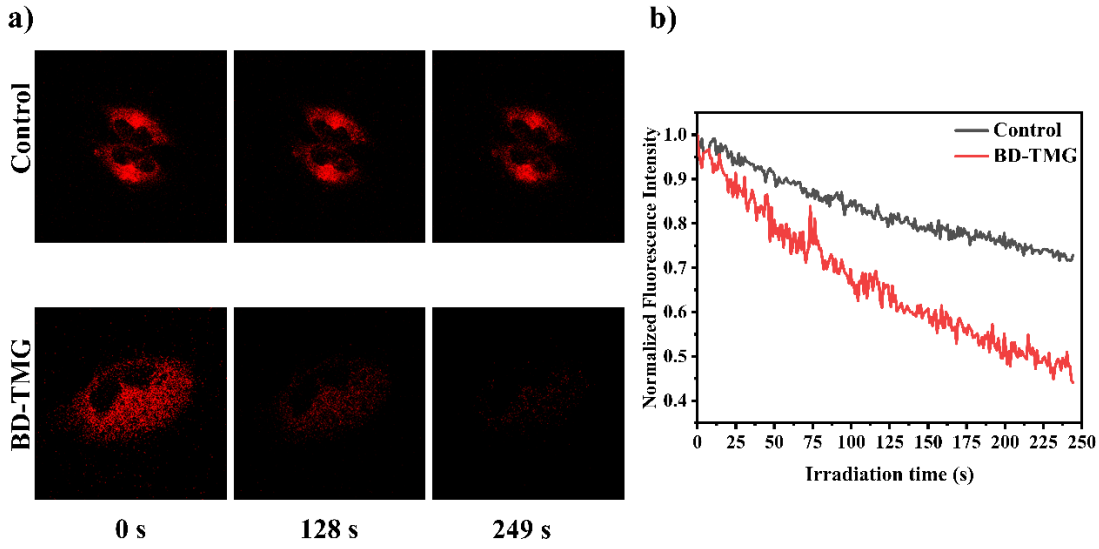

Fig 4.6 a) Time-lapse cell imaging of HeLa cells treated with 20 μM BD-TMG and 1000-fold dilution of pHLys Red, and HeLa cells only stained with pHLys Red (Control group) separately exposed to varied time of 514 nm laser light (pHLys Red Ex:561 nm, Em: 560 ~ 650 nm). b) Fluorescence intensity of BD-TMG group and control group (Fluorescence intensities were recorded by Zeiss LSM 780 confocal microscope).

Lysosomes are highly dynamic organelles that can move rapidly in cells.[156] After demonstrating the feasibility of lysosomal pH regulation using BD-TMG and light, we

then performed time-lapsed cell imaging to monitor the cells' morphologies during treatment. HeLa cells were incubated with 20 μM BD-TMG for 30 min, after washing and removing the extracellular BD-TMG, the cells were used in the light activation experiments. The sample was irradiated continuously with direct 514 nm laser light from the Zeiss LSM 780 confocal microscope, and fluorescence images were recorded from 0 to 30 min (Ex: 514 nm, Em: 530~550 nm) (As shown in Figure 4.7). The time-lapse images clearly exhibit that BD-TMG treatment resulted in fluorescent substances gradually diffuse into the cytoplasm with the laser irradiation. This change may be caused by photolyzed BD-TMG increasing lysosomal pH, thus increasing lysosomal membrane permeability, causing the leakage of BD-TMG and its photolyzed fluorescent product from the lysosomes into the cytoplasm. This phenomenon is very similar to the HCQ treatment cells, which showed leakage of lysosomal and cell structure broken.[157] We also conducted imaging experiments to observe the cell's morphology changes after light activation for varied times. HeLa cells were stained with 20 μM BD-TMG for 30 min, followed by removed extracellular BD-TMG, the treated cells were irradiated by 514 nm green laser light for 30 min. The samples were then returned to the incubator for varied times (0 min, 30 min, and 60 min) before cell imaging. As shown in Figure 4.8, the BD-TMG treated HeLa cells' morphology gradually transits from willow leaf shape to round shape as the incubation time increases. Such cell shrinkage and the loss of cell volume is a ubiquitous characteristic of programmed cell death.[158] Such programmed cell death has been reported in many cases, for example glucocorticoid (dexamethasone) treatment rat thymocytes,[159] radiation-induced cell death.[160]

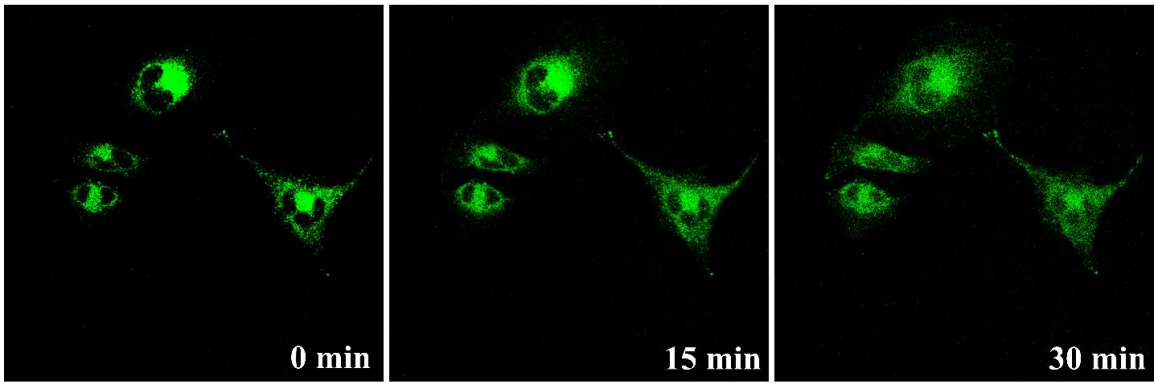

Figure 4.7 20 μM of BD-TMG-treated time-lapse cell imaging. HeLa cells were incubated with 20 μM BD-TMG for 30 min. After washing with PBS, time-lapse cell images were captured from 0 min to 30 min. (Ex: 514 nm, Em: 530~550 nm)

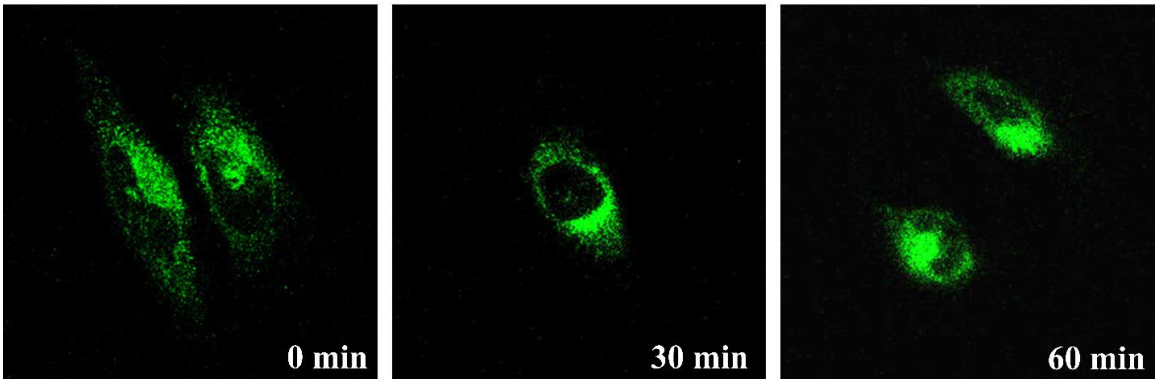

Figure 4.8 Cell imaging of HeLa cells treated with 20 μM BD-TMG and exposed to 30 min of 514 nm green laser light and then back to incubator for varied time (0 min, 30 min, 60 min).

Finally, the biocompatibility of BD-TMG in the dark and the cytotoxicity under light were evaluated using HeLa cells and MTS assays. The dark cell viability of BD-TMG showed no acute toxic effects in the range of concentrations from 1 to 40 μM. Even at 40 μM of BD-TMG, the cell viability remains over 80% (Figure. 4.9a). In addition, we utilized BD-OH (the main photolysis product of BD-TMG) as a control group to confirm the toxic effects is due to the light-triggered releasing of TMG not the byproduct BD-OH. The dark cell viability of BD-OH showed lower cytotoxicity than BD-TMG. Next, to assess the photolysis cytotoxicity of BD-TMG, irradiation time-dependent cell viability

experiments were performed (Figure. 4.9b). It is obvious that the viability of cells treated with BD-TMG and light was significantly decreased with increasing irradiation time, and the cell viability reached the minimum after 15 min under light. However, in the control group using photolysis product BD-OH, cells didn't show any cytotoxicity during the light irradiation at the same concentration. These results prove that the alkaline substances released by BD-TMG are the major cause of HeLa cell death.

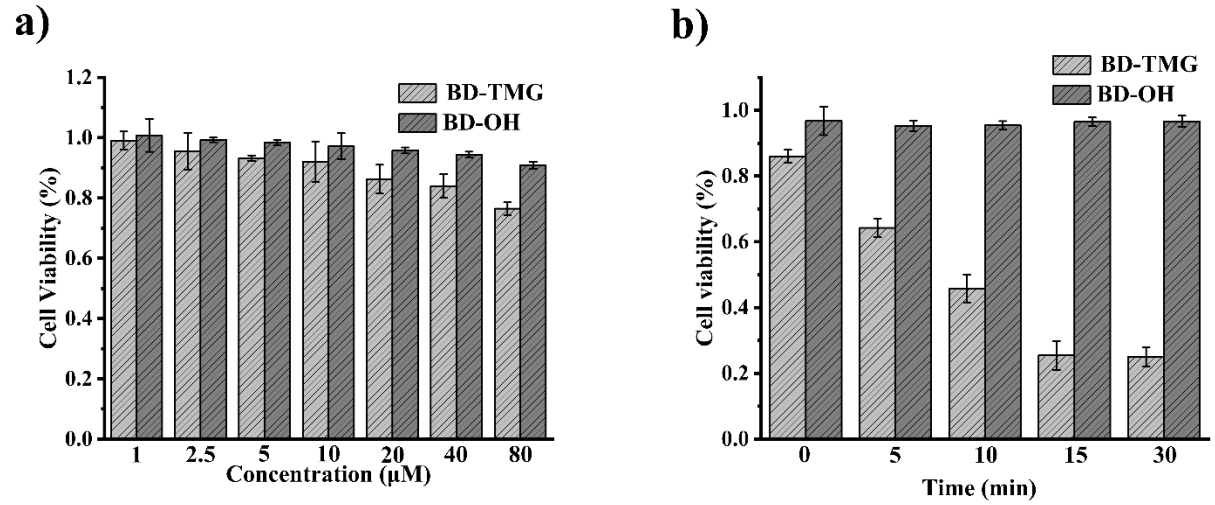

Figure 4.9 a) Dark cell viability. Cell viability of HeLa cells treated with varied concentrations (1, 2.5, 5, 10, 20, 40, and 80 μM) of BD-TMG and BD-OH at 37°C for 24 h separately. Untreated cells were classified as 100% cell viability (N=6). b) Irradiation Time-dependent cell viability. HeLa cells were treated with 20 μM BD-TMG and BD-OH for 30 min separately. After replaced fresh cell culture medium, treated cells were irradiated by Thorlabs M505L3 LED light for following time (0 min, 5 min, 10 min, 15 min and 30 min) then incubated for 24 h. Ligh source: nominal wavelength 505 nm, power density 80 mW/cm^2, irradiated distance is 1 cm. cell with no irradiation and drug treatment classified as 100%. (N=6)

4.4 Conclusion

In conclusion, we demonstrated that a BODIPY-based PBG (BD-TMG) can be used to selectively induce HeLa cell death via light-induced base release in lysosomes. This opens the possibility of using PBGs as anticancer drugs to directly regulate the pH of organelles to trigger cell death. In this work, in vitro experiments demonstrated that BD-TMG can target lysosomes and regulate lysosomal pH. Moreover, time-lapse cell imaging exhibited the morphology changes of BD-TMG treated HeLa cells. At last, cell viability demonstrated that BD-TMG was an efficient tool to induce cell death.

CHAPTER 5

FUTURE PLANS

In light of our research endeavors, we have successfully developed BODIPY-based compounds for drug delivery, base release, and fluorescence sensing applications. These derivatives have demonstrated specific utility in photopolymerization and anticancer therapy. Nevertheless, in our pursuit of enhancing the efficiency of base photo-release in the context of PBGs, further refinements are warranted. An avenue for optimization entails halogenating the BODIPY core with additional halogen atoms, such as fluorine, chlorine, bromine, or iodine. Furthermore, with respect to BD-I-TMG, where a single iodine atom is introduced into the BODIPY core, potential modifications encompass the introduction of iodine on both sides of the BODIPY core. Moreover, an alternative approach involves employing methylmagnesium bromide to replace the fluorine atom with methyl group, thereby amplifying the photo-uncaging efficacy. Detailed molecular structures are depicted in Figure 5.1 for reference.

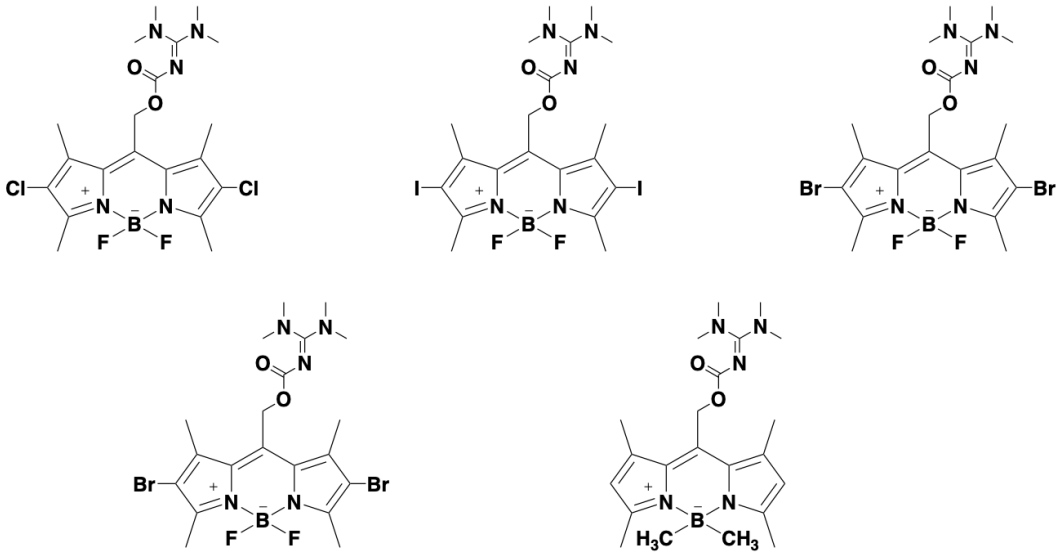

Figure 5.1 Modification of BODIPY core.

Moreover, it is worth noting that BD-TMG and BD-I-TMG exhibit absorption properties limited to the green light spectrum, thereby impinging on their suitability for certain biological applications. To address this limitation and broaden their utility, an avenue for improvement resides in the extension of their light-responsive wavelengths into the far-red range through molecular modification. For instance, a viable strategy involves the introduction of fused ring functional groups at the 3 and 5 positions of the BODIPY structure via microwave-assisted reactions, thereby enhancing the overall conjugation of the molecule. This structural refinement results in a consequential extension of both the absorption and emission wavelengths, thereby enhancing the range of potential applications. (As shown in Figure 5.2).

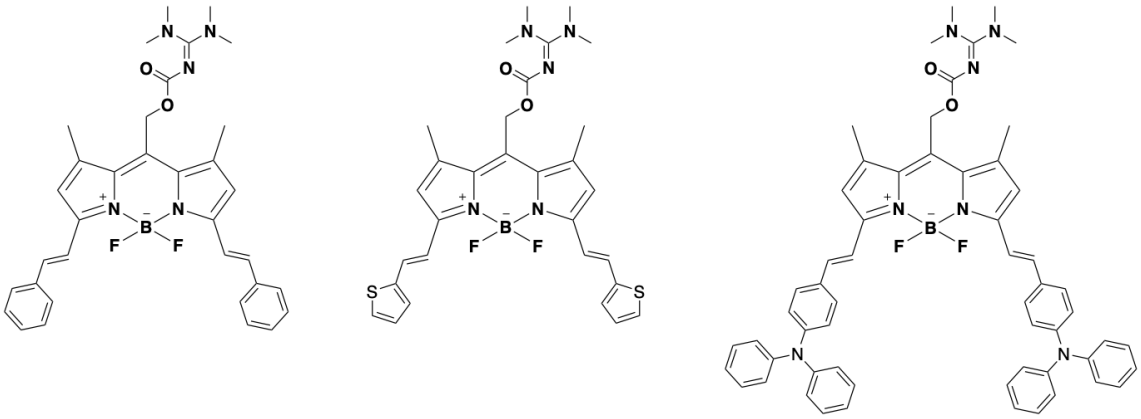

Figure 5.2 Examples of BODIPY modifications.

APPENDIX

^{1}H NMR ^{13}C NMR ^{19}F NMR AND MASS SPECTRUM

Figure A.1 to A.11 show ^{1}H NMR ^{13}C NMR ^{19}F NMR and mass spectrum of BD-OAc, BD-OH, BD-I-OH, BD-TMG, BD-I-TMG and BLG-NCA.

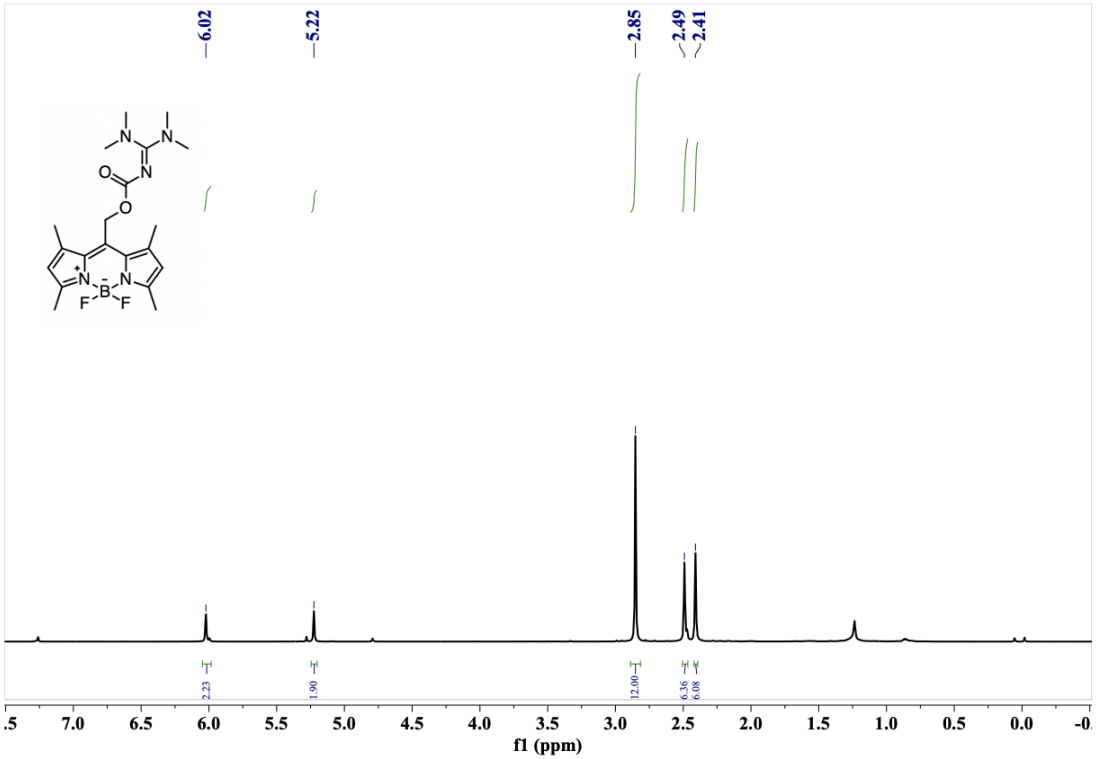

Figure A.1 ^{1}H NMR of BD-TMG.

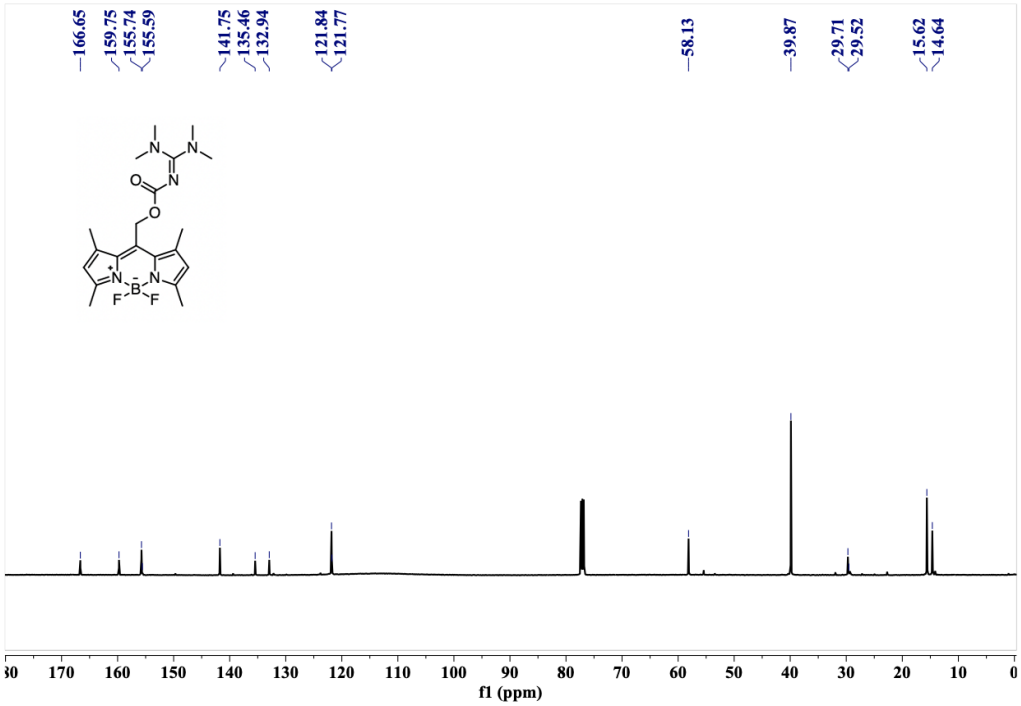

Figure A.2 ^{13}C NMR of BD-TMG.

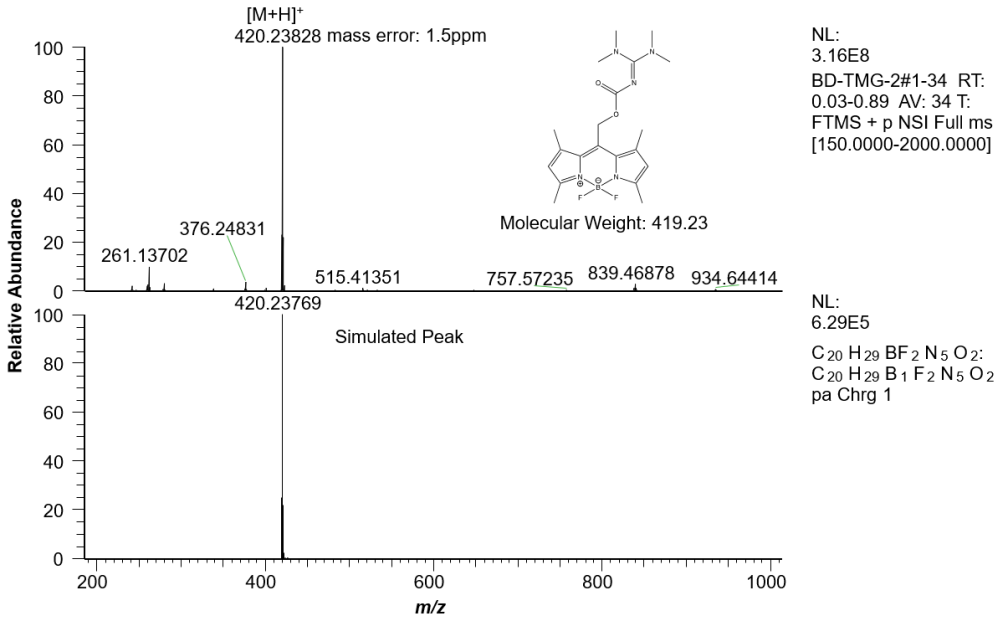

Figure A.3 Mass spectrum of BD-TMG.

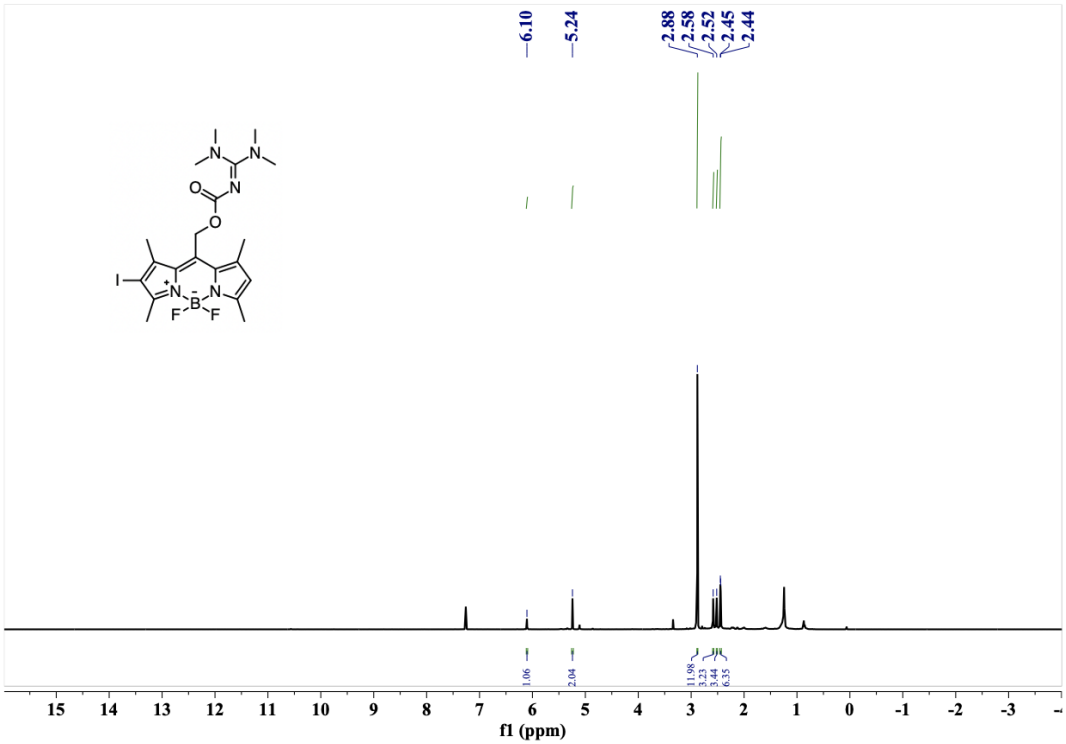

Figure A.4 ^{1}H NMR of BD-I-TMG.

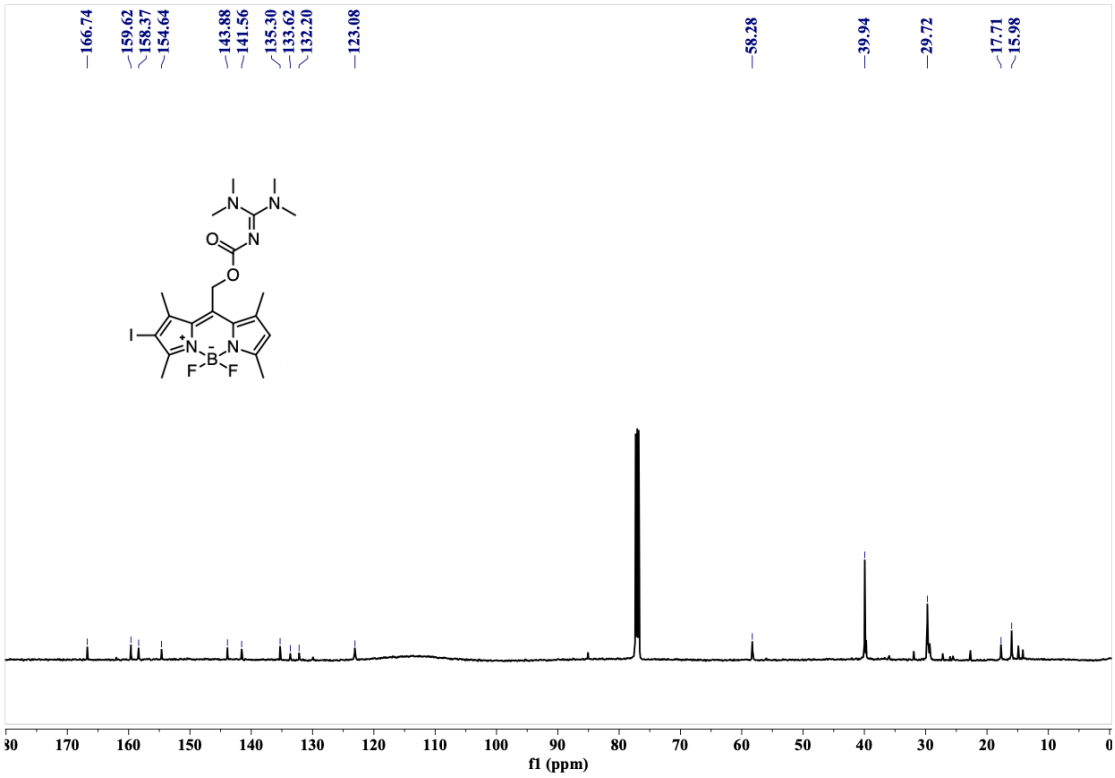

Figure A.5 ^{13}C NMR of BD-I-TMG.

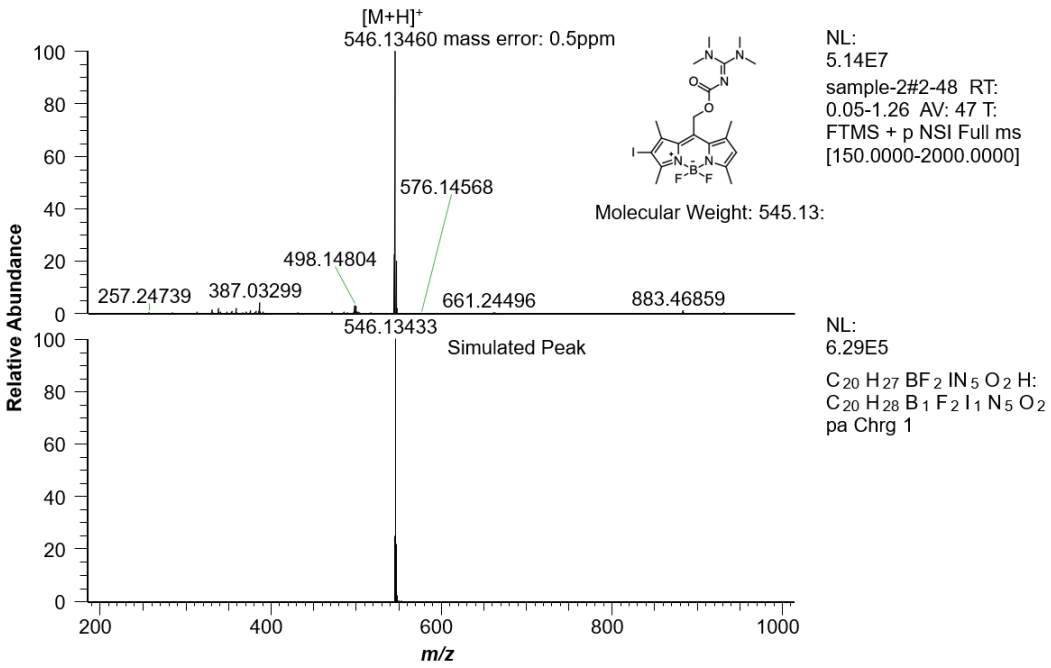

Figure A.6 Mass spectrum of BD-I-TMG.

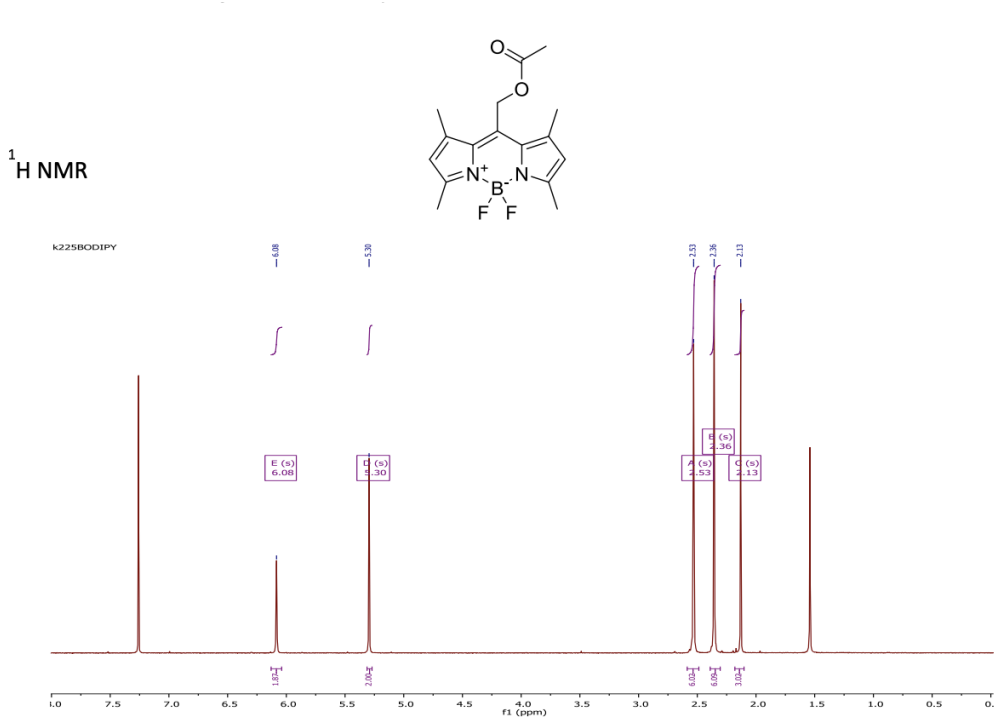

Figure A.7 ^{1}H NMR of BD-OAc.

^{19}F NMR

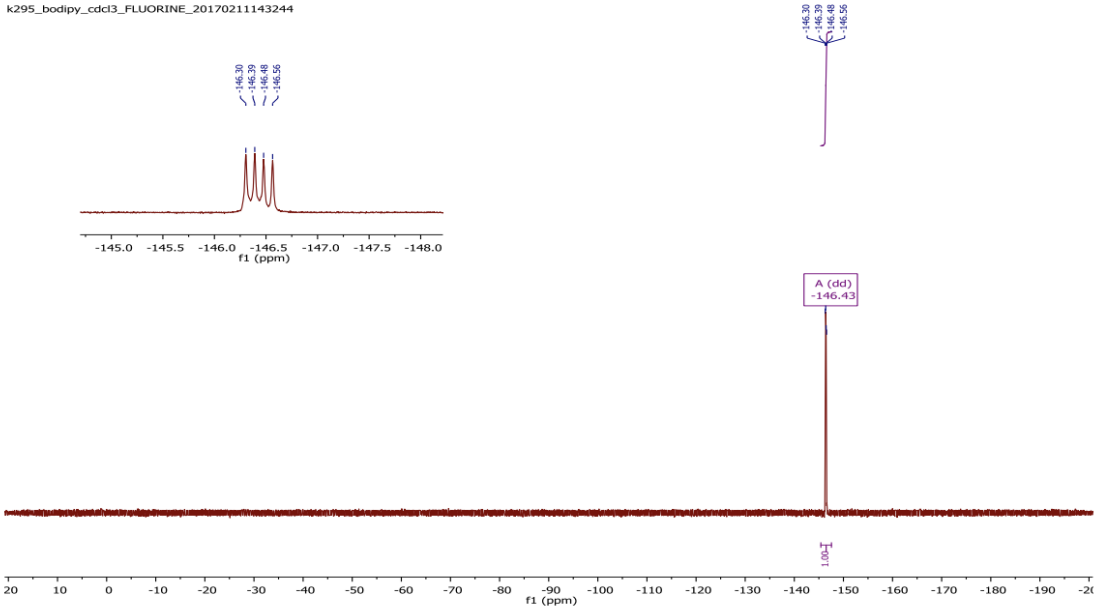

Figure A.8 ^{19}F NMR of BD-OAc.

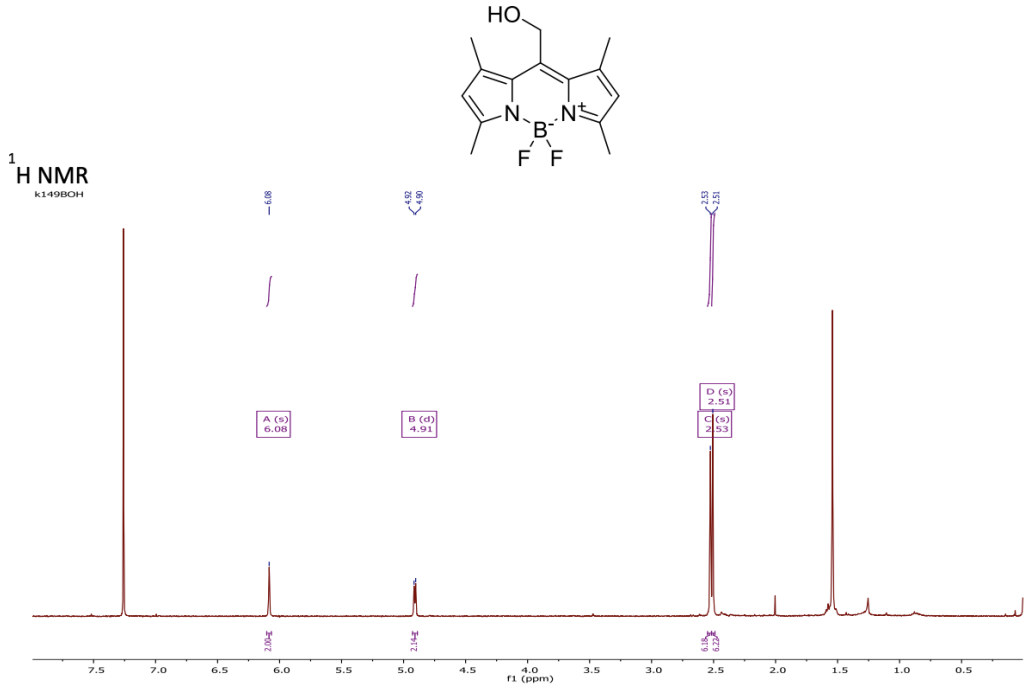

Figure A.9 ^{1}H NMR of BD-OH.

^{19}F NMR

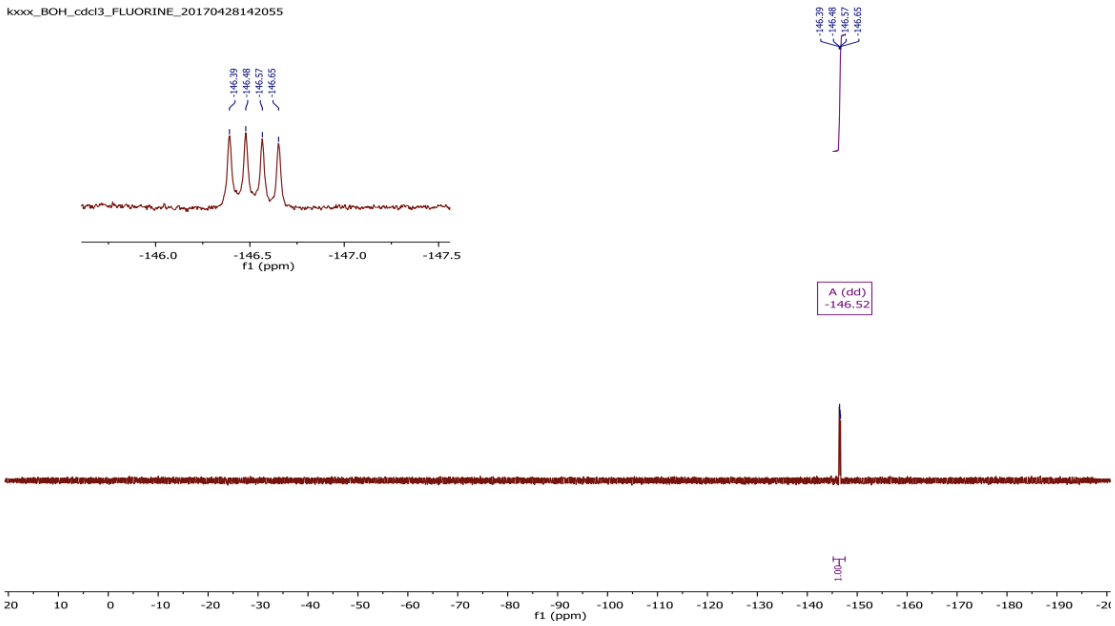

Figure A.10. ^{19}F NMR of BD-OH.

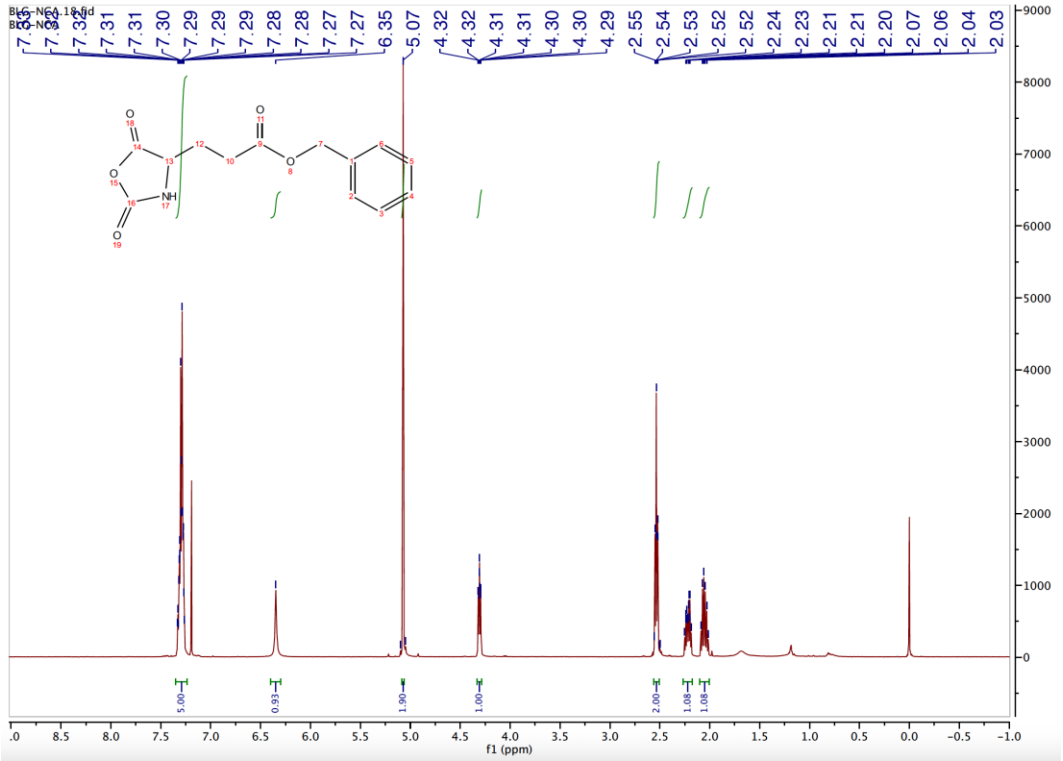

Figure A.11 ^{1}H NMR of BLG-NCA.

REFERENCES

1. Shirai, M. and Tsunooka, M., "Photoacid and photobase generators: chemistry and applications to polymeric materials." *Progress in Polymer Science* 21.1 (**1996**): 1-45.

2. Crivello, J.V. and Reichmanis, E., "Photopolymer materials and processes for advanced technologies." *Chemistry of Materials* 26.1 (**2014**): 533-548.

3. Baltazar, J., Sojoudi, H., Paniagua, S.A., Zhang, S., Lawson, R.A., Marder, S.R., Graham, S., Tolbert, L.M. and Henderson, C.L., "Photochemical doping and tuning of the work function and dirac point in graphene using photoacid and photobase generators." *Advanced Functional Materials* 24.32 (**2014**): 5147-5156.

4. Crivello, J.V. and Lam, J.H.W., "Diaryliodonium salts. A new class of photoinitiators for cationic polymerization." *Macromolecules* 10.6 (**1977**): 1307-1315.

5. Zivic, N., Bouzrati-Zerrelli, M., Villotte, S., Morlet-Savary, F., Dietlin, C., Dumur, F., Gigmes, D., Fouassier, J.P. and Lalevee, J., "A novel naphthalimide scaffold based iodonium salt as a one-component photoacid/photoinitiator for cationic and radical polymerization under LED exposure." *Polymer Chemistry* 7.37 (**2016**): 5873-5879.

6. Kumi, G., Yanez, C.O., Belfield, K.D. and Fourkas, J.T., "High-speed multiphoton absorption polymerization: fabrication of microfluidic channels with arbitrary cross-sections and high aspect ratios." *Lab on a Chip* 10.8 (**2010**): 1057-1060.

7. Cameron, J.F. and Frechet, J.M., "Base catalysis in Imaging Materials. 1. Design and synthesis of novel light-sensitive urethanes as photoprecursors of amines." *The Journal of Organic Chemistry* 55.23 (**1990**): 5919-5922.

8. Okamura, H., Terakawa, T., Suyama, K. and Shirai, M., "Reworkable photocrosslinking system using multifunctional epoxides and photobase generators." *Journal of Photopolymer Science and Technology* 19.1 (**2006**): 85-88.

9. Zivic, N., Kuroishi, P.K., Dumur, F., Gigmes, D., Dove, A.P. and Sardon, H., "Recent advances and challenges in the design of organic photoacid and photobase generators for polymerizations." *Angewandte Chemie International Edition* 58.31 (**2019**): 10410-10422.

10. Salmi, H., Allonas, X. and Ley, C., "Polythiourethane networks catalyzed by photobase generators." *Progress in Organic Coatings* 100 (**2016**): 81-85.

11. Placet, E., Pinaud, J., Gimello, O. and Lacroix-Desmazes, P., "UV-Initiated ring opening polymerization of L-lactide using a photobase generator." *ACS Macro Letters* 7.6 (**2018**): 688-692.

12. Zivic, N., Sadaba, N., Almandoz, N., Ruiperez, F., Mecerreyes, D. and Sardon, H., "Thioxanthone-Based photobase generators for the synthesis of polyurethanes via the photopolymerization of polyols and polyisocyanates." *Macromolecules* 53.6 (**2020**): 2069-2076.

13. Barner‐Kowollik, C., Bastmeyer, M., Blasco, E., Delaittre, G., Müller, P., Richter, B. and Wegener, M., "3D laser micro‐and nanoprinting: challenges for chemistry." *Angewandte Chemie International Edition* 56.50 (**2017**): 15828-15845.

14. Sarker, A.M., Kaneko, Y., Nikolaitchik, A.V. and Neckers, D.C., "Photoinduced Electron-Transfer Reactions: Highly Efficient Cleavage of C− N Bonds and Photogeneration of Tertiary Amines." *The Journal of Physical Chemistry A* 102.28 (**1998**): 5375-5382.

15. Sarker, A. and Neckers, D., "Tetraorganylborate salts as convenient precursors for photogeneration of tertiary amines." *Journal of the Chemical Society, Perkin Transactions* 2 10 (**1998**): 2315-2322.

16. Kaneko, Y., Sarker, A.M. and Neckers, D.C., "Mechanistic Studies of Photobase Generation from Ammonium Tetraorganyl Borate Salts[1]." *Chemistry of materials* 11.1 (**1999**): 170-176.

17. Sarker, A.M., Kaneko, Y. and Neckers, D.C., "Electron transfer followed by double fragmentation reactions: mechanism of photogeneration of tertiary amines and radicals from tetraorganyl borates." *Journal of Photochemistry and Photobiology A: Chemistry* 121.2 (**1999**): 83-90.

18. Suyama, K. and Shirai, M., "Photobase generators: Recent progress and application trend in polymer systems." *Progress in Polymer Science* 34.2 (**2009**): 194-209.

19. Sun, X., Gao, J.P. and Wang, Z.Y., "Bicyclic guanidinium tetraphenylborate: a photobase generator and a photocatalyst for living anionic ring-opening polymerization and cross-linking of polymeric materials containing ester and hydroxy groups." *Journal of the American Chemical Society* 130.26 (**2008**): 8130-8131.

20. Xi, W., Peng, H., Aguirre-Soto, A., Kloxin, C.J., Stansbury, J.W. and Bowman, C.N., "Spatial and temporal control of thiol-Michael addition via photocaged superbase in photopatterning and two-stage polymer networks formation." *Macromolecules* 47.18 (**2014**): 6159-6165.

21. Xi, W., Krieger, M., Kloxin, C.J. and Bowman, C.N., "A new photoclick reaction strategy: photo-induced catalysis of the thiol-Michael addition via a caged primary amine." *Chemical communications* 49.40 (**2013**): 4504-4506.

22. Zhang, X., Xi, W., Gao, G., Wang, X., Stansbury, J.W. and Bowman, C.N., "o-Nitrobenzyl-based photobase generators: efficient photoinitiators for visible-light induced thiol-michael addition photopolymerization." *ACS Macro Letters* 7.7 (**2018**): 852-857.

23. Zhang, X., Xi, W., Wang, C., Podgórski, M. and Bowman, C.N., "Visible-light-initiated thiol-Michael addition polymerizations with Coumarin-based photobase generators: another photoclick reaction strategy." *ACS Macro Letters* 5.2 (**2016**): 229-233.

24. Lalevée, J., Allonas, X., Fouassier, J.P., Tachi, H., Izumitani, A., Shirai, M. and Tsunooka, M., "Investigation of the photochemical properties of an important class of photobase generators: the O-acyloximes." *Journal of Photochemistry and Photobiology A: Chemistry* 151.1-3 (**2002**): 27-37.

25. Ohba, T., Nakai, D., Suyama, K. and Shirai, M., "Photo-crosslinking of poly (glycidyl methacrylate) using di-functional photobase generators." *Journal of Photopolymer Science and Technology* 17.1 (**2004**): 11-14.

26. Boens, N., Verbelen, B., Ortiz, M.J., Jiao, L. and Dehaen, W., "Synthesis of BODIPY dyes through postfunctionalization of the boron dipyrromethene core." *Coordination Chemistry Reviews* 399 (**2019**): 213024.

27. Chen, X., Wang, F., Hyun, J.Y., Wei, T., Qiang, J., Ren, X., Shin, I. and Yoon, J., "Recent progress in the development of fluorescent, luminescent and colorimetric probes for detection of reactive oxygen and nitrogen species." *Chemical Society Reviews* 45.10 (**2016**): 2976-3016.

28. Kolanowski, J.L., Liu, F. and New, E.J., "Fluorescent probes for the simultaneous detection of multiple analytes in biology." *Chemical Society Reviews* 47.1 (**2018**): 195-208.

29. Chen, Y., Li, L., Chen, W., Chen, H. and Yin, J., "Near-infrared small molecular fluorescent dyes for photothermal therapy." *Chinese Chemical Letters* 30.7 (**2019**): 1353-1360.

30. Kowada, T., Maeda, H. and Kikuchi, K., "BODIPY-based probes for the fluorescence imaging of biomolecules in living cells." *Chemical Society Reviews* 44.14 (**2015**): 4953-4972.

31. Fan, Y., Lu, M., Yu, X.A., He, M., Zhang, Y., Ma, X.N., Kou, J., Yu, B.Y. and Tian, J., "Targeted myocardial hypoxia imaging using a nitroreductase-activatable near-infrared fluorescent nanoprobe." *Analytical Chemistry* 91.10 (**2019**): 6585-6592.

32. He, H., "Near-infrared emitting lanthanide complexes of porphyrin and BODIPY dyes." *Coordination Chemistry Reviews* 273 (**2014**): 87-99.

33. Hermes, R.E., Allik, T.H., Chandra, S. and Hutchinson, J.A., "High‐efficiency pyrromethene doped solid‐state dye lasers." *Applied Physics Letters* 63.7 (**1993**): 877-879.

34. Loudet, A. and Burgess, K., "BODIPY dyes and their derivatives: syntheses and spectroscopic properties." *Chemical Reviews* 107.11 (**2007**): 4891-4932.

35. Zhao, J., Xu, K., Yang, W., Wang, Z. and Zhong, F., "The triplet excited state of Bodipy: formation, modulation and application." *Chemical Society Reviews* 44.24 (**2015**): 8904-8939.

36. Lu, H., Mack, J., Yang, Y. and Shen, Z., "Structural modification strategies for the rational design of red/NIR region BODIPYs." *Chemical Society Reviews* 43.13 (**2014**): 4778-4823.

37. Liu, M., Ma, S., She, M., Chen, J., Wang, Z., Liu, P., Zhang, S. and Li, J., "Structural modification of BODIPY: Improve its applicability." *Chinese Chemical Letters* 30.10 (**2019**): 1815-1824.

38. Hui-Wen, Y., Xiao-Yan, Z., Xiao-Feng, G. and Hong, W., "An amphiphilic fluorescent probe designed for extracellular visualization of nitric oxide released from living cells." *Analytical Chemistry* 88.18 (**2016**): 9014-9021.

39. Kobayashi, T., Komatsu, T., Kamiya, M., Campos, C., Gonzalez-Gaitan, M., Terai, T., Hanaoka, K., Nagano, T. and Urano, Y., "Highly activatable and environment-insensitive optical highlighters for selective spatiotemporal imaging of target proteins." *Journal of the American Chemical Society* 134.27 (**2012**): 11153-11160.

40. Nierth, A., Kobitski, A.Y., Nienhaus, G.U. and Jäschke, A., "Anthracene−BODIPY dyads as fluorescent sensors for biocatalytic diels− alder reactions." *Journal of the American Chemical Society* 132.8 (**2010**): 2646-2654.

41. Zou, B., Liu, H., Mack, J., Wang, S., Tian, J., Lu, H., Li, Z. and Shen, Z., "A new aza-BODIPY based NIR region colorimetric and fluorescent chemodosimeter for fluoride." *RSC Advances* 4.96 (**2014**): 53864-53869.

42. Huang, L., Li, Z., Zhao, Y., Zhang, Y., Wu, S., Zhao, J. and Han, G., "Ultralow-power near infrared lamp light operable targeted organic nanoparticle photodynamic therapy." *Journal of the American Chemical Society* 138.44 (**2016**): 14586-14591.

43. Ali, F., Sreedharan, S., Ashoka, A.H., Saeed, H.K., Smythe, C.G., Thomas, J.A. and Das, A., "A super-resolution probe to monitor HNO levels in the endoplasmic reticulum of cells." *Analytical Chemistry* 89.22 (**2017**): 12087-12093.

44. He, H., Ji, S., He, Y., Zhu, A., Zou, Y., Deng, Y., Ke, H., Yang, H., Zhao, Y., Guo, Z. and Chen, H., "Photoconversion‐tunable fluorophore vesicles for wavelength‐dependent photoinduced cancer therapy." *Advanced Materials* 29.19 (**2017**): 1606690.

45. Zou, J., Wang, P., Wang, Y., Liu, G., Zhang, Y., Zhang, Q., Shao, J., Si, W., Huang, W. and Dong, X., "Penetration depth tunable BODIPY derivatives for pH triggered enhanced photothermal/photodynamic synergistic therapy." *Chemical Science* 10.1 (**2019**): 268-276.

46. Yamazawa, S., Nakashima, M., Suda, Y., Nishiyabu, R. and Kubo, Y., "2, 3-naphtho-fused BODIPYs as near-infrared absorbing dyes." *The Journal of Organic Chemistry* 81.3 (**2016**): 1310-1315.

47. Slanina, T., Shrestha, P., Palao, E., Kand, D., Peterson, J.A., Dutton, A.S., Rubinstein, N., Weinstain, R., Winter, A.H. and Klan, P., "In search of the perfect photocage: structure–reactivity relationships in meso-methyl BODIPY photoremovable protecting groups." *Journal of the American Chemical Society* 139.42 (**2017**): 15168-15175.

48. Peterson, J.A., Wijesooriya, C., Gehrmann, E.J., Mahoney, K.M., Goswami, P.P., Albright, T.R., Syed, A., Dutton, A.S., Smith, E.A. and Winter, A.H., "Family of BODIPY photocages cleaved by single photons of visible/near-infrared light." *Journal of the American Chemical Society* 140.23 (**2018**): 7343-7346.

49. Decker, C. and Moussa, K., "Kinetic study of the cationic photopolymerization of epoxy monomers." *Journal of Polymer Science Part A: Polymer Chemistry* 28.12 (**1990**): 3429-3443.

50. Zhao, T., Wan, Z., Sambath, K., Yu, S., Uddin, M.N., Zhang, Y. and Belfield, K.D., "Regulating mitochondrial pH with light and implications for chemoresistance." *Chemistry–A European Journal* 27.1 (**2021**): 247-251.

51. Fouassier, J.P. and Lalevée, J., *Photoinitiators for Polymer Synthesis: Scope, Reactivity, and Efficiency*; Wiley-VCH: Weinheim, 2012.

52. Tachi, H., Shirai, M. and Tsunooka, M., "Photolysis of quaternary ammonium dithiocarbamates and their use as photobase generators." *Journal of Photopolymer Science and Technology* 13.1 (**2000**): 153-156.

53. Salmi, H., Allonas, X., Ley, C., Defoin, A. and Ak, A., "Quaternary ammonium salts of phenylglyoxylic acid as photobase generators for thiol-promoted epoxide photopolymerization." *Polymer Chemistry* 5.22 (**2014**): 6577-6583.

54. Zhang, X., Wang, X., Chatani, S. and Bowman, C.N., "Phosphonium tetraphenylborate: a photocatalyst for visible-light-induced, nucleophile-initiated thiol-Michael addition photopolymerization." *ACS Macro Letters* 10.1 (**2020**): 84-89.

55. Suyama, K., Fuke, K., Yamamoto, T., Kurokawa, Y., Tsunooka, M. and Shirai, M., "Photochemical formation of ammonium/thiolate complexes from quaternary ammonium thiocyanates and its use in crosslinking of polymers." *Journal of Photochemistry and Photobiology A: Chemistry* 179.1-2 (**2006**): 87-94.

56. Klán, P., Solomek, T., Bochet, C.G., Blanc, A., Givens, R., Rubina, M., Popik, V., Kostikov, A. and Wirz, J., "Photoremovable protecting groups in chemistry and biology: reaction mechanisms and efficacy." *Chemical Reviews* 113.1 (**2013**): 119-191.

57. Hillel, A.T., Unterman, S., Nahas, Z., Reid, B., Coburn, J.M., Axelman, J., Chae, J.J., Guo, Q., Trow, R., Thomas, A. and Hou, Z., "Photoactivated composite biomaterial for soft tissue restoration in rodents and in humans." *Science Translational Medicine* 3.93 (**2011**): 93ra67-93ra67.

58. Karami, P., Rana, V.K., Zhang, Q., Boniface, A., Guo, Y., Moser, C. and Pioletti, D.P., "NIR Light-Mediated Photocuring of Adhesive Hydrogels for Noninvasive Tissue Repair via Upconversion Optogenesis." *Biomacromolecules* 23.12 (**2022**): 5007-5017.

59. Engelke, J. and Truong, V.X., "Visible light enabled para-fluoro-thiol ligation." *Polymer Chemistry* 11.44 (**2020**): 7015-7019.

60. Sitkowska, K., Feringa, B.L. and Szymański, W., "Green-light-sensitive BODIPY photoprotecting groups for amines." *The Journal of Organic Chemistry* 83.4 (**2018**): 1819-1827.

61. Wijesooriya, C.S., Peterson, J.A., Shrestha, P., Gehrmann, E.J., Winter, A.H. and Smith, E.A., 2018. "A Photoactivatable BODIPY Probe for Localization‐Based Super‐Resolution Cellular Imaging." *Angewandte Chemie* 130.39 (**2018**): 12867-12871.

62. Sambath, K., Liu, X., Wan, Z., Hutnik, L., Belfield, K.D. and Zhang, Y., "Potassium ion fluorescence probes: structures, properties and bioimaging." *ChemPhotoChem* 5.4 (**2021**): 317-325.

63. Yeh, S.A., Hou, J., Wu, J.W., Yu, S., Zhang, Y., Belfield, K.D., Camargo, F.D. and Lin, C.P., "Quantification of bone marrow interstitial pH and calcium concentration by intravital ratiometric imaging." *Nature Communications* 13.1 (**2022**): 393.

64. Zhang, X., Xiao, Y., Qi, J., Qu, J., Kim, B., Yue, X. and Belfield, K.D., "Long-wavelength, photostable, two-photon excitable BODIPY fluorophores readily modifiable for molecular probes." *The Journal of Organic Chemistry* 78.18 (**2013**): 9153-9160.

65. Sui, B., Bondar, M.V., Anderson, D., Rivera-Jacquez, H.J., Masunov, A.E. and Belfield, K.D., "New two-photon absorbing BODIPY-based fluorescent probe: Linear photophysics, stimulated emission, and ultrafast spectroscopy." *The Journal of Physical Chemistry C* 120.26 (**2016**): 14317-14329.

66. Li, W., Xie, Z. and Jing, X., "BODIPY photocatalyzed oxidation of thioanisole under visible light." *Catalysis Communications* 16.1 (**2011**): 94-97.

67. Sambath, K., Wan, Z., Wang, Q., Chen, H. and Zhang, Y., "BODIPY-Based Photoacid Generators for Light-Induced Cationic Polymerization." *Organic Letters* 22.3 (**2020**): 1208-1212.

68. Digby, E.M., Ayan, S., Shrestha, P., Gehrmann, E.J., Winter, A.H. and Beharry, A.A., "Photocaged DNA-Binding Photosensitizer Enables Photocontrol of Nuclear Entry for Dual-Targeted Photodynamic Therapy." *Journal of Medicinal Chemistry* 65.24 (**2022**): 16679-16694.

69. Kim, B., Sui, B., Yue, X., Tang, S., Tichy, M.G. and Belfield, K.D., "In Vitro Photodynamic Studies of a BODIPY‐Based Photosensitizer." *European Journal of Organic Chemistry* 2017.1 (**2017**): 25-28.

70. Ulrich, G., Ziessel, R. and Harriman, A., "The chemistry of fluorescent bodipy dyes: versatility unsurpassed." *Angewandte Chemie International Edition* 47.7 **(2008**): 1184-1201.

71. Ni, Y. and Wu, J., "Far-red and near infrared BODIPY dyes: synthesis and applications for fluorescent pH probes and bio-imaging." *Organic and Biomolecular Chemistry* 12.23 (**2014**): 3774-3791.

72. Kand, D., Liu, P., Navarro, M.X., Fischer, L.J., Rousso-Noori, L., Friedmann-Morvinski, D., Winter, A.H., Miller, E.W. and Weinstain, R., "Water-soluble

BODIPY photocages with tunable cellular localization." *Journal of the American Chemical Society* 142.11 (**2020**): 4970-4974.

73. Kue, C.S., Ng, S.Y., Voon, S.H., Kamkaew, A., Chung, L.Y., Kiew, L.V. and Lee, H.B., "Recent strategies to improve boron dipyrromethene (BODIPY) for photodynamic cancer therapy: an updated review." *Photochemical and Photobiological Sciences* 17 (**2018**): 1691-1708.

74. Wan, Z., Yu, S., Wang, Q., Tobia, J., Chen, H., Li, Z., Liu, X. and Zhang, Y., "A BODIPY‐Based Far‐Red‐Absorbing Fluorescent Probe for Hypochlorous Acid Imaging." *ChemPhotoChem* 6.4 (**2022**): e202100250.

75. Weinstain, R., Slanina, T., Kand, D. and Klan, P., "Visible-to-NIR-light activated release: from small molecules to nanomaterials." *Chemical Reviews* 120.24 (**2020**): 13135-13272.

76. Sánchez-Carnerero, E.M., Russo, M., Jakob, A., Muchová, L., Vítek, L. and Klán, P., "Effects of Substituents on Photophysical and CO-Photoreleasing Properties of 2, 6-Substituted meso-Carboxy BODIPY Derivatives." *Chemistry* 3.1 (**2021**): 238-255.

77. Lv, W., Li, Y., Li, F., Lan, X., Zhang, Y., Du, L., Zhao, Q., Phillips, D.L. and Wang, W., "Upconversion-like photolysis of BODIPY-based prodrugs via a one-photon process." *Journal of the American Chemical Society* 141.44 (**2019**): 17482-17486.

78. Slanina, T., Shrestha, P., Palao, E., Kand, D., Peterson, J.A., Dutton, A.S., Rubinstein, N., Weinstain, R., Winter, A.H. and Klan, P., "In search of the perfect photocage: structure–reactivity relationships in meso-methyl BODIPY photoremovable protecting groups." *Journal of the American Chemical Society* 139.42 (**2017**): 15168-15175.

79. Stafford, A., Ahn, D., Raulerson, E.K., Chung, K.Y., Sun, K., Cadena, D.M., Forrister, E.M., Yost, S.R., Roberts, S.T. and Page, Z.A., "Catalyst halogenation enables rapid and efficient polymerizations with visible to far-red light." *Journal of the American Chemical Society* 142.34 (**2020**): 14733-14742.

80. Lv, W., Li, Y., Li, F., Lan, X., Zhang, Y., Du, L., Zhao, Q., Phillips, D.L. and Wang, W., "Upconversion-like photolysis of BODIPY-based prodrugs via a one-photon process." *Journal of the American Chemical Society* 141.44 (**2019**): 17482-17486.

81. Sitkowska, K., Feringa, B.L. and Szymański, W., "Green-light-sensitive BODIPY photoprotecting groups for amines." *The Journal of Organic Chemistry* 83.4 (**2018**): 1819-1827.

82. Slanina, T., Shrestha, P., Palao, E., Kand, D., Peterson, J.A., Dutton, A.S., Rubinstein, N., Weinstain, R., Winter, A.H. and Klan, P., "In search of the perfect photocage: structure–reactivity relationships in meso-methyl BODIPY photoremovable protecting groups." *Journal of the American Chemical Society* 139.42 (**2017**): 15168-15175.

83. Chung, K.Y., Halwachs, K.N., Lu, P., Sun, K., Silva, H.A., Rosales, A.M. and Page, Z.A., "Rapid hydrogel formation via tandem visible light photouncaging and bioorthogonal ligation." *Cell Reports Physical Science* 3.12 (**2022**).

84. Lin, Q., Yang, L., Wang, Z., Hua, Y., Zhang, D., Bao, B., Bao, C., Gong, X. and Zhu, L., "Coumarin Photocaging Groups Modified with an Electron‐Rich Styryl Moiety at the 3‐Position: Long‐Wavelength Excitation, Rapid Photolysis, and Photobleaching." *Angewandte Chemie International Edition* 57.14 (**2018**): 3722-3726.

85. Ortiz, M.J., Agarrabeitia, A.R., Duran-Sampedro, G., Prieto, J.B., Lopez, T.A., Massad, W.A., Montejano, H.A., García, N.A. and Arbeloa, I.L., "Synthesis and functionalization of new polyhalogenated BODIPY dyes. Study of their photophysical properties and singlet oxygen generation." *Tetrahedron* 68.4 (**2012**): 1153-1162.

86. Sambath, K., Zhao, T., Wan, Z. and Zhang, Y., "Photo-uncaging of BODIPY oxime ester for histone deacetylases induced apoptosis in tumor cells." *Chemical Communications* 55.94 (**2019**): 14162-14165.

87. Goswami, P.P., Syed, A., Beck, C.L., Albright, T.R., Mahoney, K.M., Unash, R., Smith, E.A. and Winter, A.H., "BODIPY-derived photoremovable protecting groups unmasked with green light." *Journal of the American Chemical Society* 137.11 (**2015**): 3783-3786.

88. Kolb, H.C., Finn, M.G. and Sharpless, K.B., "Click chemistry: diverse chemical function from a few good reactions." *Angewandte Chemie International Edition* 40.11 (**2001**): 2004-2021.

89. Nair, D.P., Podgorski, M., Chatani, S., Gong, T., Xi, W., Fenoli, C.R. and Bowman, C.N., "The thiol-Michael addition click reaction: a powerful and widely used tool in materials chemistry." *Chemistry of Materials* 26.1 (**2014**): 724-744.

90. Chatani, S., Gong, T., Earle, B.A., Podgorski, M. and Bowman, C.N., "Visible-light initiated thiol-Michael addition photopolymerization reactions." *ACS Macro Letters* 3.4 (**2014**): 315-318.

91. Sutherland, B.P., Kabra, M. and Kloxin, C.J., "Expanding the thiol–X toolbox: photoinitiation and materials application of the acid-catalyzed thiol–ene (ACT) reaction." *Polymer Chemistry* 12.10 (**2021**): 1562-1570.

92. Kumar, R., Santa Chalarca, C.F., Bockman, M.R., Bruggen, C.V., Grimme, C.J., Dalal, R.J., Hanson, M.G., Hexum, J.K. and Reineke, T.M., "Polymeric delivery of therapeutic nucleic acids." *Chemical Reviews* 121.18 (**2021**): 11527-11652.

93. Najafi, F., Salami-Kalajahi, M. and Roghani-Mamaqani, H., "Synthesis of amphiphilic Janus dendrimer and its application in improvement of hydrophobic drugs solubility in aqueous media." *European Polymer Journal* 134 (**2020**): 109804.

94. Pashaei-Sarnaghi, R., Najafi, F., Taghavi-Kahagh, A., Salami-Kalajahi, M. and Roghani-Mamaqani, H., "Synthesis, photocrosslinking, and self-assembly of coumarin-anchored poly (amidoamine) dendrimer for smart drug delivery system." *European Polymer Journal* 158 (**2021**): 110686.

95. Li, H., Tang, S., Zhou, Q., Chen, W., Yang, X., Xing, T., Zhao, Y. and Chen, G., "Durable superhydrophobic cotton fabrics prepared by surface-initiated electrochemically mediated ATRP of polyhedral vinylsilsesquioxane and subsequent fluorination via thiol-Michael addition reaction." *Journal of Colloid and Interface Science* 593 (**2021**): 79-88.

96. Reese, C.M., Thompson, B.J., Logan, P.K., Stafford, C.M., Blanton, M. and Patton, D.L., "Sequential and one-pot post-polymerization modification reactions of thiolactone-containing polymer brushes." *Polymer Chemistry* 10.36 (**2019**): 4935-4943.

97. Yee, D.W., Schulz, M.D., Grubbs, R.H. and Greer, J.R., "Functionalized 3D Architected Materials via Thiol‐Michael Addition and Two‐Photon Lithography." *Advanced Materials* 29.16 (**2017**): 1605293.

98. Berry, D.R., Díaz, B.K., Durand-Silva, A. and Smaldone, R.A., "Radical free crosslinking of direct-write 3D printed hydrogels through a base catalyzed thiol-Michael reaction." *Polymer Chemistry* 10.44 (**2019**): 5979-5984.

99. Rossegger, E., Höller, R., Hrbinič, K., Sangermano, M., Griesser, T. and Schlögl, S., "3D Printing of Soft Magnetoactive Devices with Thiol‐Click Photopolymer Composites." *Advanced Engineering Materials* 25.7 (**2023**): 2200749.

100. Zhang, Y., Li, X., Zhu, Q., Wei, W. and Liu, X., "Photocurable hyperbranched polymer medical glue for water-resistant bonding." *Biomacromolecules* 21.12 (**2020**): 5222-5232.

101. Daglar, O., Gungor, B., Guric, G., Gunay, U.S., Hizal, G., Tunca, U. and Durmaz, H., "Rapid Hyperbranched Polythioether Synthesis Through Thiol‐Michael Addition Reaction." *Journal of Polymer Science* 58.6 (**2020**): 824-830.

102. Sinha, J., Soars, S. and Bowman, C.N., "Enamine Organocatalysts for the Thiol-Michael Addition Reaction and Cross-Linking Polymerizations." *Macromolecules* 54.4 (**2021**): 1693-1701.

103. McNair, O.D., Brent, D.P., Sparks, B.J., Patton, D.L. and Savin, D.A., "Sequential thiol click reactions: formation of ternary thiourethane/thiol–ene networks with enhanced thermal and mechanical properties." *ACS Applied Materials and Interfaces* 6.9 (**2014**): 6088-6097.

104. Nuyken, O. and Pask, S.D., "Ring-opening polymerization—an introductory review." *Polymers* 5.2 (**2013**): 361-403.

105. Nguyen, T.P., Easley, A.D., Kang, N., Khan, S., Lim, S.M., Rezenom, Y.H., Wang, S., Tran, D.K., Fan, J., Letteri, R.A. and He, X., "Polypeptide organic radical batteries." *Nature* 593.7857 (**2021**): 61-66.

106. Song, Z., Fu, H., Wang, R., Pacheco, L.A., Wang, X., Lin, Y. and Cheng, J., "Secondary structures in synthetic polypeptides from N-carboxyanhydrides: design, modulation, association, and material applications." *Chemical Society Reviews* 47.19 (**2018**): 7401-7425.

107. Deming, T.J., "Synthesis of side-chain modified polypeptides." *Chemical Reviews* 116.3 **(2016**): 786-808.

108. Li, K., Li, Z., Shen, Y., Fu, X., Chen, C. and Li, Z., "Organobase 1, 1, 3, 3-tetramethyl guanidine catalyzed rapid ring-opening polymerization of α-amino acid N-carboxyanhydrides adaptive to amine, alcohol and carboxyl acid initiators." *Polymer Chemistry* 13.5 (**2022**): 586-591.

109. Liu, Y., Li, D., Ding, J. and Chen, X., "Controlled synthesis of polypeptides." *Chinese Chemical Letters* 31.12 (**2020**): 3001-3014.

110. Soria‐Carrera, H., Franco‐Castillo, I., Romero, P., Martín, S., de la Fuente, J.M., Mitchell, S.G. and Martín‐Rapún, R., "On‐POM Ring‐Opening Polymerisation of N‐Carboxyanhydrides." *Angewandte Chemie* 133.7 (**2021**): 3491-3495.

111. Vacogne, C.D. and Schlaad, H., "Primary ammonium/tertiary amine-mediated controlled ring opening polymerisation of amino acid N-carboxyanhydrides." *Chemical Communications* 51.86 (**2015**): 15645-15648.

112. Zou, J., Fan, J., He, X., Zhang, S., Wang, H. and Wooley, K.L., "A facile glovebox-free strategy to significantly accelerate the syntheses of well-defined polypeptides by N-carboxyanhydride (NCA) ring-opening polymerizations." *Macromolecules* 46.10 (**2013**): 4223-4226.

113. Wu, L., Zou, Y., Deng, C., Cheng, R., Meng, F. and Zhong, Z., "Intracellular release of doxorubicin from core-crosslinked polypeptide micelles triggered by both pH and reduction conditions." *Biomaterials* 34.21 (**2013**): 5262-5272.

114. Rabnawaz, M., Wyman, I., Auras, R. and Cheng, S., "A roadmap towards green packaging: the current status and future outlook for polyesters in the packaging industry." *Green Chemistry* 19.20 (**2017**): 4737-4753.

115. Brannigan, R.P. and Dove, A.P., "Synthesis, properties and biomedical applications of hydrolytically degradable materials based on aliphatic polyesters and polycarbonates." *Biomaterials Science* 5.1 (**2017**): 9-21.

116. Kuroishi, P.K. and Dove, A.P., "Photoinduced ring-opening polymerisation of L-lactide via a photocaged superbase." *Chemical Communications* 54.49 (**2018**): 6264-6267.

117. Dechy-Cabaret, O., Martin-Vaca, B. and Bourissou, D., "Controlled ring-opening polymerization of lactide and glycolide." *Chemical Reviews* 104.12 (**2004**): 6147-6176.

118. Kamber, N.E., Jeong, W., Waymouth, R.M., Pratt, R.C., Lohmeijer, B.G. and Hedrick, J.L., "Organocatalytic ring-opening polymerization." *Chemical Reviews* 107.12 (**2007**): 5813-5840.

119. Nederberg, F., Connor, E.F., Möller, M., Glauser, T. and Hedrick, J.L., "New paradigms for organic catalysts: the first organocatalytic living polymerization." *Angewandte Chemie* 113.14 (**2001**): 2784-2787.

120. Yamago, S. and Nakamura, Y., "Recent progress in the use of photoirradiation in living radical polymerization." *Polymer* 54.3 (**2013**): 981-994.

121. Chen, M., Zhong, M. and Johnson, J.A., "Light-controlled radical polymerization: mechanisms, methods, and applications." *Chemical Reviews* 116.17 (**2016**): 10167-10211.

122. Pan, X., Tasdelen, M.A., Laun, J., Junkers, T., Yagci, Y. and Matyjaszewski, K., "Photomediated controlled radical polymerization." *Progress in Polymer Science* 62 (**2016**): 73-125.

123. Leibfarth, F.A., Mattson, K.M., Fors, B.P., Collins, H.A. and Hawker, C.J., "External regulation of controlled polymerizations." *Angewandte Chemie International Edition* 52.1 (**2013**): 199-210.

124. Yang, F., Dong, B., Nie, K., Shi, H., Wu, Y., Wang, H. and Liu, Z., "Light-directed synthesis of high-density peptide nucleic acid microarrays." *ACS Combinatorial Science* 17.10 (**2015**): 608-614.

125. Wöll, D., Smirnova, J., Galetskaya, M., Prykota, T., Bühler, J., Stengele, K.P., Pfleiderer, W. and Steiner, U.E., "Intramolecular Sensitization of Photocleavage of the Photolabile 2‐(2‐Nitrophenyl) propoxycarbonyl (NPPOC) Protecting Group: Photoproducts and Photokinetics of the Release of Nucleosides." *Chemistry–A European Journal* 14.21 (**2008**): 6490-6497.

126. Wöll, D., Walbert, S., Stengele, K.P., Albert, T.J., Richmond, T., Norton, J., Singer, M., Green, R.D., Pfleiderer, W. and Steiner, U.E., "Triplet‐sensitized photodeprotection of oligonucleotides in solution and on microarray chips." *Helvetica chimica acta* 87.1 (2004): 28-45.

127. Zhitomirsky, B. and Assaraf, Y.G., "Lysosomes as mediators of drug resistance in cancer." *Drug Resistance Updates* 24 (**2016**): 23-33.

128. Perera, R.M. and Zoncu, R., "The lysosome as a regulatory hub." *Annual Review of Cell and Developmental Biology* 32 (**2016**): 223-253.

129. De Duve, C., Pressman, B.C., Gianetto, R., Wattiaux, R. and Appelmans, F., "Tissue fractionation studies. 6. Intracellular distribution patterns of enzymes in rat-liver tissue." *Biochemical Journal* 60.4 (**1955**): 604.

130. Papadopoulos, C., Kravic, B. and Meyer, H., "Repair or lysophagy: dealing with damaged lysosomes." *Journal of Molecular Biology* 432.1 (**2020**): 231-239.

131. Zhu, S.Y., Yao, R.Q., Li, Y.X., Zhao, P.Y., Ren, C., Du, X.H. and Yao, Y.M., "Lysosomal quality control of cell fate: a novel therapeutic target for human diseases." *Cell Death and Disease* 11.9 (**2020**): 817.

132. Boya, P., "Lysosomal function and dysfunction: mechanism and disease." *Antioxidants and Redox Signaling* 17.5 (**2012**): 766-774.

133. Wang, C., Telpoukhovskaia, M.A., Bahr, B.A., Chen, X. and Gan, L., "Endo-lysosomal dysfunction: a converging mechanism in neurodegenerative diseases." *Current Opinion in Neurobiology* 48 (**2018**): 52-58.

134. Neufeld, E.F., Lim, T.W. and Shapiro, L.J., "Inherited disorders of lysosomal metabolism." *Annual Review of Biochemistry* 44.1 (**1975**): 357-376.

135. Neufeld, E.F., Lim, T.W. and Shapiro, L.J., "Lysosomal abnormalities in cardiovascular disease." *International Journal of Molecular Sciences* 21.3 (**2020**): 811.

136. Yue, X., Yanez, C.O., Yao, S. and Belfield, K.D., "Selective cell death by photochemically induced pH imbalance in cancer cells." *Journal of the American Chemical Society* 135.6 (**2013**): 2112-2115.

137. Muz, B., de la Puente, P., Azab, F. and Kareem Azab, A., "The role of hypoxia in cancer progression, angiogenesis, metastasis, and resistance to therapy." *Hypoxia* (**2015**): 83-92.

138. Adar, Y., Stark, M., Bram, E.E., Nowak-Sliwinska, P., Van Den Bergh, H., Szewczyk, G., Sarna, T., Skladanowski, A., Griffioen, A.W. and Assaraf, Y.G., "Imidazoacridinone-dependent lysosomal photodestruction: a pharmacological Trojan horse approach to eradicate multidrug-resistant cancers." *Cell Death and Disease* 3.4 (**2012**): e293-e293.

139. Li, Y., Han, W., Gong, D., Luo, T., Fan, Y., Mao, J., Qin, W. and Lin, W., "A self-assembled nanophotosensitizer targets lysosomes and induces lysosomal membrane permeabilization to enhance photodynamic therapy." *Chemical Science* 14.19 (**2023**): 5106-5115.

140. Cai, H., Wu, X., Jiang, L., Yu, F., Yang, Y., Li, Y., Zhang, X., Liu, J., Li, Z. and Bi, H., "Lysosome-targeted carbon dots with a light-controlled nitric oxide releasing property for enhanced photodynamic therapy." *Chinese Chemical Letters* (**2023**): 108946.

141. Zeng, J., Shirihai, O.S. and Grinstaff, M.W., "Modulating lysosomal pH: A molecular and nanoscale materials design perspective." *Journal of life sciences (Westlake Village, Calif.)* 2.4 (**2020**): 25.

142. Zeng, J., Shirihai, O.S. and Grinstaff, M.W., "Degradable nanoparticles restore lysosomal pH and autophagic flux in lipotoxic pancreatic beta cells." *Advanced Healthcare Materials* 8.12 (**2019**): 1801511.

143. Jones, T.M., Espitia, C., Wang, W., Nawrocki, S.T. and Carew, J.S., "Moving beyond hydroxychloroquine: the novel lysosomal autophagy inhibitor ROC-325 shows significant potential in preclinical studies." *Cancer Communications* 39.1 (**2019**): 1-3.

144. Domagala, A., Fidyt, K., Bobrowicz, M., Stachura, J., Szczygiel, K. and Firczuk, M., "Typical and atypical inducers of lysosomal cell death: a promising anticancer strategy." *International Journal of Molecular Sciences* 19.8 (**2018**): 2256.

145. Ferreira, P.M.P., de Sousa, R.W.R., de Oliveira Ferreira, J.R., Militão, G.C.G. and Bezerra, D.P., "Chloroquine and hydroxychloroquine in antitumor therapies based on autophagy-related mechanisms." *Pharmacological Research* 168 (**2021**): 105582.

146. McAfee, Q., Zhang, Z., Samanta, A., Levi, S.M., Ma, X.H., Piao, S., Lynch, J.P., Uehara, T., Sepulveda, A.R., Davis, L.E. and Winkler, J.D., "Autophagy inhibitor Lys05 has single-agent antitumor activity and reproduces the phenotype of a

genetic autophagy deficiency." *Proceedings of the National Academy of Sciences* 109.21 (**2012**): 8253-8258.

147. Yu, K., Ding, Y., Yu, H., Zhu, W., Yu, H., Luo, Y., Zheng, X., Huang, Y., Lu, Z. and Wang, X., "Visualizing lysosomal positioning with a fluorescent probe reveals a new synergistic anticancer effect." *ACS Sensors* 7.7 (**2022**): 1867-1873.

148. Shao, M., Zhu, W., Lv, X., Yang, Q., Liu, X., Xie, Y., Tang, P. and Sun, L., "Encapsulation of chloroquine and doxorubicin by MPEG-PLA to enhance anticancer effects by lysosomes inhibition in ovarian cancer." *International Journal of Nanomedicine* (**2018**): 8231-8245.

149. Stamelos, V.A., Fisher, N., Bamrah, H., Voisey, C., Price, J.C., Farrell, W.E., Redman, C.W. and Richardson, A., "The BH3 mimetic obatoclax accumulates in lysosomes and causes their alkalinization." *PloS One* 11.3 (**2016**): e0150696.

150. Champa, D., Orlacchio, A., Patel, B., Ranieri, M., Shemetov, A.A., Verkhusha, V.V., Cuervo, A.M. and Di Cristofano, A., "Obatoclax kills anaplastic thyroid cancer cells by inducing lysosome neutralization and necrosis." *Oncotarget* 7.23 (**2016**): 34453.

151. Guntuku, L., Gangasani, J.K., Thummuri, D., Borkar, R.M., Manavathi, B., Ragampeta, S., Vaidya, J.R., Sistla, R. and Vegi, N.G., "IITZ-01, a novel potent lysosomotropic autophagy inhibitor, has single-agent antitumor efficacy in triple-negative breast cancer in vitro and in vivo." *Oncogene* 38.4 (**2019**): 581-595.

152. Becker, P., Duhamel, T., Martínez, C. and Muñiz, K., "Designing Homogeneous Bromine Redox Catalysis for Selective Aliphatic C− H Bond Functionalization." *Angewandte Chemie International Edition* 57.18 (**2018**): 5166-5170.

153. Yu, S., Reddy, O., Abaci, A., Ai, Y., Li, Y., Chen, H., Guvendiren, M., Belfield, K.D. and Zhang, Y., "Novel BODIPY-Based Photobase Generators for Photoinduced Polymerization." *ACS Applied Materials & Interfaces* 15.38 (**2023**): 45281-45289.

154. Mlejnek, P., Havlasek, J., Pastvova, N., Dolezel, P. and Dostalova, K., "Lysosomal sequestration of weak base drugs, lysosomal biogenesis, and cell cycle alteration." *Biomedicine and Pharmacotherapy* 153 (**2022**): 113328.

155. Zhitomirsky, B. and Assaraf, Y.G., "The role of cytoplasmic-to-lysosomal pH gradient in hydrophobic weak base drug sequestration in lysosomes." *Target* 4 (**2015**): 7.

156. Cabukusta, B. and Neefjes, J., "Mechanisms of lysosomal positioning and movement." *Traffic* 19.10 (**2018**): 761-769.

157. Boya, P., Gonzalez-Polo, R.A., Poncet, D., Andreau, K., Vieira, H.L., Roumier, T., Perfettini, J.L. and Kroemer, G., "Mitochondrial membrane permeabilization is a critical step of lysosome-initiated apoptosis induced by hydroxychloroquine." *Oncogene* 22.25 (**2003**): 3927-3936.

158. Bortner, C.D. and Cidlowski, J.A., "Uncoupling cell shrinkage from apoptosis reveals that Na+ influx is required for volume loss during programmed cell death." *Journal of Biological Chemistry* 278.40 (**2003**): 39176-39184.

159. Benson, R.S., Heer, S., Dive, C. and Watson, A.J., "Characterization of cell volume loss in CEM-C7A cells during dexamethasone-induced apoptosis." *American Journal of Physiology-Cell Physiology* 270.4 (**1996**): C1190-C1203.

160. Klassen, N.V., Walker, P.R., Ross, C.K., Cygler, J. and Lach, B., "Two-stage cell shrinkage and the OER for radiation-induced apoptosis of rat thymocytes." *International Journal of Radiation Biology* 64.5 (**1993**): 571-581.